Developing a Model of H5N1 Influenza Pathogenesis in Precision-Cut Human Lung Slices

by

Gwenddolen Kettenburg

BS, Keystone College, 2018

Submitted to the Graduate Faculty of the

Department of Infectious Diseases and Microbiology

Graduate School of Public Health in partial fulfillment

of the requirements for the degree of

Master of Science

University of Pittsburgh

2020

UNIVERSITY OF PITTSBURGH

GRADUATE SCHOOL OF PUBLIC HEALTH

This thesis was presented

by

Gwenddolen Kettenburg

It was defended on

May 27, 2020

and approved by

Joshua T. Mattila, PhD
Assistant Professor
Infectious Diseases and Microbiology
Graduate School of Public Health
University of Pittsburgh

Simon C. Watkins, PhD
Distinguished Professor and Vice Chair
Department of Cell Biology
University of Pittsburgh

Thesis Director:
Simon Barratt-Boyes, BVSc, PhD
Professor
Infectious Diseases and Microbiology
Graduate School of Public Health
University of Pittsburgh

Simon Barratt-Boyes BVSc, PhD, DACVIM

Developing a Model of H5N1 Influenza Pathogenesis in Precision-Cut Human Lung Slices

Gwenddolen Kettenburg, MS

University of Pittsburgh, 2020

Abstract

Highly pathogenic avian H5N1, known as HPAI H5N1, is a strain of influenza that is highly contagious in poultry and is occasionally spread to people that have had close contact with infected poultry. In humans, the fatality rate is 60%, though person-to-person transmission rarely occurs. HPAI H5N1 causes severe acute respiratory distress syndrome (ARDS), fluid buildup in the lung alveoli, making it hard for the lungs to get adequate oxygen due to a severe inflammatory response, followed by an inflammatory response and subsequent epithelial cell death in the lungs. The mechanism for ARDS is poorly understood. While models of infection exist in lab animals, a representative *ex vivo* model of infection in humans is needed to study the severe outcome of disease. An emerging alternative to animal models and immortalized cell culture models is precision-cut tissue slices of the organ of interest, using human donors as a source of tissue. In this study, I developed a model of H5N1-infected precision-cut lung porcine then human slices and utilized said model to elucidate the mechanism of ARDS by selectively inhibiting members of cell death pathways and observe changes in downstream cytokines. Fluorescent immunohistochemistry was used to visualize and quantify markers of cell death and infection using image quantification. Changes in IL-1β were observed by enzyme-linked immunosorbent assay (ELISA). Here, I demonstrate that pyroptotic cell death is induced in response to H5N1 infection

ex vivo as demonstrated by reduced IL-1β levels in response to a caspase-1/4 inhibitor and a gasdermin-D (GSDMD) inhibitor. This approach could prove public health relevance in developing novel, host-directed therapies to treat severe influenza infection in humans by providing a model to easily test human responses.

Table of Contents

List of Tables

List of Figures

List of Abbreviations

7-AAD – 7-amino-actinomycin D

AEC- Alveolar epithelial cells

AIM2 – Absent in melanoma 2

AM – Alveolar macrophage

ARDS – Acute respiratory distress syndrom

ASC – Apoptosis-associated speck like protein containing a caspase recruitment domain

BCL2– B-cell lymphoma 2

BCL2L1 – BCL2 Like 1

Bid – BH3 interacting-domain death agonist

BSA – Bovine serum albumin

BSL3 – Biosafety level 3

COPD – Chronic obstructive pulmonary disease

CXCL10 – C-X-C motif chemokine ligand 10

DAMPs – Damage associated molecular patterns

DAPI – 4',6-diamindino-2-phenyindole

DIC – Differential interference contrast

DIVA – Differentiating infected from vaccinated animals

DMSO – Dimethylsulfoxide

ELISA – Enzyme-linked immunosorbent assay

Gal – Galactose

GSDMD – Gasdermin-D

HA- Hemagglutinin

HPAI – Highly pathogenic avian influenza

HPI – Hours post infection

IAV – Influenza type A virus

IFN-α - Interferon alpha

IHC – Immunohostochemistry

IIAM – International Institute for the Advancement of Medicine

IL-1β - Interleukin 1 beta

IL-18 – Interleukin 18

IL-6 – Interleukin 6

ISG – Interferon stimulating genes

LDH – Lactate dehydrogenase

LPAI – Low pathogenic avian influenza

LPS – Lipopolysaccharide

LSMM – Lung slice maintenance media

M1 – Matrix protein 1

M2 – Matrix protein 2

MDCK – Madin-Darby canine kidney

MERS-CoV - Middle East respiratory syndrome coronavirus

MIP-1A – Macrophage inflammatory protein 1A

MLKL – Mixed lineage kinase domain like pseudokinase

MxA – orthoMyxovirus-resistant protein A

NA – Neuraminidase

NET – Neutrophil extracellular trap

NHP – Non-human primate

NK – Natural killer

NLRP3 – NOD-,LRR-, and pyrin domain containing protein 3

NP – Nucleoprotein

NS1 – Nonstructural protein 1

NS2 – Nonstructural protein 2

PA- Polymerase acidic protein

PAMPs – Pathogen-associated molecular pattern molecules

PB1 – Polymerase basic protein 1

PB2 – Polymerase basic protein 2

PCLS – Precision-cut lung slices

PFA – Paraformaldehyde

PFU – Plaque forming units

PPE – Personal protective equipment

RIPA – Radioimmunoprecipitation assay buffer

SA – Sialyloligosaccharides

SARS-CoV - Severe acute respiratory syndrome coronavirus

SARS-CoV-2 - Severe acute respiratory syndrome coronavirus 2

STAT3 – Signal transducer and activator of transcription 3

TC – Tissue culture

TNF-α - Tumor necrosis factor alpha

TRAIL – TNF-related apoptosis-inducing ligand

Preface

I would like to offer my gratitude to Dr. Simon Barratt-Boyes for allowing me to join his lab and eventually hire me as a research technician. Over the past 2 years I feel that I have developed a wide array of laboratory skills that will stick with me throughout my scientific career, and feel especially thankful that I was given the opportunity to work in a high biocontainment setting and hone my skills as a researcher. Both past and present lab members were instrumental to my training and I want to especially thank Priscila Castanha and Jacque Corry for giving me excellent mentorship and training, along with wonderful friendship throughout this experience. I cannot express my gratitude enough.

None of this work would be possible without an excellent network of collaborations that were essential include: Rojas lab for use of his lab's vibratome, and the Center for Biological Imaging, along with funding from the Department of Defense to investigate this exciting area of research.

1.0 Introduction

1.1 HPAI H5N1 Influenza

1.1.1 Highly Pathogenic Avian Influenza H5N1 Virology

Influenza viruses are diverse members of the *Orthomyxoviridae* family, possessing a single stranded RNA genome consisting of eight segments (1-3). These eight segments encode 11 proteins (4). Hemagglutinin (HA) and neuraminidase (NA) are surface glycoproteins that play roles in entry/exit of virus particles and are used to subtype influenza type A viruses (IAV) (1, 2, 4). Polymerase basic protein 2 (PB2), polymerase basic protein 1 (PB1), polymerase basic protein 1-F2 (PB1-F2), and polymerase acidic protein (PA) are polymerase subunits that play a role in mRNA cap recognition and RNA elongation, and protease activity (2, 4). Nucleoprotein (NP) is an RNA binding protein that plays a role in nuclear import (2, 4). Matrix protein 1 (M1) is a matrix protein that plays a role in viral export and RNA nuclear export, while matrix protein 2 (M2) is an ion channel protein that assists in virus uncoating (2, 4). Nonstructural protein 1 (NS1) is an antagonist of interferon, and nonstructural protein 2 (NS2) plays a role in RNA nuclear export (2, 4).

Influenza A and B viruses are clinically relevant human pathogens, and influenza C and D viruses also exist (5), but for the purpose of this study the focus will be on highly pathogenic avian influenza H5N1 (HPAI H5N1), an influenza A virus. IAV can be further subtyped into combinations of 18 known HA and 11 known NA subtypes (5). Wild aquatic birds are the natural hosts of IAV (5). HPAI subtypes that pose risk to both poultry and human health are the H5, H7,

and H9 subtypes, and are deadlier to humans than seasonal strains (1-3, 5, 6). Seasonal IAV subtypes are the H1, H2, and H3 subtypes that circulate in the human population and cause illness every year (2, 3, 7).

IAV viruses enter cells by binding to sialic acid receptors, more specifically receptors that are linkages between sialyloligosaccharides (SA) and galactose (Gal). The two most important sialic acid receptors are SA-α2,6-Gal and SA-α2,3-Gal (3, 4, 7-11). Circulating seasonal IAVs preferentially bind to SA-α2,6-Gal receptors, while avian IAVs preferentially bind SA-α2,3-Gal receptors (3, 4, 7-11). This is suspected to be because SA-α2,3-Gal is readily expressed in avian airways and intestines but found in the lower respiratory tract in humans, whereas SA-α2,6-Gal receptors are predominantly in the upper respiratory tract of humans (2, 3, 9, 11). Other differences such as temperature of the upper and lower respiratory tract along with target cells also play a role in the differing routes of infection (2, 3, 9, 11). Avian influenza viruses on their own are fairly stable in their aquatic bird reservoirs, but concern is raised that HPAI H5N1 could reassort in a "mixing vessel" host such as a pig, which has both SA-α2,6-Gal and SA-α2,3-Gal receptors, in the same manner which created the 2009 H1N1 pandemic IAV, along with the 1957 H2N2 "Asian influenza" and 1968 H3N2 "Hong Kong influenza" (12-15). In contrast, the 1918 H1N1 pandemic IAV had avian origins but did not go through a reassortment event, instead resulting from a bird-to-human transmission (12).

HPAI H5N1 preferentially binds to non-ciliated cells, and it is thought that the most favored cellular target for infection of HPAI H5N1 is type II pneumocytes in the alveoli (8, 10, 11). Human IAVs in general preferentially bind to ciliated cells, and it is thought that the most favored cellular target for infection is type I pneumocytes in the alveoli, in comparison (8, 10, 11). Human disease from HPAI H5N1 usually arises when domestic poultry are infected and infection

is passed to people in close contact with these animals, although due to the preferential binding to receptors in the lower respiratory tract of people, it is extremely difficult for HPAI H5N1 to spread between people, as with other avian IAV (1, 2, 4, 6, 16, 17).

1.1.2 Epidemiology and Ecology

HPAI H5N1 circulates naturally in wild aquatic birds such as ducks and gulls, usually asymptomatically (15, 18). The terms highly pathogenic avian influenza (HPAI) and low pathogenic avian influenza (LPAI) refers to disease outcome in domestic poultry, and does not coincide with disease presentation in humans; H5N1 can spread rapidly throughout a poultry stock once infected with high mortality rates (around 90%) after coming into contact with surfaces shared between infected birds, close contact, or through contact with contaminated feces (13, 15, 18-20). IAVs are notorious for undergoing antigenic drift and shift. Antigenic drift produces the seasonal strains every year that differ from the previous year through small mutations in the HA and NA proteins, and antigenic shift is a large change in the virus that can produce a new subtype by which people have no preexisting immunity (5). These changes often yield reassortments between one to two different subtypes, making vaccine design a difficult challenge (15, 21, 22).

To date, there have been 861 cases of H5N1 infection in humans with 455 of these confirmed cases resulting in death (20), although these are severe cases and the true case count may be much higher due to mild cases going unreported (13, 15, 18, 23, 24). Outbreaks of H5N1 have been notable in Asia, with the first detection arising in southern China shortly preceding the first reported human cases in Hong Kong, with the majority of human cases now taking place in Indonesia, Vietnam, Egypt, China, Thailand, and Bangladesh (13, 15, 22, 24-26). It should be noted that outbreaks occur in poultry in the same areas where human infections have been detected

3

(the Asian lineage of HPAI H5N1), but also in North America, where the lineage has rarely been found to infect people (18). Other avian IAV viruses (H7 and H9 subtypes) have been found to infect people as well, but have not been found to be as pathogenic, with H9 IAV infections resulting in mild seasonal flu-like clinical manifestations and H7 IAV infections also resulting in mild symptoms with the exception of some severe cases (27-29). Still, HPAI H5N1 Asian lineage remains the most fatal influenza strain to humans, with a reported mortality rate of about 52%; although with the assumption that mild cases go unreported due to many people with flu-like symptoms never seeking testing and treatment, some research suggests that the true mortality rate may be closer to 30% (13, 15, 18, 23, 24).

1.1.3 Clinical Manifestation, Treatment, and Prevention

HPAI H5N1 infection in humans presents with symptoms of normal respiratory illness: fever, cough, shortness of breath along with other typical seasonal influenza symptoms such as headache, tiredness, and sore throat (30, 31). However, disease progression then leads to more severe complications like pneumonia and acute respiratory distress syndrome (ARDS), with evidence showing that infection can spread throughout the body and past the respiratory system (30-32). Pigs have been shown to be infected with HPAI H5N1, although replication and subsequent titers remained low and were accompanied by mild and asymptomatic infection, further highlighting their possible role as an intermediate host (33, 34).

Currently, as with most viral infections without a current vaccine, prevention is the best method in disease reduction. For HPAI H5N1, since infection usually happens at the poultry-human interface, mitigation is best done at this step by taking basic personal protective equipment (PPE) precautions such as washing hands after coming in contact with birds, and wearing a mask

(18). Also, vaccination for the seasonal influenza strains to generate potential cross-protection, and reducing exposure to sick and/or dead birds can also help in mitigation (18). These are prevention measures that can be completed on an individual level, but other more aggressive/widespread concepts have been suggested, such as a more controlled approach to poultry rearing with active surveillance to limit exposure of domestic poultry to wild birds, live bird market changes to instill more sanitary and safe practices if not disband the practice overall, and finally, potential vaccination of humans once an appropriate vaccine has been developed (18, 35). As for a drug treatment, oseltamivir and zanamivir are approved for prophylactic use (18, 36, 37).

In the past there have been some investigations into vaccination programs for poultry, rather than focusing efforts solely on human vaccination and are available, but in the most affected countries many have deemed the cost of the service unsustainable, and coverage of flocks was low; these vaccines would be useful if implemented in combination with increased biosafety measures (35, 38, 39). In the United States, the standard for curbing HPAI H5N1 in poultry is to cull the flocks because the method of differentiating infected from vaccinated animals (DIVA) is difficult due to shortcomings in serological testing. The pursuit of a vaccine for HPAI H5N1 has made progress, but the attention has shifted to a different IAV vaccine approach, targeting the more conserved HA stem region rather than the HA globular head, which would allow for broad protection to both seasonal IAV strains and avian IAV strains without the urgent need to develop a new formulation every year to match the circulating strains (40-42).

1.1.4 HPAI H5N1 Pathogenesis in Humans Leads to ARDS

The innate immune response dominates the host's response to HPAI H5N1 infection, as demonstrated by a multitude of studies showing an increase in proinflammatory cytokines (cell

signaling molecules) and mobilization of macrophages, particularly alveolar macrophages (AMs) (Figure 1), followed by recruitment of neutrophils to the lung in response to infection (43-54). Hallmarks specifically include an increase in interferon-α (IFNα) production, interleukin-6 (IL-6), C-X-C motif chemokine ligand 10 (CXCL10), tumor necrosis factor-α (TNF-α), interleukin-1 beta (IL-1β), and interleukin-18 (IL-18) (43-46, 48, 49, 51-54). Interferon-stimulated gene (ISG)-induction was also linked to disease pathology, more specifically a type I IFN signaling response to generate antiviral activity through secretion of IFN-α and IFN-β, with some reports demonstrating similar responses to what was seen in the 1918 H1N1 pandemic (46, 47, 50, 54-57). Alveolar epithelial cells (AECs) are the main cellular targets of H5N1, and through lung damage to AECs plasma leakage into the airways happened as a result (Figure 1) (43). AMs are also susceptible to infection, and it is suspected that H5N1 recruitment of neutrophils and macrophages disrupts the epithelial-endothelial barriers and therefore leading to alveolar damage (Figure 1) (43, 45, 46, 51, 53, 58-60). A primary disease outcome of H5N1 infection is ARDS, which is still poorly characterized, as are some parts of H5N1 pathogenesis itself; more research into the cytokine response and cell death mechanisms that accompany this response would be beneficial to prevention and treatment of the disease (43, 45, 46, 51, 52, 58). While causing severe disease in humans, pigs generally have mild disease, and generally pathogenesis in these hosts is controlled by alveolar macrophages in addition to lower titers in the lungs overall, possibly losing their pathogenicity in this intermediate host (14, 61, 62).
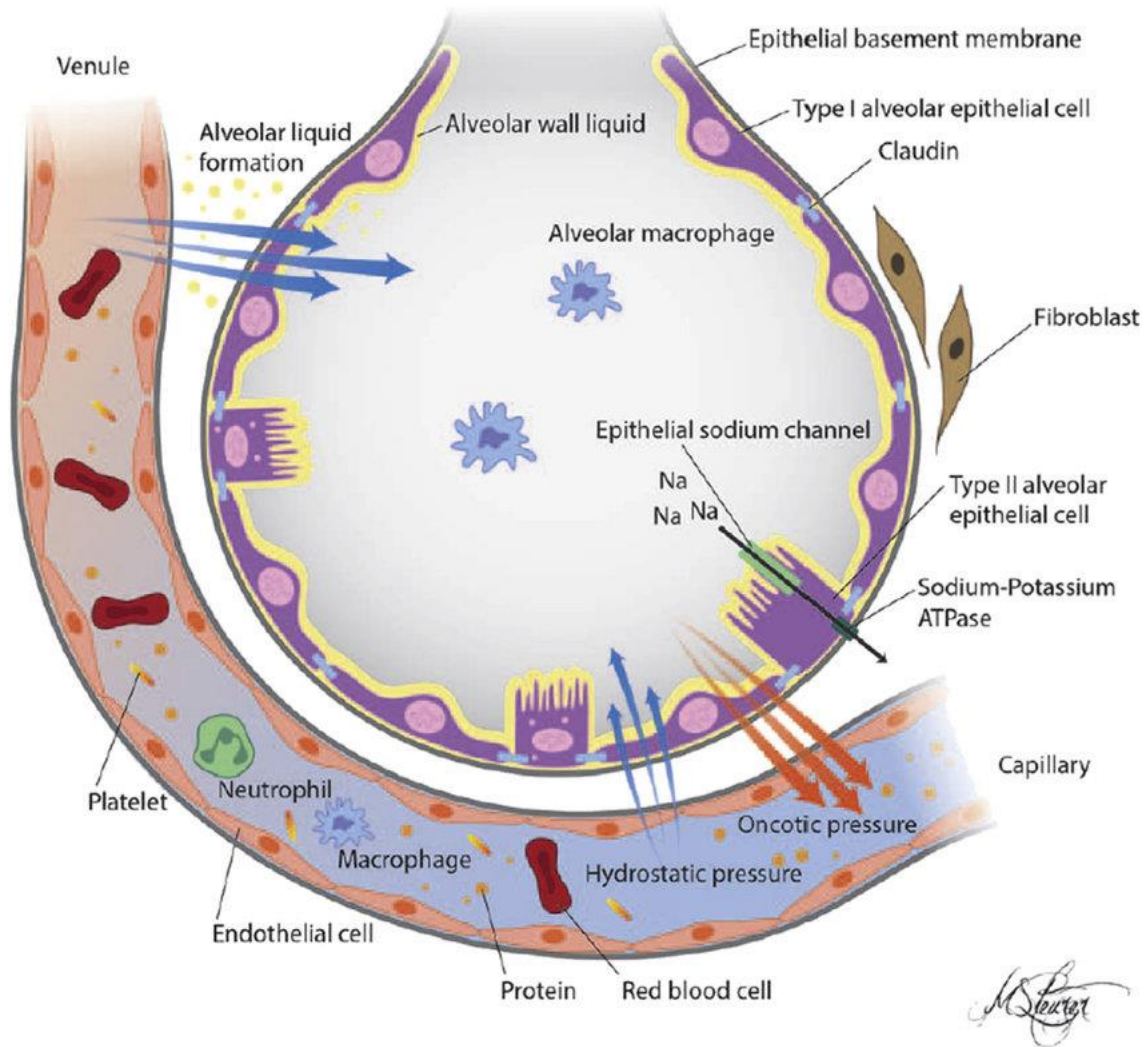
Figure 1: Schematic of Lung Alveolar Epithelium

Diagram demonstrating location of AECs (type I and type II pneumocytes) and macrophages (63).

1.2 Animal Models of H5N1 Infection

Animal models are a necessary and more sophisticated method of studying diseases that provide a better picture of how a disease may progress in a human as opposed to cell culture. For HPAI H5N1, mice, ferrets, and non-human primates (NHPs) have all been used (43, 64-71). In mice, the BALB/c model is most frequently used and infection is simulated through the intranasal

route, without adapting the virus to the mice first (64, 67, 68). Adaptation of influenza to the animal model is unfavorable because it promotes loss of pathogenicity (to humans) through lung-to-lung serial passages, and gain of characteristics that make the virus pathogenic in mice or other animal models like ferrets, effectively testing something that is not representative of a human infection (72).

Ferrets are a more representative model than mice, due to their respiratory system similarities to the human respiratory system, and they are also susceptible to infection without adaptation (64, 65, 67, 71). There are other benefits that make ferrets a better small animal model, such as the ability for infected ferrets to transit disease to uninfected ferrets and their competence in vaccine efficacy research. However, there is a limit on the amount of ferret specific reagents available, their caging and care requirements are more costly, and lack of influenza virus seronegative ferrets make mice preferred to many researchers (64, 65).

NHPs remain the gold standard of disease modeling, due to their similarities to humans. However, the costs associated with this model make it a less favorable option unless other small animal models have already been used to investigate, along with variability of viral titers and gross pathology within groups that can make statistical analysis difficult, and ethical issues (64). For NHP, both models of aerosol delivery and intranasal/intratracheal route have been established and have been used to evaluate vaccine efficacy, antiviral treatments, and natural disease progression (43, 64, 66, 69, 70). However, the problem still remains that working with HPAI H5N1 in biosafety level 3 (BSL3) conditions is cumbersome when working with animals. A more representative model of infection than cell culture that capitulates a natural human response would be helpful in screening treatments and investigating novel pathogenesis mechanisms before moving to an animal model.

8

1.2.1 Previous Model of HPAI H5N1 Induced ARDS

Our lab has established an aerosolized model of HPAI H5N1 infection in cynomolgus macaques that has shown an increase in IL-1β with other proinflammatory cytokines along with destruction of alveolar macrophages can lead to ARDS and therefore serve as a model for severe infection with disease (43). This being an aerosol model allows for the virus to reach the alveoli, which are believed to be the site of ARDS, whereas intranasal and intratracheal methods of infection do not allow for this deep lung infection that is a hallmark of a lethal H5N1 infection. We have also shown through RNA expression profiles from these macaques that genes involved with the pyroptotic pathway (GSDMD, NLRP3, AIM2, caspase-4, caspase-5, and AIM2) are upregulated in comparison to control animals, and that apoptotic genes (caspase-3, caspase-8, BCL2, and BCL2L1) remain largely comparable to mock animals, with the exception of caspase-9 which was lower in infected animals (Corry *et al.* manuscript in preparation). This, in combination with the lack of exploration of pyroptosis in a representative model of H5N1 has prompted further interest into the topic for our group, which is partially explored in this research project.

1.3 Apoptosis

Apoptosis is a programmed cell death mechanism that has two general pathways: the intrinsic and extrinsic pathways, triggered either by the death ligand or cellular stress, and a granzyme B pathway (which is less common but is carried out by cytotoxic T-cell activities (73-76). Caspases (protease enzymes that are involved in cell death pathways) play a significant role

in this pathway, and procaspases are the inactive precursors of caspases. The extrinsic pathway follows a sequence of events that starts with death ligand activation and procaspase-8 may cleave itself into caspase-8 that goes on to activate caspase-3, which is the most significant member of the apoptotic pathway, and caspases-6 and -7 (73, 74, 76). The intrinsic pathway is induced by stimuli that is not receptor associated such as DNA damage and oxidative stress, which then goes on to induce the anti-apoptotic B-cell lymphoma 2 (Bcl-2) protein family to interact with the mitochondria to release cytochrome-c, eventually activating procaspase-9 and procaspase-3, and finally inducing apoptosis (73, 74, 76). In the intrinsic pathway, caspase-8 can also go on to cleave proapoptotic protein BH3 interacting-domain death agonist (Bid) that interacts with the mitochondria and continue to follow the events of the intrinsic pathway, linking the two (73, 74, 76). Most importantly, apoptosis is considered a "silent" form of cell death, meaning there is no inflammatory reaction (77). An outline of this pathway is seen in figure 2.
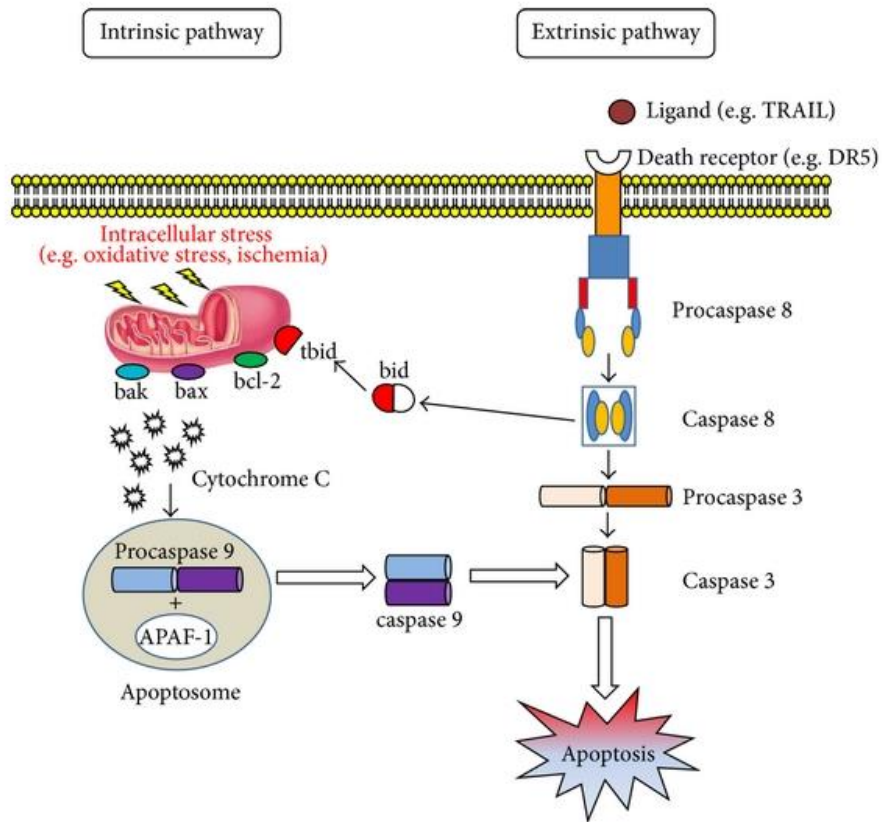
Figure 2: Apoptotic Pathway

Figure showing the intrinsic and extrinsic pathways of apoptosis (78).

1.3.1 Apoptosis and HPAI H5N1

Apoptosis has been suggested to play a role in the cytokine dysregulation events that could lead to severe pathogenesis in H5N1 disease (49, 79-85). H5N1 has been shown to activate caspases-8 and -9 in alveolar epithelial cells, but had also delayed apoptosis through its upregulation of TNF-related apoptosis-inducing ligand (TRAIL) and signal transducer and activator of transcription 3 (STAT3) (85). Additionally, research has found that H5N1 can directly infect natural killer (NK) cells and induce apoptosis of the cells in an effort to evade NK immunity and cytotoxicity, allowing for increased replication (82). In humans, apoptosis of alveolar

macrophages is found to be delayed by H5N1 because the peak in apoptotic cells was not seen until 48 hours post infection (hpi) as observed through TRAIL expression, possibly allowing for a chance for extended replication in the lungs (79). Finally, NS1 of H5N1 has the ability to induce apoptosis through both the intrinsic and extrinsic pathways (84).

In duck embryonic fibroblasts and chicken embryonic fibroblasts, there has been evidence shown to suggest that non-cytokine related events may lead to apoptosis, more specifically through an influx of extracellular calcium, therefore leading to mitochondrial dysregulation through both caspase independent and dependent events (81). Another study in duck embryonic fibroblasts showed that apoptosis was carried out in a caspase-dependent matter in avian cells, specifically caspases-8 and -9, but also with caspase-3 (83). Pigs are already more resistant to H5N1 pathogenesis, but this is hypothesized to be in part mediated by early apoptotic events in porcine alveolar macrophages through PB1-F2 through induction of inflammation, and therefore there are less virus progeny produced (86).

While apoptosis has been implicated as a method of pathogenesis, the fact that it is not associated with an inflammatory response does not explain the massive inflammatory response that is seen in ARDS following infection. Also, much of the research into cell death mechanisms are done in cell culture and mice, which may not be completely representative of what happens in an appropriate animal model (49, 79, 81-86). An inflammatory response to ARDS in our aerosolized macaque model has led us to believe that another form of cell death, pyroptosis, may be contributing to pathogenesis instead.

1.4 Pyroptosis

Pyroptosis is a programmed cell mechanism that ends in rupturing of the cell membrane, making this method of cell death classified as "fiery" because it induces an inflammatory response after inflammasome activation (87-94). The pyroptotic pathway starts with either intracellular pathogen-associated molecular pattern molecules (PAMPs) that are derived from pathogenic sources (i.e. bacteria and viruses) that signal the immune system to respond, or damage-associated molecular patterns (DAMPs) that are released from dying cells to signal an inflammatory response (87, 90, 91, 93, 94). These signal to the inflammasome complex, molecular units that trigger pro-inflammatory cytokine production, with apoptosis-associated speck like protein containing a caspase recruitment domain (ASC) which then signals procaspase-1, further cleaving itself into caspase-1 which then cleaves GSDMD (87, 90, 91, 93, 94). Additionally, through caspase-1 cleavage, further cleavage events of pro-IL-1β into IL-1β and pro-IL-18 into IL-18 go on to be released from the cell through potassium efflux which can trigger further NOD-,LRR-, and pyrin domain containing protein 3 (NLRP3) inflammasome activation, denoted as the canonical pathway (87, 90, 91, 93, 94).

The non-canonical pathway involves the cleavage of procaspase-11 into caspase-11 upon PAMP and DAMP signaling, leaving to cleavage of GSDMD by caspase-4, upon which the N terminus can go on to either cause mitochondrial damage from the N-terminus of cleaved or assemble into pores in the inner cell membrane leaflet to allow for IL-1β and IL-18 to leave the cell upon cleavage from caspase-4/5 (87, 89, 91, 93, 94).

With this pathway newer to discovery than other for more well-known cell death mechanisms, the master executioner of the pathway, GSDMD, is only in recent years being recognized for its role in cytokine release, although caspase-1 is also a very important member of

the pathway (87, 88, 90, 91, 93, 94). Because it is involved in both canonical and non-canonical pyroptotic pathways, GSDMD and the cleavage events of caspase-1 and caspase-4/5 are ideal targets for inhibition when studying the role of pyroptosis in disease pathogenesis (88). Outlines of this pathway are seen in figure 3.
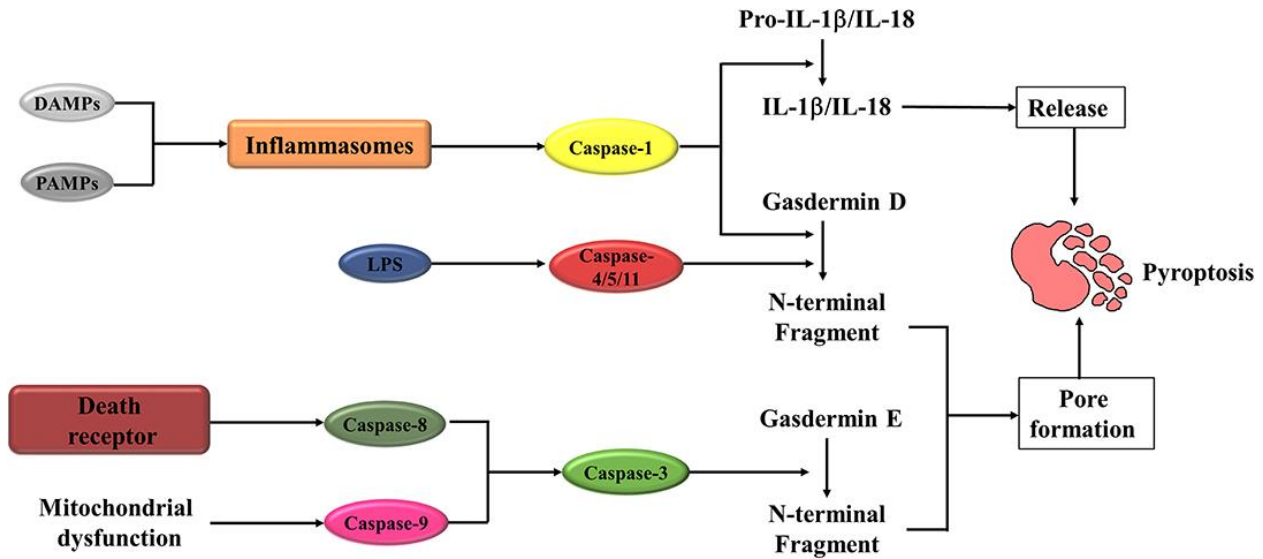
Figure 3: Pyroptotic Pathway

Figure demonstrating the components of the pyroptotic pathway (95).

1.4.1 Pyroptosis and HPAI H5N1

Unlike literature linking apoptosis and H5N1 pathogenesis, there is not much research into the possibility of pyroptosis playing a role in H5N1 pathogenesis. To explain the massive proinflammatory response, one study has linked induction of type I IFN signaling to trigger pyroptosis in immortalized airway epithelial cells, and various caspase inhibitors were used to determine which pathway was most prominent upon infection (56). ASC and caspase-1 have demonstrated role in the adaptive response to IAV after challenge, recruiting macrophages, dendritic cells, NK cells, and neutrophils to the lung, but also shown that they are required for

14

release of IL-1β and IL-18 in IAV infection (96, 97). A study in rhesus macaques showed that genes NLRP3 and IL-1β were downregulated after infection with H5N1 in the bronchus, however in this experiment the virus was delivered via multiple routes: intratracheal, intranasal, intraocular, and oral, which may not be representative of a natural aerosol infection (98). Conversely, in a macaque model of aerosolized H5N1 infection, downstream cytokines of pyroptosis such as IL-1β were found to be upregulated after infection (43). In response to seeing a proinflammatory response upon aerosol H5N1 challenge, transcriptomics revealed an increase in RNA expression in GSDMD, caspase-1, ASC, NLRP3, and absent in melanoma 2 (AIM2), indicating that a canonical pyroptotic response is happening (Corry *et al.* Manuscript in preparation).

1.5 Precision-Cut Lung Slices

Precision-cut lung slices (PCLS) are a valuable culture system that are more representative of a whole lung than normal immortalized cell culture because they represent all cell types, structure, and accurately reflect changes to the extracellular matrix that may happen with disease, but are more easily generated than performing animal research by providing an *ex vivo* platform (99-104). These are thin sections of sectioned tissue that are derived from a live organ that can be put into culture and kept alive, and have the benefit of creating a "snapshot" of the cells in that particular area of the tissue while retaining their immune cells (99-104). PCLS are more sophisticated than transwell systems, which allow for study for cellular interactions and crosstalk, but do not accurately recapitulate the air and liquid flow as it would happen *in vivo* (100). PCLS provide an alternative to these more sophisticated *in vivo* models that are difficult to create and have reliance on artificial scaffolds by creating a mechanistically useful model (100). Finally,

PCLS have also been shown to be viable after cryopreservation, allowing for the researcher to make full use of hard to procure lungs for future studies (100). Most attractive, the PCLS model maintains a 3-dimensional architecture of the lung, which cannot be attained in *in vivo* models (105).

As with all model systems, there are disadvantages that include a lack of a recruitable immune response, not every slice has the exact same cellular makeup, and the fact that this is regarded universally "static" system as opposed to a breathing system, especially with no air-liquid interface (100). In short, PCLS provide a platform to model diseases up to two weeks, but anything longer should warrant the investment into another model system, making them ideal for observing a short-term response (100, 102-104).

Interestingly, there has been some evidence that PCLS can generate a re-call immune response to antigens from routine vaccines such as influenza (104). Traditionally, PCLS are used to study chronic respiratory diseases such as chronic obstructive pulmonary disease (COPD) and asthma, although there has been some exploration into infectious respiratory pathogens including swine influenza virus, *S. aureus*, *Y. pestis*, *C. burnetii*, Jaagsiekte sheep retrovirus (99-101, 103, 106-108). As mentioned in previous sections, animal models are not human models, no matter how sophisticated, and are difficult to manipulate in high biosafety conditions. A massive cytokine influx is thought to be the mechanism of which ARDS causes lung damage, but the processes behind this are poorly understood. A PCLS system using inhibitors to block cell death pathways would allow us to pinpoint the mechanism by which ARDS leads to cell death in an easy to manipulate model system.

2.0 Public Health Significance

With the risks that the constantly mutating seasonal influenza viruses pose to human health and the strain they put on the public health system, it is only natural to wonder if HPAI H5N1 or other avian influenza strains could mutate to adapt to person-to-person spread and cause another flu pandemic (18, 109, 110). Gain of function experiments completed on HPAI H5N1 demonstrated that airborne transmission was possible between infected and healthy ferrets by generating mutations from serial passaging in ferrets, but there was a loss of pathogenesis (111). The same observation was made by generating viruses that are comprised of the HA protein from HPAI H5N1 and seven gene segments from the 1918 pandemic H1N1, with several mutations to the HA segment that allowed for easier transmission between mammals, but again a loss of pathogenicity occurred over passages (112). Both of these studies, while ultimately demonstrating that over serial passages and selective mutations H5N1 loses pathogenicity, still show the alarming potential of HPAI H5N1 to possibly mutate to gain the ability to spread person-to-person.

Research to understand the mechanisms that contribute to pathogenesis and how to block those said mechanisms in the absence of the vaccine are necessary to prepare for a potential HPAI H5N1 pandemic. Drugs to block cell death mechanisms of disease could be especially useful to Middle Eastern and Asian countries where outbreaks of H5N1 happen most often, but also to provide broadly acting solutions to other viruses of concern in the same areas, such as Middle East respiratory syndrome coronavirus (MERS-CoV) and severe acute respiratory syndrome coronavirus 2 (SARS-CoV-2) (18). In fact, while understanding the pathogenesis of SARS-CoV-2 is only in the early stages, some research has suggested that pyroptosis may contribute to pathogenesis (113, 114), as my data and our lab's previous data into HPAI H5N1 pathogenesis

suggests. These data together highlight the need for a model of HPAI H5N1 that is easy to generate,

representative of human infection, and susceptible to testing of new treatments.

3.0 Hypothesis and Specific Aims

Previously, we have started to pinpoint the cell death mechanism of ARDS using our lethal HPAI H5N1 aerosol model (43). From transcriptomic analyses of the lungs from this study, we have started to analyze the cell death mechanisms that may be causing ARDS; genes involved with the pyroptotic pathway such as ASC, NLRP3, caspase-1, AIM2, and GSDMD were upregulated in infected macaques in relation to naïve macaques (Corry *et al*. manuscript in preparation). Genes involved with the apoptotic pathway such as caspase-3, caspase-8, and antiapoptotic genes BCL2 and BCL2L1 remained the same between infected and naïve macaques (Corry *et al*. manuscript in preparation). My overarching hypothesis is that lung damage from HPAI H5N1 infection is a result of pyroptosis. This project's main focus will be to establish a protocol for generating PCLS from pig lungs and eventually from human lungs and be able to establish successful infection of HPAI H5N1 in these lung slices. Once infection is established in these models, I will focus on blocking main members of the pyroptotic pathway (using caspase 1/4 inhibitor VX-765 and GSDMD inhibitor disulfiram) and the apoptotic pathway (caspase-3 inhibitor Z-DEVD-FMK), along with a pan-caspase inhibitor Z-VAD-FMK. I aim to assess the success of these inhibitors by imaging certain cell markers for members of the pyroptotic pathway, cell death, cell markers, and infection, along with performing assays to measure downstream IL-1ß.

3.1 Aim 1: Develop an *Ex Vivo* Model of Porcine and Human PCLS

This aim seeks to successfully develop a protocol to generate PCLS from two relevant hosts of HPAI H5N1 infection: pigs and humans. I carried this out by procuring lungs from respective sources, infused the lung with low melting point agarose, then sliced small cores of the lung with a vibratome in order to generate 400-micron thick lung slices that were of appropriate thickness to mount on a microscope slide. I used viability staining and differential interference contrast (DIC) imaging to assess the structural integrity and general health of the slices, and finally established a working protocol for either host that would be appropriate for infection.

3.2 Aim 2: Determine if PCLS Can Be Productively Infected with HPAI H5N1 and Determine Cellular Targets of Infection

This aim allowed for me to see if the PCLS and specific cell types within those PCLS are susceptible to being infected with HPAI H5N1, and if the slices were generating virus progeny. I carried this out by taking supernatant from the lung slices and performed plaque assays to look for replicating virus, along with using immunohistochemistry (IHC) to use a microscope to look for markers of infection such as influenza A NP and influenza NS1. I was also interested in observing the susceptibility of AECs's and alveolar AM's to HPAI H5N1 infection. Prior to infection, I propagated H5N1 A/Vietnam/1203/2004 virus stock in chicken eggs and used this stock throughout the project.

3.3 Aim 3: Determine the Contribution of Pyroptosis to Lung Damage in H5N1 Infection

This aim sought to explore the role of pyroptosis in HPAI H5N1 pathogenesis, and blocked cell death by treating PCLS with VX-765. To do this, I treated the lung slices with DMSO as a vehicle control, VX-765 as a caspase-1/4 inhibitor (inhibit pyroptosis), Z-DEVD-FMK as a caspase-3 inhibitor (inhibit apoptosis), and Z-VAD-FMK as a pan-caspase inhibitor. I also explored the potential of disulfiram as a GSDMD inhibitor (inhibit pyroptosis). To observe cell death, I used fluorescent-labeled inhibitor of caspases (FLICA), a marker of active caspase-1, and 7-aminoactinomycin D (7-AAD), a marker of cells with compromised membranes, to observe the changes in cell death in response to drug treatments through IHC. Other markers such as IL-1ß, ASC, human myxovirus resistance protein 1 (MxA/Mx1), and IFNα were also observed through IHC. Finally, ELISAs for IL-1ß were performed on supernatants collected from PCLS to quantify the changes in this late stage cytokine released in response to pyroptosis.

4.0 Methods and Materials

4.1 H5N1 Influenza Propagation in Chicken Eggs

Embryonated pathogen-free chicken eggs (Charles River Laboratories) were incubated in a rocking egg incubator (GQF MFG Co. Inc) at 35°C at 60% humidity for 11 days before infection and were checked by candling (shining a light on the eggs in a dark room to observe the inside) on day 1, day 8, and day of infection. Eggs with blood rings, evidence of bacterial contamination, or eggs that were not fertilized were discarded (Figure 4). The H5N1 A/Vietnam/1203/2004 stock virus previously provided by Dr. S. Mark Tompkins at the Department of Infectious Diseases, University of Georgia was diluted to 1×10^4 PFU/mL (determined to be optimal titer in pilot egg inoculation experiment) in 1x antibiotic-antimycotic (Thermo Fisher). Using a 20-gauge needle, a hole was pierced on the top of the air sac, and a 27-gauge needle was used to inoculate the allantoic sac by dispensing contents at a 45-degree angle through the previously made hole. The eggs were sealed with glue and disinfected with 70% alcohol and incubated in a static humidified incubator at 37°C for 24 hours. Eggs were then placed at 4°C overnight to kill the embryo and constrict the blood vessels. The allantoic fluid was then collected without blood contamination, pooled into one container, then centrifuged to remove debris. Supernatant was aliquoted and flash frozen before storage at -80°C. Virus titer was verified to be 7.25×10^8 PFU/mL in Madin-Darby canine-kidney (MDCK) cells by plaque assay, and virus stock was analyzed via whole-genome sequencing as previously described (43) and no significant amino acid changes were found. All work with H5N1 was performed at the University of Pittsburgh Regional Biocontainment Laboratory under BSL3 conditions.
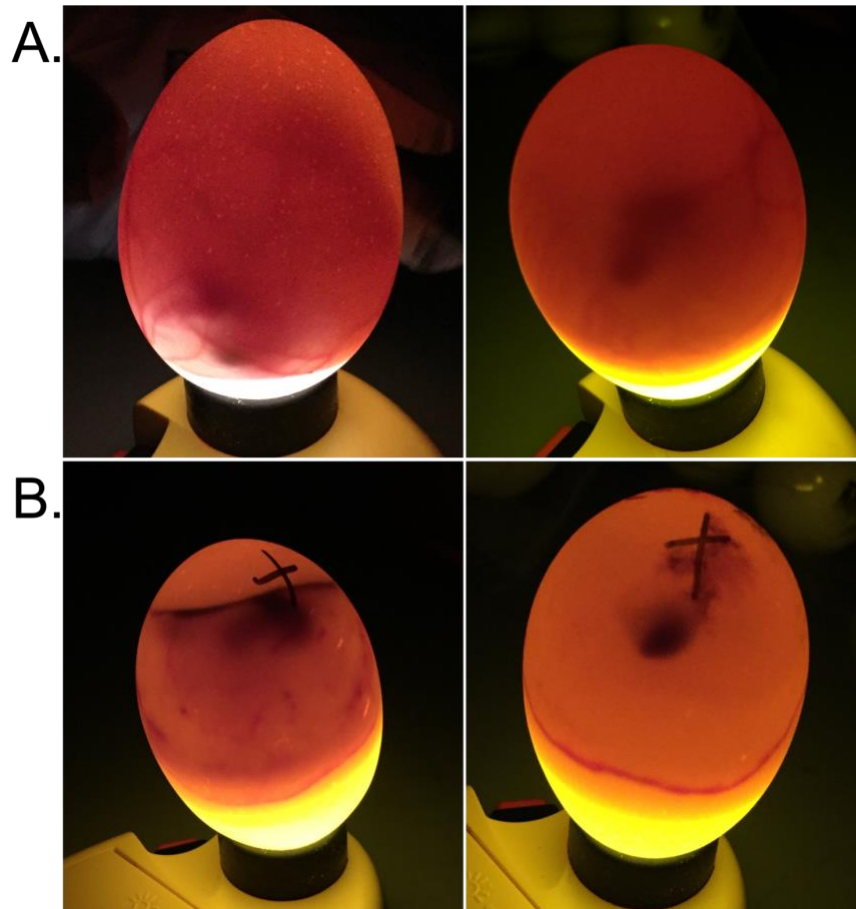
Figure 4: Egg Candling

Examples of eggs used in experiment to generate H5N1 A/Vietnam/1203/2004 stock. (A) These eggs are considered healthy and preferable to infect due to the presence of a developing embryo and developed veins. (B) These eggs are not viable as demonstrated by a ring of bacterial contamination and dead embryo (left) and presence of a blood ring and dead embryo (right).

4.2 Acquisition of Porcine and Human Lungs and Tissue Processing

Human lungs were acquired from the International Institute for the Advancement of Medicine (IIAM) postmortem and were delivered within 48 hours of cross-clamp time (Table 1), then upon arrival were warmed in a 37°C water bath for 1 hour. Porcine lungs were acquired from Thoma Meat Market from pigs that were sacrificed on day of lung collection for other purposes

(Table 1), and upon arrival were warmed in a 37°C water bath for 1 hour. Next, lungs were perfused with 2% low-melting point agarose (Thermo Fisher) and allowed to solidify at room temperature. Lung was further separated into 0.5-inch sections and cored with an 8mm biopunch. The cores were embedded in petri dishes with 2% low-melting point agarose (Thermo Fisher) and sectioned into either 400-micron or 900-micron human PCLS with a vibratome (Leica VT1200s). Slices were washed 3 times with DMEM media (Gibco) containing 50 U/mL penicillin/streptomycin (Gibco), 0.2 μg/mL gentamicin (Gibco), and 1.25 μg/mL amphotericin B (Gibco) (lung slice wash media) to reduce contamination before culturing in lung slice wash media with 10% FBS (Gemini) (lung slice maintenance media is LSMM). Slices were cultured overnight in 0.5 mL media in 48 well tissue culture (TC)-treated plates on a rocker at 37°C and 5% CO_2 before infection the following day.

Table 1: Lung Donor Demographic Information

A.

Lung ID (L/R)	Cause of death	Age	Sex	Appearance	
AGDO365	Stroke	64	M	Grey from smoking, light in color, not obviously heavily damaged from smoking	
AGET446	Anoxia	60	F	Pink and healthy in appearance	
AGFH249	Stroke	71	F	Black coloration from smoking, brown when cut into	*
AGGL489 (R)	Head trauma	75	M	Pale, black debris present in lower lobes	
AGHH267	Stroke	52	F	Overall healthy, lower lobe was a little bluish in color	
AGIE005 (R)	Anoxia	29	F	No smoking history but black debris present	*donor had Lupus
AHAU189	Head trauma	59	M	Overall healthy and pink	
AHCG011	Stroke	57	F	Overall healthy and pink	*nasal swab positive for CoV HKU1

*Used in model development, data not shown

B.

Lung and date	Description	
Porcine lungs 3/2019	Bloody and hemorrhaged	
Porcine lungs 4/2019	Bloody and hemorrhaged	*
Porcine lungs 6/20/19	Bloody and hemorrhaged	
Porcine lungs 8/19	Bloody and hemorrhaged	
Porcine lungs 11/19	Bloody and hemorrhaged	

*Used in model development, data not shown

Summary demographic data of lungs used in this study. (A) Demographic and descriptive data of human lungs.   (B) Description of porcine lungs and date acquired.

4.3 Infection, Sample Collection, and Fixation of PCLS

PCLS were placed one per well in a 48 well TC-treated plate with 0.5mL LSMM either on

its own as a mock condition, 100ng/mL lipopolysaccharide (LPS) (Novus Biological), or highly

pathogenic avian influenza A/Vietnam/1203/2004 (H5N1) virus at MOI 10. The media was further

treated with vehicle control, inflammasome control, caspase inhibitors, or GSDMD inhibitors. PCLS were left to infect rocking at 37°C and 5% CO_2 until various timepoints were reached. At the end of timepoints (24, 48, or 72 hpi depending on experiment), the slice was washed with 1x PBS and moved to fixing in 2% paraformaldehyde for 4 hours if used for IHC or pooled in a tube and treated with radioimmunoprecipitation assay buffer (RIPA) buffer to generate protein lysates. Supernatant was collected at time points (24, 48, or 72 hpi depending on experiment) and treated with non-denaturing lysis buffer (NDLB) before freezing at -80°C.

4.4 Drug Treatments

LPS (Thermo Fisher) was used as a positive inflammasome control initially at a concentration of 10ng/mL before changing to a concentration of 100ng/mL due to low inflammasome activation observed at the lower dose. Dimethylsulfoxide (DMSO) 1% (Sigma) was used as a vehicle control in all conditions, as this is the solvent that the caspase and GSDMD inhibitors used in this study are reconstituted in. Caspase-1/4 inhibitor VX-765 (Sigma) was used at a concentration of 10 μM, caspase-3 inhibitor Z-DEVD-FMK (Fisher Scientific) was used at a concentration of 100 μM, pan-caspase inhibitor Z-VAD-FMK (Fisher Scientific) was used at a concentration of 100 μM, and GSDMD inhibitor disulfiram (Fisher Scientific) was originally used at a concentration of 100 μM before changing to 5 μM over toxicity concerns. Once reconstituted in DMSO, inhibitors were further diluted in LSMM before being added to PCLS.

4.5 Fluorescence Microscopy

4.5.1 Precision-Cut Lung Slices

PCLS were fixed in 2% paraformaldehyde (PFA) for 4 hours then permeabilized in 0.25% Triton-X 100 for 10 minutes before blocking in a solution containing 5% goat serum for 1 hour at room temperature. Slices were then incubated in primary antibody in a solution containing 0.5% goat serum for overnight at 4°C, followed by incubation with Alexa-Fluor conjugated secondary antibodies for 45 minutes at room temperature. DAPI was used to identify cellular nuclei. Slices were flattened on microscope slides and mounted under coverslips with ProLong Diamond Antifade Mountant (Thermo Fisher). 7-AAD staining was completed before fixing with 2% PFA by diluting 1:200 in 1xPBS and incubating for 30 minutes on ice, then moved to fixing.

The following primary antibodies were used and diluted at 1:100 (except 7-AAD at 1:200): mouse anti-human anti pan-cytokeratin (AE1/AE3; Abcam), mouse anti-human anti-influenza A nucleoprotein (DPJY03; BEI resources), mouse anti-human anti-caspase-1 (D-3; Santa Cruz), 7-AAD (Immunohistochemistry Technologies), mouse anti-human anti-ASC (B-3; Santa Cruz), mouse anti-human anti-MxA/Mx1 (4812; Novus Biological), mouse anti-human anti-IFN alpha (MMHA-2; PBL Assay Science), and mouse anti-human anti-IL-1ß/IL-1F2 (11E5; Novus Biologicals).

Secondary antibodies were all from Thermo Fisher and included goat anti-mouse IgG1 Alexa Fluor 546, goat anti-mouse IgG2a Alexa Fluor 647, goat anti-mouse IgG2a Alexa Fluor 488, donkey anti-rabbit IgG Alexa Fluor 488, and goat anti-mouse IgG2b Alexa Flour 647, all diluted at 1:250. Isotype controls were all from Invitrogen and included: rabbit anti-IgG, mouse anti-IgG2a clone 20102, mouse anti-IgG1 clone 11711, and mouse anti-IgG2b. Staining controls

included an isotype control with matching secondary antibody or just secondary antibody alone. PCLS were imaged using either an Olympus FluoView FV1000 confocal microscope or an Olympus Multiphoton microscope and analyzed using NIS elements software (Nikon).

4.5.2 Macaque Study Samples

Tissues from macaques were part of the study in 2016 that developed a lethal model of HPAI H5N1 ARDS, and serves as the prerequisite for this study, and were animals M139-15 (naïve control animal) and 103799 M138-15 (infected with 6.57 $\log_{10}$ PFU H5N1 A/Vietnam/1203/2004 and was humanely sacrificed on day 4) (43). These macaques were cynomologus females exposed to aerosolized H5N1 A/Vietnam/1203/2004 at varying concentrations via head-only Aeroneb Solo Nebulizer (Aerogen) exposure unit and monitored for disease status until the animal needed to be humanely sacrificed due to disease progression. At necropsy, tissue chunks were fixed in 2% paraformaldehyde for four hours followed by immersion in 30% sucrose overnight before being flash frozen and stores at -80°C until sliced. From here, tissue sections were cut using a cryostat microtome at 7 microns thick and were attached to warmed microscope slides and stored at -20°C until stained. From here, tissue sections were permeabilized, stained, and imaged with the same equipment and in the same manner as PCLS.

The primary antibodies used for macaque lungs were diluted 1:100 and were: mouse anti-human anti-MxA/Mx1 (4812; Novus Biological) and mouse anti-human anti-IFN alpha (MMHA-2; PBL Assay Science). The secondary antibodies used, all from Thermo Fisher, were diluted 1:250 and were goat anti-mouse IgG1 Alexa Fluor 546 and goat anti-mouse IgG2a Alexa Fluor 488. Isotype controls were carried out in the same manner as PCLS.

4.6 Plaque Assays

MDCK cells were grown until 90% confluent in cell media consisting of DMEM (Gibco) with 20% FBS (Gemini), 200mM L-glutamine (Gibco), 1M HEPES buffer (Gibco), and Penicillin/Streptomycin 10,000 U/mL/10,000 μg/mL (Gibco). All cell cultures used were below passage 20. This suspension is split into 6-well TC-treated plates and left to incubate overnight (or until 90% confluency was reached) at 37°C at 5% CO_2. Media was then removed from the cells immediately prior to infection, and 0.2mL of diluted virus in virus growth media (DMEM with 1M HEPES buffer, Penicillin/Streptomycin 10,000 U/mL/10,000 μg/mL, 1:40 bovine serum albumin fraction V 7.5%, and 1:1000 2mg/mL TPCK-trypsin; all reagents from Gibco). Plates were rocked, then placed at 4°C for 15 minutes followed by 37°C at 5% CO_2 for 45 minutes. A 1:1 mixture of 2% agarose (Invitrogen) and MEM media (2x MEM with 1M HEPES (Gibco), Penicillin/Streptomycin 10,000 U/mL/10,000 μg/mL (Gibco), 1:20 bovine serum albumin fraction V 7.5% (Gibco), with 1:800 2mg/mL TPCK-trypsin (Thermo Fisher)) was applied per well. The plates were incubated at 37°C at 5% CO_2 for 3-5 days, then agarose plugs are removed, and plates are fixed with 37% formaldehyde (Fisher Scientific). Plates were stained with 25%EtOH/0.1% crystal violet (Fisher Scientific) and plaques were counted.

4.7 Cytokine Analysis

IL-1β enzyme-linked immunosorbent assays (ELISAs) (R&D systems) were performed according to manufacturer's protocol on supernatant collected from PCLS. Supernatants were treated with non-denaturing lysis buffer (2mM EDTA, 50mM Tris-HCL, 1% Triton X-100,

150mM NaCL, and water) to inactivate H5N1 infected samples to perform the assay under biosafety level 2 (BSL2) conditions. Mock and LPS treated samples were also treated with non-denaturing lysis buffer. Capture antibody coated a high-binding 96-well plate overnight, followed by blocking with 1% bovine serum albumin (BSA) before sample addition. Following incubation of samples, detection antibody was added to the plates followed by Streptavidin-HRP. Finally, a mixture of H_2O_2 and tetramethylbenzidine was added to trigger a colorimetric reaction that was stopped with sulfuric acid before being read using a BioTek ELx800 microplate reader at 450nm with 540nm correction.

4.8 Lactate Dehydrogenase Assay

Lactate dehydrogenase (LDH) assays (Thermo Fisher Scientific) were performed under BSL3 conditions with supernatants that were collected from PCLS. Supernatants and a 1X LDH positive control were treated with a mix of substrate mix and assay buffer (included in kit) and left to incubate at room temperature for 30 minutes in a flat bottom 96-well plate before the reaction was stopped by the addition of stop solution (included in kit). Total absorbance of released red formazan product was measured at 490-680nm using a Synergy LX Multi-Mode microplate reader.

4.9 Generation of Protein Lysates

900-micron thick lung slices were collected and pooled at various timepoints (either n=2 or n=3, depending on experiment) and weighed. RIPA buffer (10mM Tris-Cl pH 8.0, 1mM EDTA,

1% Triton X-100, 0.1% sodium deoxycholate, 0.1% SDS, 140mM NaCl) was added to the slices in a volume (in microliters) that was 3 times the weight of the slices (in milligrams) and small scissors were used to shear the sample. Keeping sample on ice, the sample was vortexed then placed at -80°C to fully freeze. After thawing, samples were centrifuged, and supernatant was collected and stored at -80°C until Bicinchoninic acid (BCA) protein assays and Western blots could be performed.

4.10 Image Analysis and Quantification

TIFF images taken from microscopy sessions were analyzed using NIS Elements version 4.50.00. Regions of interest (ROIs) were drawn to encapsulate lung tissue and exclude edges of tissue/airways in the tissue where no tissue is present. Microscope slides were imaged non-repetitively, and the total number of images per slide varies by experiment but for quantification a minimum of 5 images was used and a maximum of 10 images were used. For confocal images presented, the focal plane varied by sample but was consistently taken near the top of the tissue section. Multiphoton images are Z-stacks of a defined depth that varies per image anywhere from 40 to 70 microns, depending on the upper and lower limit of tissue determined by viewing through the objective. Stains of interest were then quantified by recording the binary area (recorded as pixels) and averaging the values to generate individual data points per donor, and summary quantification of stains of interest per panel. General image edits such as scale bars were done in ImageJ version 2.0.0-rc-69/1.52p.

4.11 Statistical Analysis

Statistical analyses were completed using GraphPad Prism software version 8.3.1 (332). The alpha value in all tests was set to 0.05. All tests were determined to be best run as non-parametric and therefore median values were displayed on graphs instead of mean values, as determined through Shapiro-Wilk tests. Comparisons within groups of three treatments or more were subject to Kruskal-Wallis test followed by multiple comparisons. Comparisons between groups of two treatments were subject to two-tailed Mann-Whitney U tests. The averages of $\log_{10}$ were calculated as geometric means, and values that originally were zero were given an arbitrary value of 1 before log transforming.

5.0 Results

5.1 Aim 1: Develop an *Ex Vivo* Model of Porcine and Human PCLS

The purpose of this aim was to develop an *ex vivo* PCLS model first in porcine lungs then in human lungs. This will be carried out by acquiring lungs from a butcher for pig lung and from the transplant network IIAM, then perfusing with low melting agarose to provide stability and allow for soft tissue to be cut into slices. Various viability methods were employed to assess quality of tissue effectiveness of processing protocols.

5.1.1 Establishment of Lung Processing Protocol

The lung processing protocol that I have developed in this study was derived from a study that generated a PCLS model in sheep lung to study various gene therapy vectors (115). Through practice with various porcine lungs and early human lungs (Table 1), I have had great success in being able to perfuse lungs with low melting point agarose until stiff to the touch, generate small lung cores to be sectioned on a vibratome (Leica VT1200s), generating 400-micron thick slices for microscopy, and 900-micron thick slices for downstream western blotting, and supernatant collection to measure downstream cytokines and replicating virus through plaque assays (Figure 5).
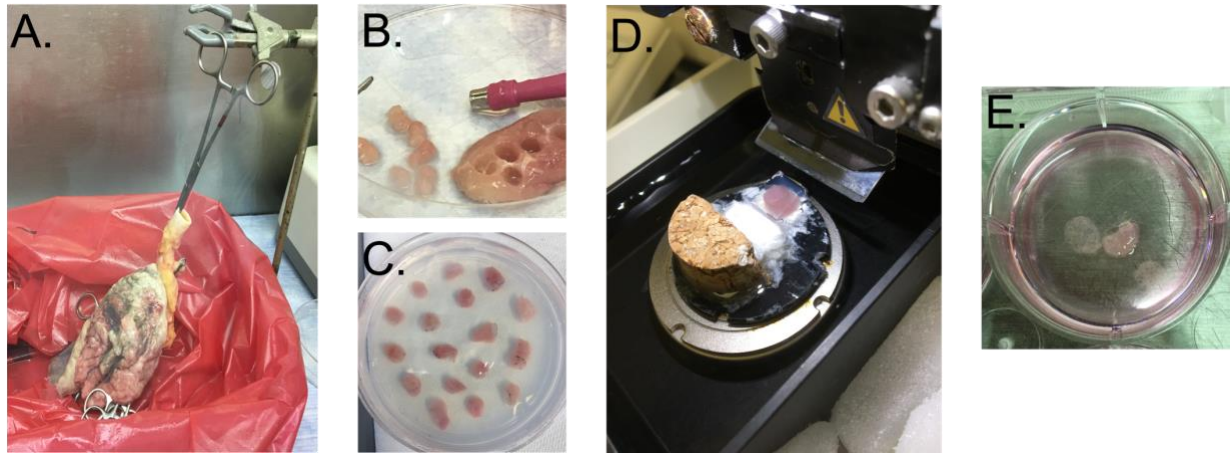
Figure 5: Workflow of Processing Lungs

Sequence of processing events to generate PCLS. (A) Setup of lung in BSC and elevation to allow for lung to be perfused with low melting point agarose. (B) A 1 inch thick section of lung cut from organ, and small 8mm biopunch cores generated from this section. (C) Lung cores embedded in low melting point agarose for stability. (D) Setup of lung core on vibratome ready to be sliced. (E) 400 micron thick lung slice (left) and 900 micron thick lung slice (right) in culture.

To image the structural integrity of the PCLS, I acquired differential interference contrast (DIC) images through confocal microscopy throughout the study to observe any changes in tissue upon processing and between donors. DIC imaging allowed for fine details in transparent tissue to be observed that would not be seen with normal fluorescent microscopy. Figure 6 represents structural makeup of a pig lung and human lung AHCG011. The most noticeable difference in gross lung pathology has to do with the way the lungs are procured. While the human lungs are taken from relatively healthy donors and processed as if they were going toward a transplant, the porcine lung is obtained from a local butcher. This concludes that the lung processing protocol does not interfere with the structural integrity of the lung slices.
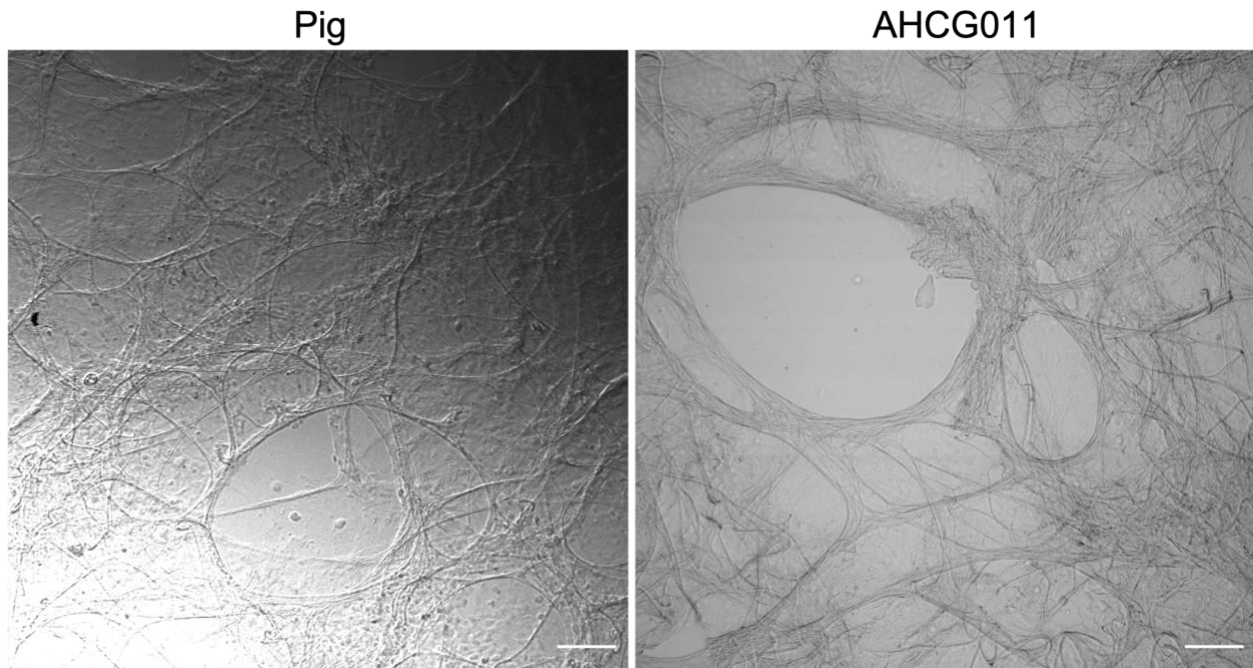
Figure 6: Imaging of PCLS

Differential interference contrast microscopy shows structural makeup of porcine PCLS (left) and human PCLS (right) from donor AHCG011. Scale bar is 100μm.

5.1.2 Establishment of Lung Culturing Protocols

In order to determine viability of PCLS in culture following processing, I employed viability staining with SYTO10, a nucleic acid stain that is cell membrane permeable and will label all cells, and DEADRed, a stain that only labels cells with compromised membranes (Thermo Fisher). This method was used in the study with sheep lung that was a foundational basis for the development of our model system (115). In the following experiments, the day 0 timepoint refers to PCLS that were cultured for one hour in LSMM on day of acquisition and processing. After processing, media was changed daily. These results indicate that for a porcine lung, the values are not significantly different from each other, suggesting that rather than being more viable on a

certain day porcine PCLS can successfully be maintained in culture for at least 3 days without viability loss. I had investigated whether leaving the lung cores in their embedded agarose petri dishes then slicing on the vibratome at a later date would become an alternate in case infection could not be completed on the same day as processing, but the viability tests revealed that these slices were not ideal (Figure 7).

Figure 7: Viability of Porcine Lung Slices

(A) Porcine PCLS stained for SYTO10 (green) and DEADRed (red) at day 0, 3, and 7 timepoints. One slice was cultured normally and one slice was treated with 10% Triton X-100 as a death control for each timepoint. Scale bar is 100μm. (B) Quantification of cell markers for SYTO10 and DEADRed within PCLS. Horizontal lines on graphs represent medians and results were statistically analyzed through Kruskal-Wallis tests followed by Dunn's multiple comparisons. *$p < 0.05$.

Viability testing was also completed with human lung with the same viability testing kit, but modifications were made to test whether PCLS were more viable when incubated with or

without gentle rocking during incubation. A day 1 timepoint was added to assess whether infection was best done the day PCLS were generated or after an acclimation period, with the media changed daily. Again, the day 0 timepoint refers to PCLS that were cultured for one hour in LSMM on day of acquisition and processing. These data indicate that the viability of human PCLS remain relatively level over 3 days in culture, as seen in the porcine lung viability experiment (Figure 8). In the study with sheep lung that serves as a basis for this study, the researchers found that culturing slices for 3 days before infection yielded greater infection and transduction efficacy (103). This certainly reduces the risk of bacterial or fungal contaminants, and this may make the slices more vulnerable to infection when the normal lung flora is not competing with the pathogen of interest. However, this study's purpose was to generate a maintained infection in PCLS, whereas I am looking at short term, within 72 hours, infection effects in PCLS. So, day of infection is most likely best done the day of or day after processing for H5N1 infection. In the human lung, there is some staining of SYTO-10 of elastin and collagen, which is also observed in later multiphoton imaging. The implementation of the shaking platform was included after porcine lung experiments were complete but will be included in any future experiments with them. Going forward with this, a shaking platform will also be used to keep the slices in motion after infection with H5N1 or treatment with LPS. LPS is known to be an inducer of the non-canonical inflammasome pathway, specifically by activating the NLRP3 inflammasome (116, 117). This will be used as a positive control for inflammasome activation at a concentration of 100ng/mL, which in literature is considered a high dose without being toxic to the cells (118-120). A lower concentration of 10ng/mL was initially used but was changed after inflammasome activation was not happening (data not shown).

A.

AHAU189

Mock Triton X-100 treated

d. 0

Stationary Shake

Mock Triton X-100 treated Mock Triton X-100 treated

d. 1

d. 3

d. 6

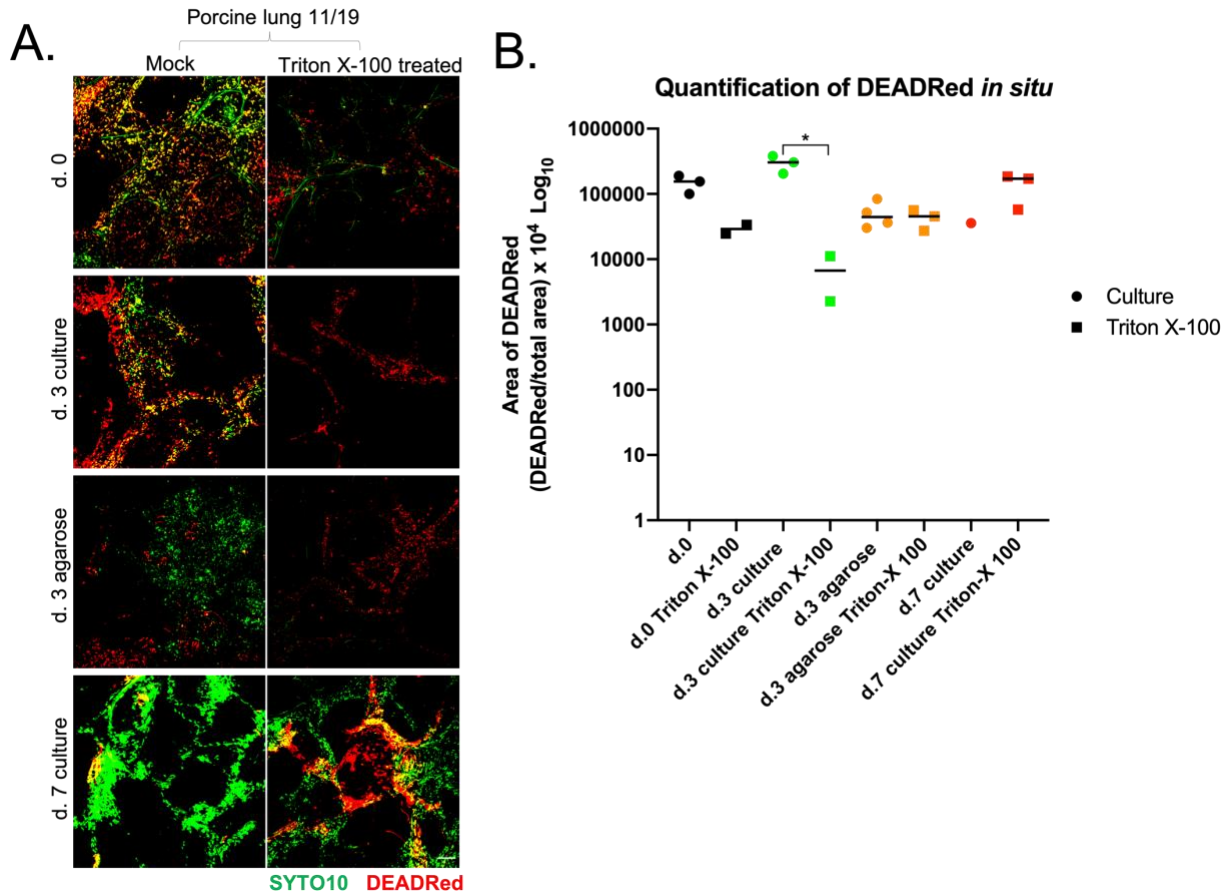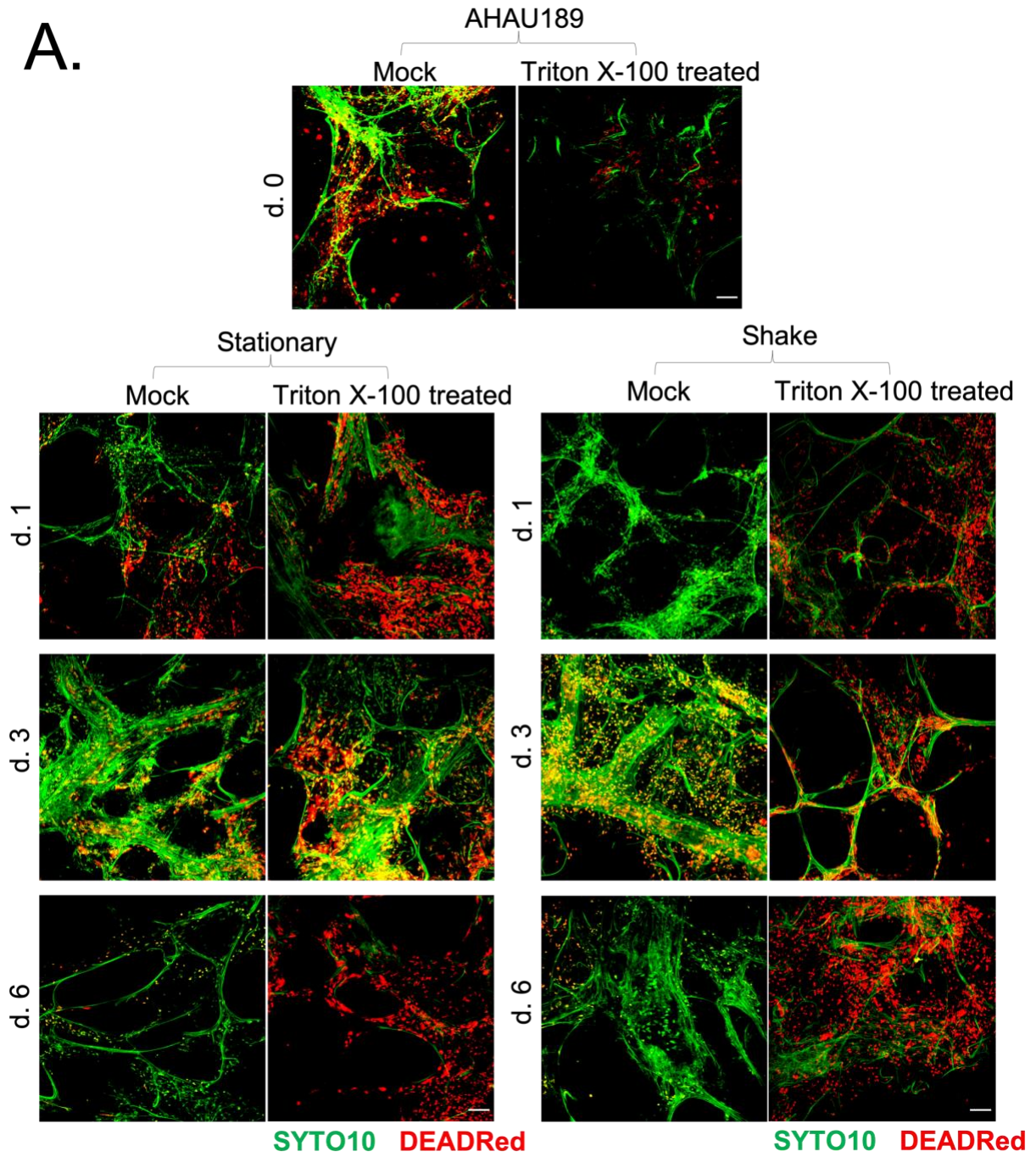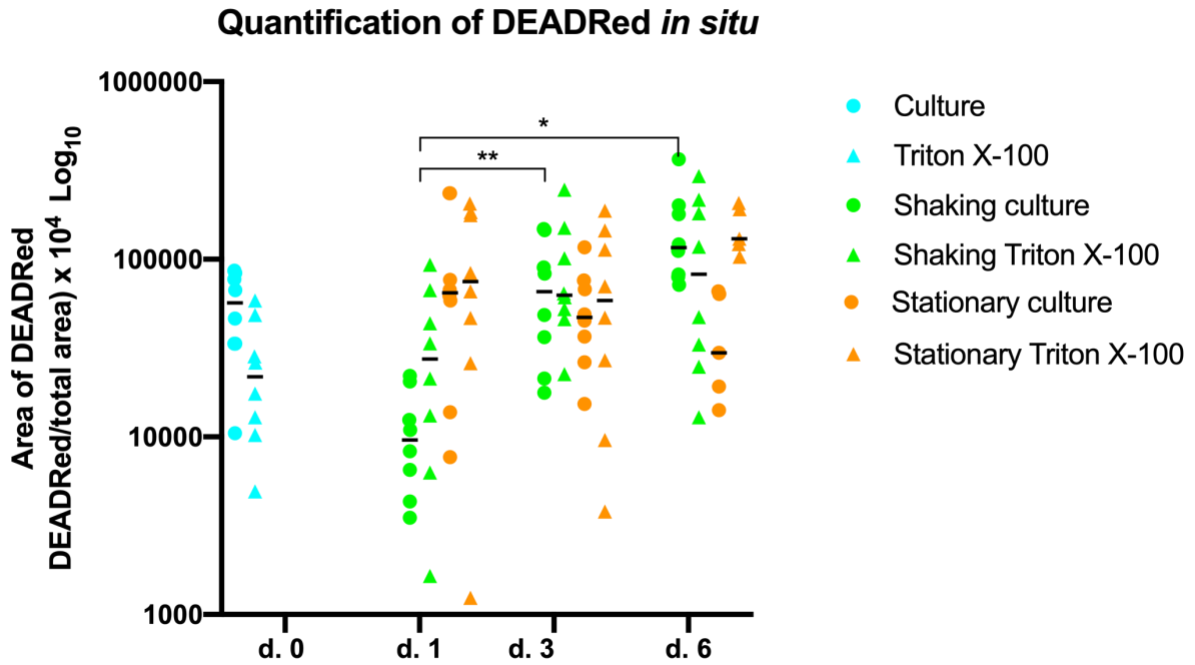SYTO10 DEADRed SYTO10 DEADRed

B.

Figure 8: Viability of Human Lung AHAU189

(A) Porcine PCLS stained for SYTO10 (green) and DEADRed (red) at day 0, 1, 3 and 7 timepoints. One slice was cultured normally and one slice was treated with 10% Triton X-100 as a death control for each timepoint. Per timepoint and per culture/death control, one slice was cultured stationary and one was cultured on a rocker. Scale bar is 100μm. (B) Quantification of cell marker for SYTO10 and DeadRed within PCLS. Horizontal lines on graphs represent medians and results were statistically analyzed through Kruskal-Wallis tests followed by Dunn's multiple comparisons. *$p<0.05$, **$p<0.01$.

5.1.3 Aim 1 Conclusions

In conclusion, in aim 1 I successfully modified a PCLS model that can go on to be tested with different treatment and exposure conditions that can be used for porcine and human lungs. Both porcine and human lung slices remain viable in culture after processing, allowing for flexibility in planning experiments and generally healthy slices that are suitable to be infected with HPAI H5N1.

5.2 Aim 2: Determine if PCLS Can Be Productively Infected with HPAI H5N1 and Determine Cellular Targets of Infection

Aim 2 seeks to take the PCLS model to the next level and determine its ability to ultimately be infected with H5N1 and determine if H5N1's target cells for replication, alveolar epithelial cells (AEC's) are susceptible within PCLS. Evidence of infection will be observed by using IHC and will be supported with plaque assay results taken from supernatant of infected PCLS. The stock of H5N1 A/Vietnam/1203/2004 that I have generated in chicken eggs was used for all infections throughout this study. The parent stock of this virus was also used to infect macaques in the 2016 study (43) (Table 1).

5.2.1 HPAI H5N1 Can Infect and Replicate in Porcine PCLS

Throughout this study, multiple compounds were used to manipulate cell death conditions to observe the role of H5N1 in cell death pathways (specifically pyroptosis). DMSO 1% will be used as a vehicle control in all conditions, as this is the solvent that the caspase and GSDMD inhibitors used in this study are reconstituted in. Caspase 1/4 inhibitor VX-765 (Millipore Sigma) will be used at a concentration of $10\mu M$ throughout the study, as it has been shown to be effective at this concentration in cell culture (121), and in animal models, other cell culture models, and is approved for clinical use (122-124). Z-DEVD-FMK (R&D Systems) is a caspase-3 inhibitor and Z-VAD-FMK (R&D Systems) is a pan-caspase inhibitor, both used at a concentration of $100\mu M$. There is some evidence that Z-VAD-FMK completely inhibits caspase-1 activity and prevents over 50% of cell death at a lower concentration of $30-40\mu M$ (125). In comparison, Z-VAD-FMK did not prove to be any more effective than Z-DEVD-FMK against influenza A infection at a

concentration of around 40μM (126) and a concentration of 20μM (127). One study found Z-VAD-FMK effective at reducing cytopathogenicity of H5N1 at 200μM (128). Finally, GSDMD inhibitor disulfiram was initially used at 100μM, but was dropped to 5μM after concerns of cell toxicity, and to be more comparable to what has been seen in other studies (125).

Plaque assay results were performed on supernatant collected from 400-micron PCLS used in IHC and from 900-micron PCLS used for further western blot analysis. In 400-micron PCLS, titers were highest after 48 hours in comparison to the input virus but dropped after 72 hours (Figure 9). This is most likely due to the fact that the porcine lung is not in great condition to begin with the lung slices may have begun to die and not be able to support replication. In comparison, 900-micron lung slices supported better replication, with all conditions yielding a higher titer than the input virus titer (Figure 9). At 24 hours, all drug treatments yielded similar titers, but after 48 hours VX-765 and Z-DEVD-FMK increased by almost 2 logs in comparison with their 24-hour counterparts (Figure 9). After 72 hours, titers were overall higher than 24 hours but still lower than 48 (Figure 9), which once again suggests that these porcine PCLS are just not as healthy, especially after being exposed to a virus.
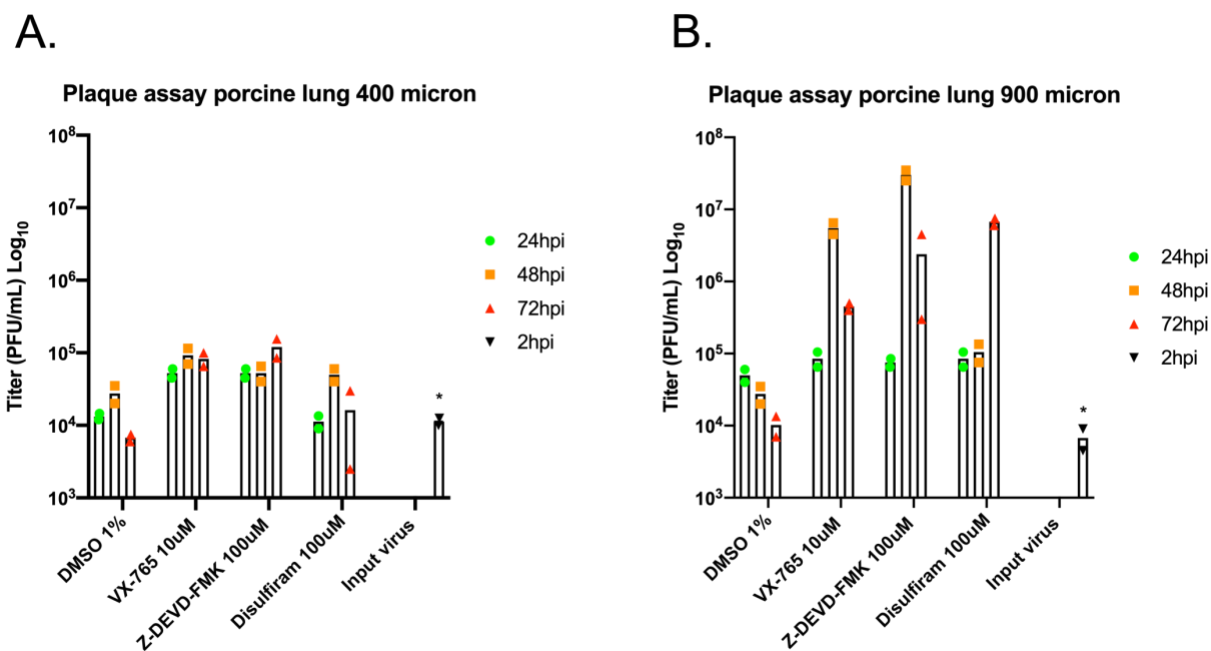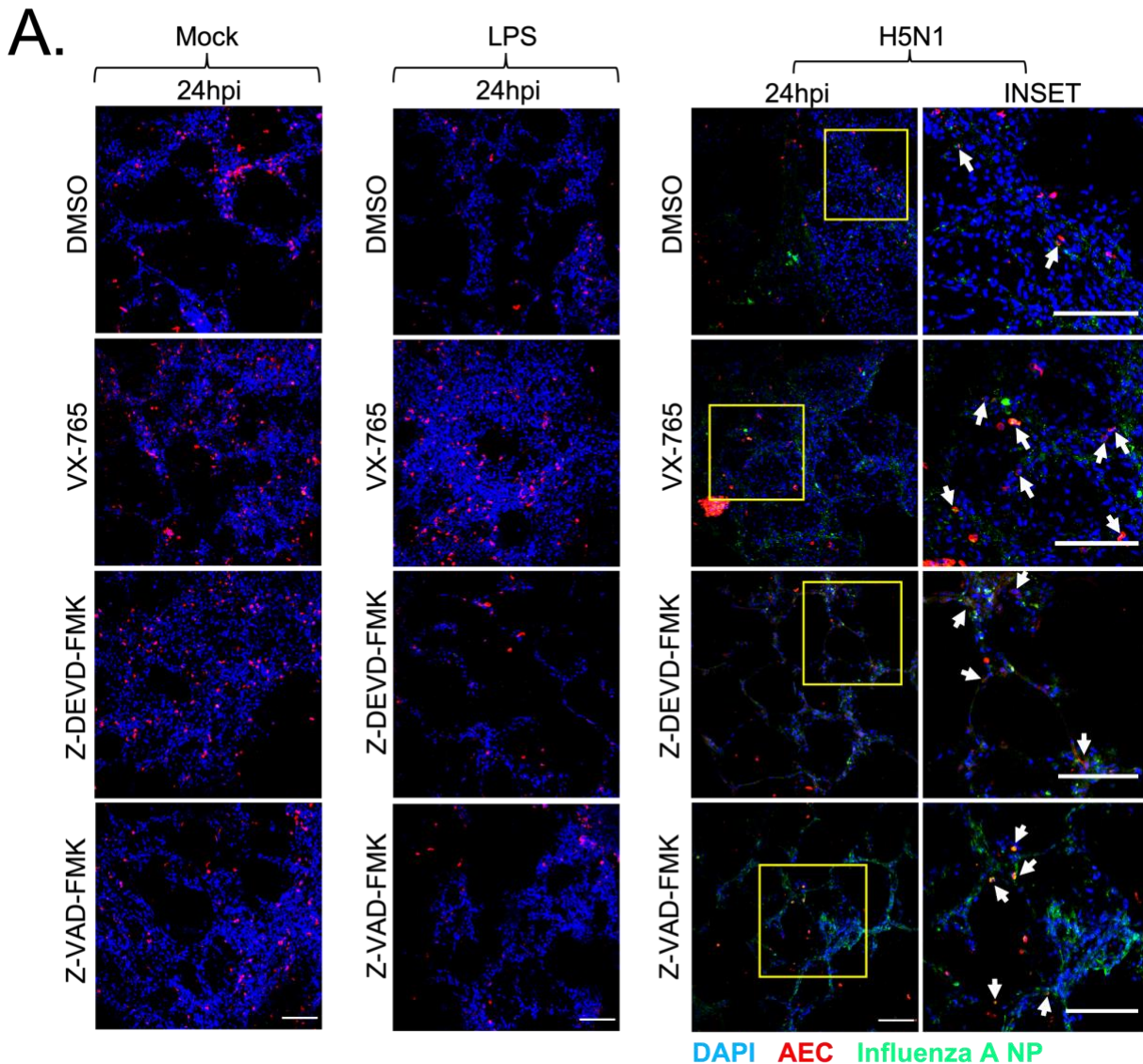
Figure 9: H5N1 Titers of Porcine Lung

Supernatant was collected from (A) 400 micron PCLS and (B) 900 micron porcine lung PCLS from one donor and titer was determined through plaque assays on MDCK cells. Bars on graphs represent medians and results were statistically analyzed through Kruskal-Wallis tests followed by Dunn's multiple comparisons. All tested treatments were significantly higher than the input virus. *$p<0.05$.

There is evidence that H5N1 can infect pigs, but their susceptibility to infection is low and titers from infected lungs are lower than other animals that are infected such as ferrets and NHPs, which may have to do with the PB1-F2 protein promoting recruitment of macrophages, monocytes, and NK cells, with early apoptotic events then taking place in alveolar macrophages (33, 86, 129). I see that in our PCLS model, H5N1 does infect porcine lung slices in what appears to be mild (Figure 10), supporting other evidence showing pigs as a potential mixing vessel and allowing us to study a comparable model to human lung. There is some colocalization that supports the idea that H5N1 infects AEC (Figure 10), and there is more virus detected after treatment with VX-765 (Figure 10B). Caspase-1 knockout mice were shown to be more susceptible to influenza infection, implicating that I might be seeing higher levels of HPAI H5N1 because dampening the

42

cell death response to infection may allow for the cells to survive and allow for further replication (130). AEC presence in lung tissue remained comparable across drug treatments in mock and LPS treated conditions, but dropped after infection with H5N1, suggesting that H5N1 infection may be destroying these target cells (Figure 10). This could be further analyzed by using panels for markers 7-AAD to measure cell death, AEC, and influenza A NP to observe through IHC.
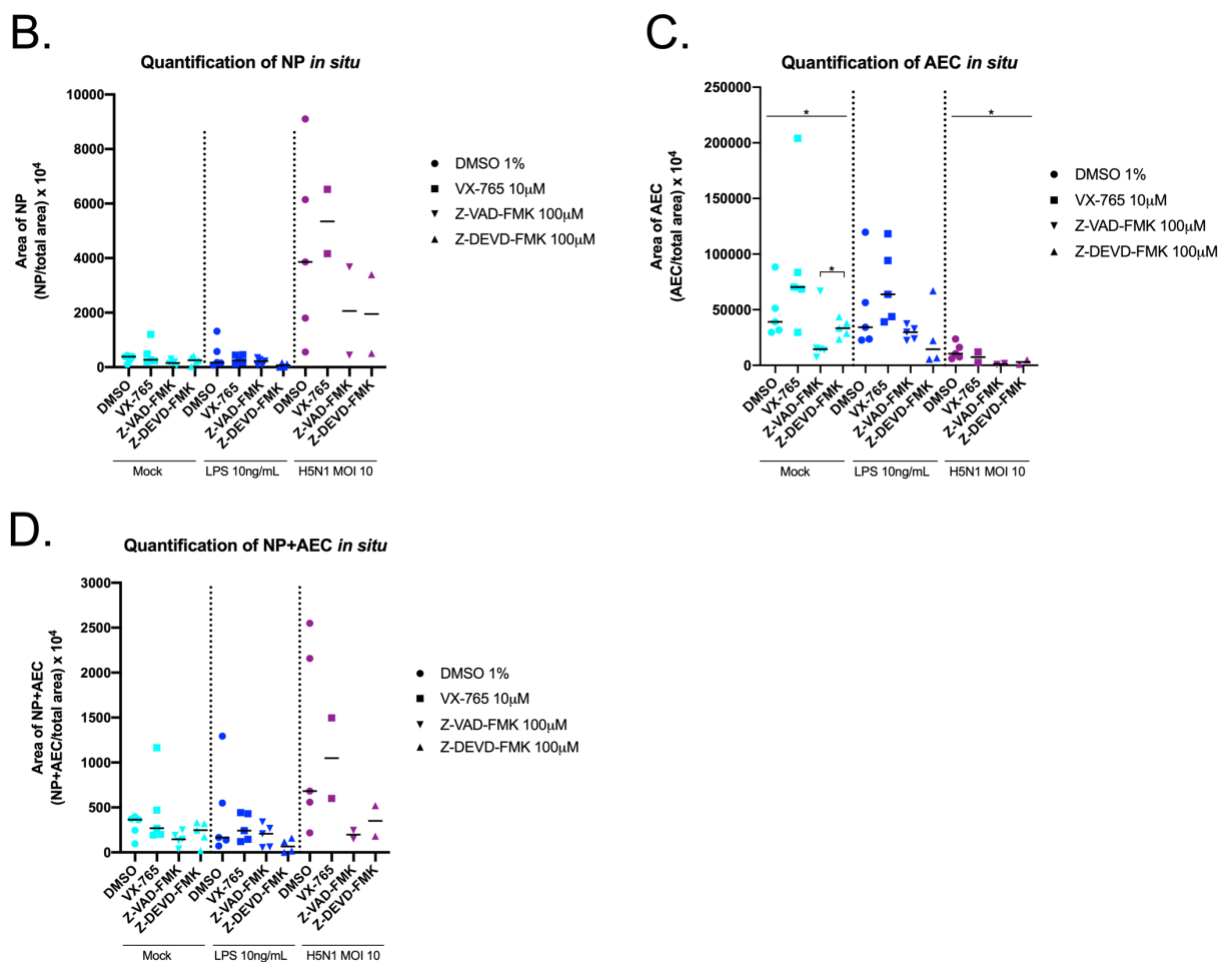
B.

Quantification of NP *in situ*

C.

Quantification of AEC *in situ*

D.

Quantification of NP+AEC *in situ*

Figure 10: Infection of Porcine Lung with H5N1

(A) Porcine lung PCLS stained with antibodies to AEC (red) and influenza A NP (green). DAPI was used to identify nuclei in cells. Scale bar is 100µm. Arrowheads point to representative co-localization. (B) Quantification of cell marker for NP within PCLS. (C) Quantification of cell marker for AEC within PCLS. (D) Quantification of colocalization of cell markers for AEC and NP within PCLS. Horizontal lines on graphs represent medians and results were statistically analyzed through Kruskal-Wallis tests followed by Dunn's multiple comparisons. *$p<0.05$. Conditions: H5N1 MOI 10, LPS 100ng/mL. Treatments: DMSO 1%, VX-765 10µM, Z-DEVD-FMK 100µM, Z-VAD-FMK 100µM. Each dot is an individual image and this figure represents one donor.

5.2.2 HPAI H5N1 Can Infect and Replicate in Human PCLS

Plaque assay results were generated by taking supernatant from 400-micron PCLS used in

IHC analysis and from 900-micron PCLS used for further western blot analysis. Because cell death

became a presumed issue with PCLS health in the porcine lung, I decided to replace the media

with drugs daily, but not LPS of H5N1 in human lung AHAU189, making each timepoint after 24hpi a non-cumulative titer (Figure 11). Titers of all timepoints and drug treatments were higher than the input titer, showing successful virus replication in PCLS. As with porcine lung, more replication was observed in 900-micron, but human lung had overall higher titers than porcine lung, indicating the humans are better hosts for H5N1 replication than pigs, supporting evidence that has already been seen to implicate pigs as a mixing vessel (33, 43, 86, 129, 131) (Figures 9 and 11).
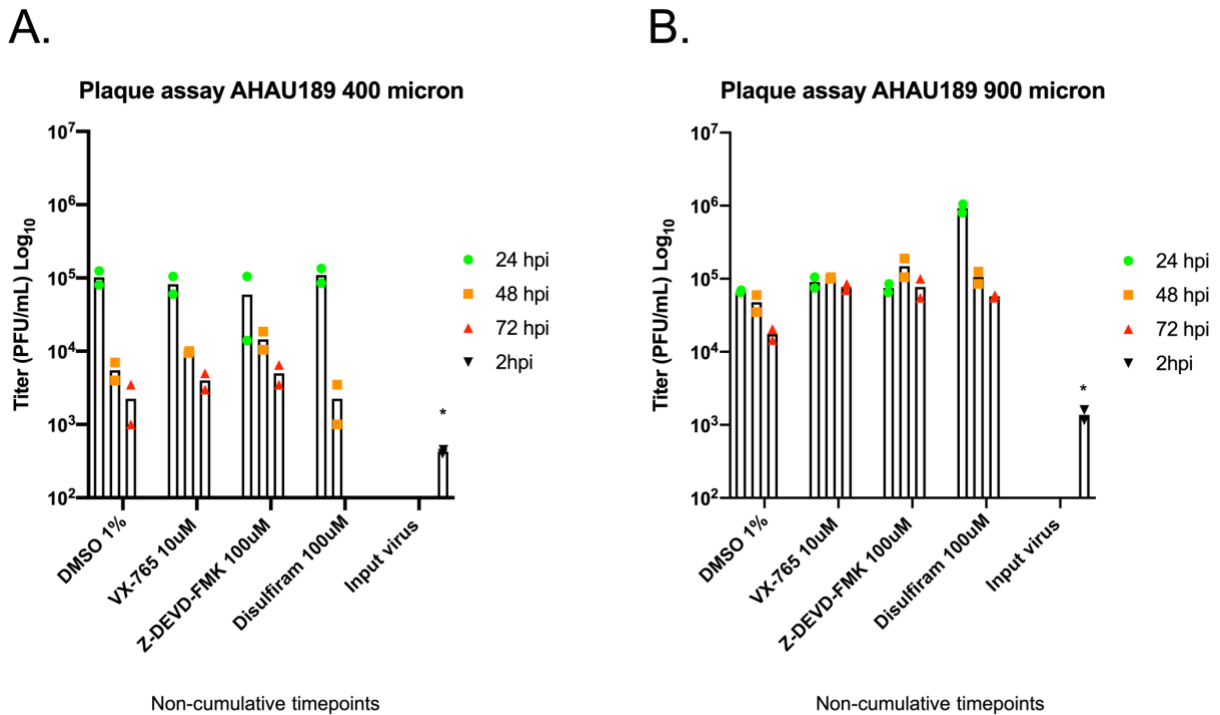
Figure 11: H5N1 Titers of Human Lung AHAU189

Supernatant was collected from (A) 400 micron PCLS and (B) 900 micron human lung AHAU189 PCLS and titer was determined through plaque assays on MDCK cells. Bars on graphs represent medians and results were statistically analyzed through Kruskal-Wallis tests followed by Dunn's multiple comparisons. All tested treatments were significantly higher than the input virus. *$p<0.05$.

Next, human PCLS were infected and evaluated for their competence as a model. Through IHC, I observed the presence of AEC's in human PCLS and showed that as in porcine lung (Figure

10), human PCLS could be infected with H5N1 as observed through representative colocalization (Figure 12). As with porcine lung, treatment with VX-765 appears to illicit more infection than its DMSO vehicle control, possibly implicating caspase-1 as an important player in infection (Figure 12). The amount of NP colocalized with AEC was also higher in VX-765 treated PCLS (Figure 12D). I believe that both type I pneumocytes, filamentous red stained region near the alveolar epithelial spaces, and type II pneumocytes, round and red stained cells, are representatively stained in this tissue. HPAI H5N1 is also preferentially infecting type II pneumocytes in PCLS, corroborating what is seen in literature (132).
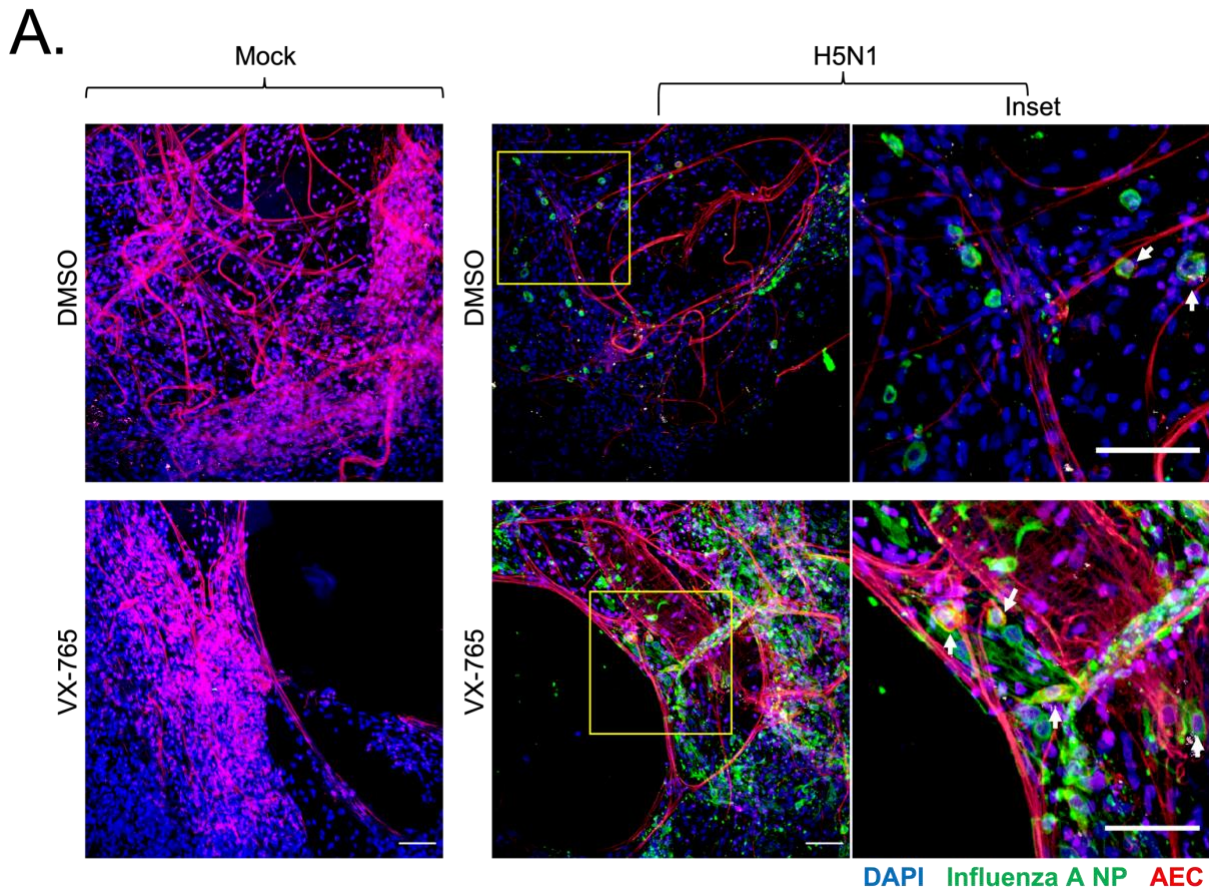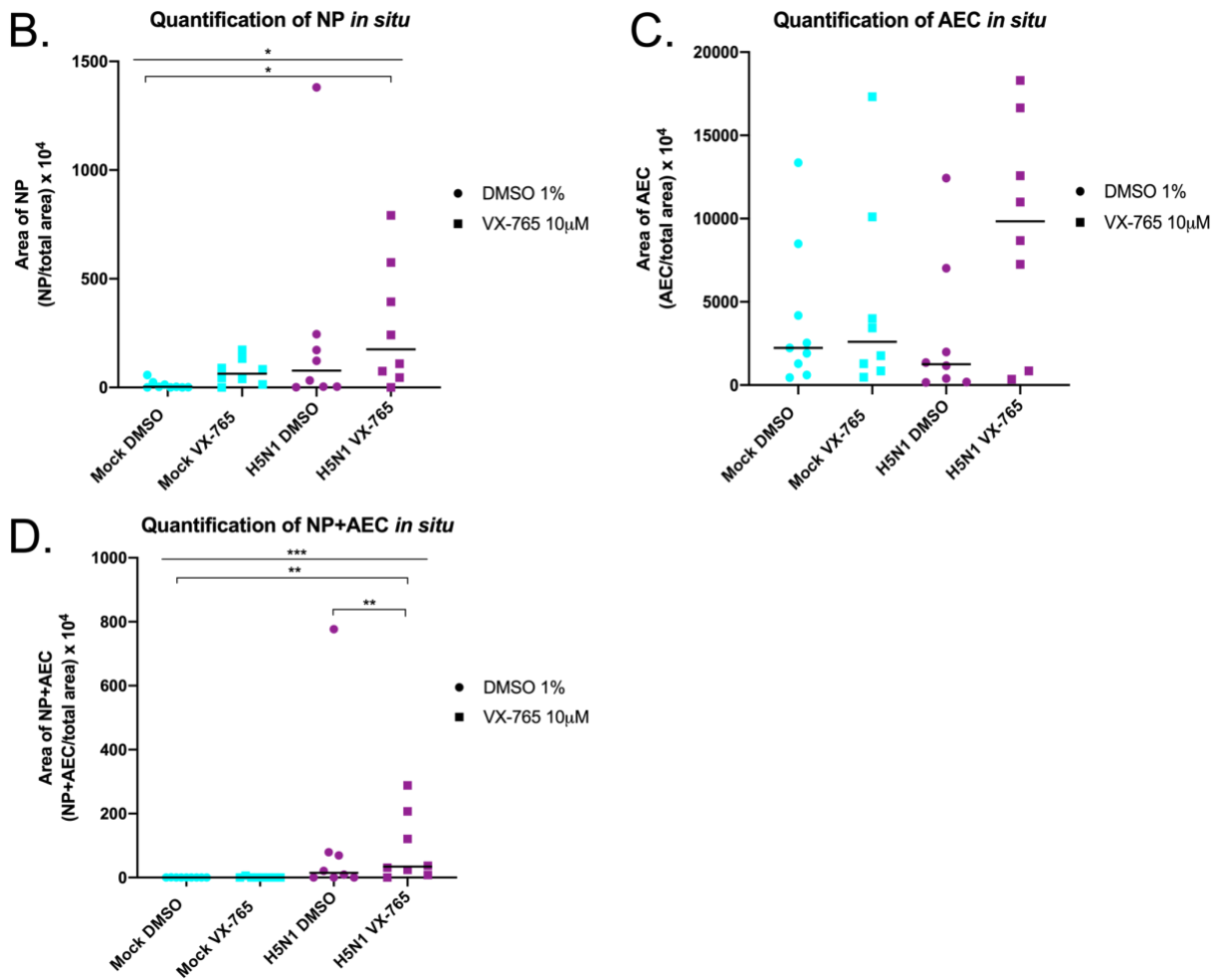
Figure 12: Infection of AHAU189 Human Lung with H5N1

(A) Human lung AHAU189 PCLS stained with antibodies to AEC (red) and influenza A NP (green). DAPI was used to identify nuclei in cells. Scale bar is 100µm. Arrowheads point to representative co-localization. Images are Z-stack projections taken on an Olympus Multiphoton microscope of 20 images encompassing a 2 micron thick section per image. (B) Quantification of NP in PCLS. (C) Quantification of AEC in PCLS. (D) Quantification of colocalization of NP and AEC in PCLS. Bars on graphs represent medians and results were statistically analyzed through Kruskal-Wallis tests followed by Dunn's multiple comparisons. *$p<0.05$, **$p<0.01$, ***$p<0.001$. Conditions: H5N1 MOI 10. Treatments: DMSO 1%, VX-765 10µM. Each dot is an individual image and this figure represents one donor.

While I have shown that AECs can be infected with H5N1, I have also seen in previous studies that H5N1 can destroy AM's in both human and porcine lungs (43, 86). To evaluate whether the same thing happens in human and porcine PCLS, PCLS were stained with antibodies to CD163 and influenza A NP. I found that in human lungs, there appeared to be fewer AMs after H5N1 infection, and some colocalization showed H5N1 infected AMs (Figure 13A). The same

47

observation was seen in porcine lungs (Figure 13B). Interestingly, the influenza A NP seemed to infect this porcine lung (Figure 13B) more than the previous porcine lung (Figure 10), despite the same dose of H5N1 being delivered and the lungs being treated in the same manner. This could be due to variation between animals and general health of the pig donor that was used, which I do not have information for. It is less likely due to the PCLS coming from different areas of the lung since all lung cores are taken from the lower lobe, and while the possibly of having sample variation of cell populations is present it cannot be controlled more closely.
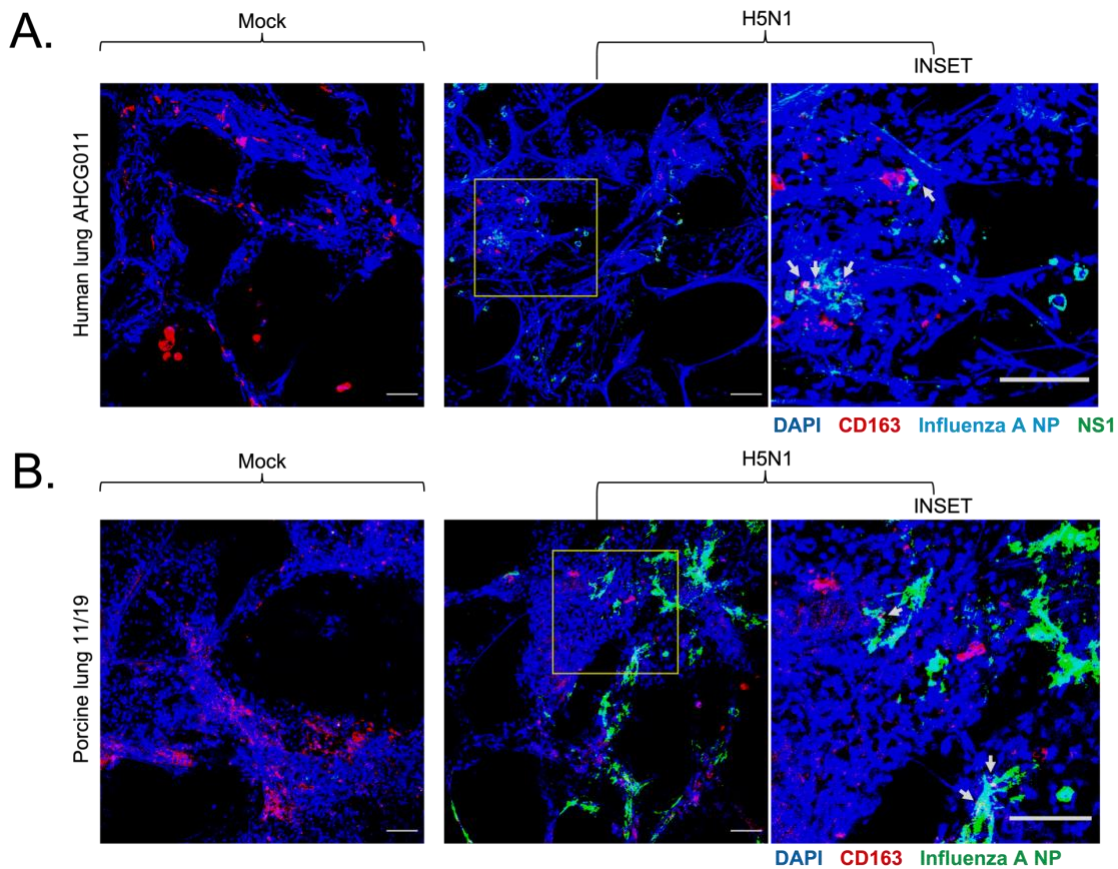

Figure 13: Alveolar Macrophages in H5N1 Infected Lungs

(A) Human lung AHCG011 PCLS stained with antibodies to CD163 (red), NS1 (green), and influenza A NP (cyan).

(B) Porcine lung PCLS stained with antibodies to CD163 (red) and Influenza A NP (green). Scale bar is 100μm.

Arrowheads point to representative co-localization. Conditions: H5N1 MOI 10.

5.2.3 Aim 2 Conclusions

In this aim I showed that the PCLS model system can successfully be infected with H5N1 and produce replicating virus. I also showed that H5N1 can infect AECs and AMs in both human and porcine lungs, showing that this model can recapitulate what is seen in other cell culture and animal models after H5N1 infection, suggesting that our model can be used to assess the role of cell death in response to infection. This important step also allows for our lab to investigate other cell death pathways in the future and assess more cell death inhibitors now that a model system has been established.

5.3 Aim 3: Determine the Contribution of Pyroptosis to Lung Damage in H5N1 Infection

In this extensive aim I plan to examine the role of cell death upon H5N1 infection, using LPS as a positive control for inflammasome activation and observing the impact of caspase and GSDMD inhibitors to try and reverse cell death. I will use 7-AAD as a marker of dead cells with compromised membranes in addition to FLICA to label active caspase-1 in living cells as a main indicator of drug effectiveness. I will also investigate the levels of secreted IL-1β to confirm that downstream cytokines are also impacted. Finally, ASC and IL-1β will be observed in IHC, along with IFNα and MxA/Mx1.

5.3.1 Cell Death is Observed in Porcine PCLS and Affected by Caspase Inhibitors

In porcine lung, mock conditions have lower levels of FLICA and 7-AAD than the LPS control and H5N1 conditions (Figure 14). The most dramatic visual change is in H5N1 infected PCLS, FLICA stained cells dropped in number after treatment with caspase-1/4 inhibitor VX-765 (Figure 14). On the contrary, the amount of 7-AAD stained cells remained largely unchanged after infection with H5N1 and across all drug treatments but was highest after exposure to disulfiram (Figure 14). Experiments with this porcine lung and human lung AHAU189 where the concentration of disulfiram was 100μM showed an increase of 7-AAD stained cells, and separate experiments in isolated and selected AMs from porcine lung showed toxicity from disulfiram at this concentration as determined by flow cytometry staining with 7-AAD. A lower concentration of 5μM was shown to be non-toxic to isolated AMs, so this concentration will be used in PCLS in the future.

A.
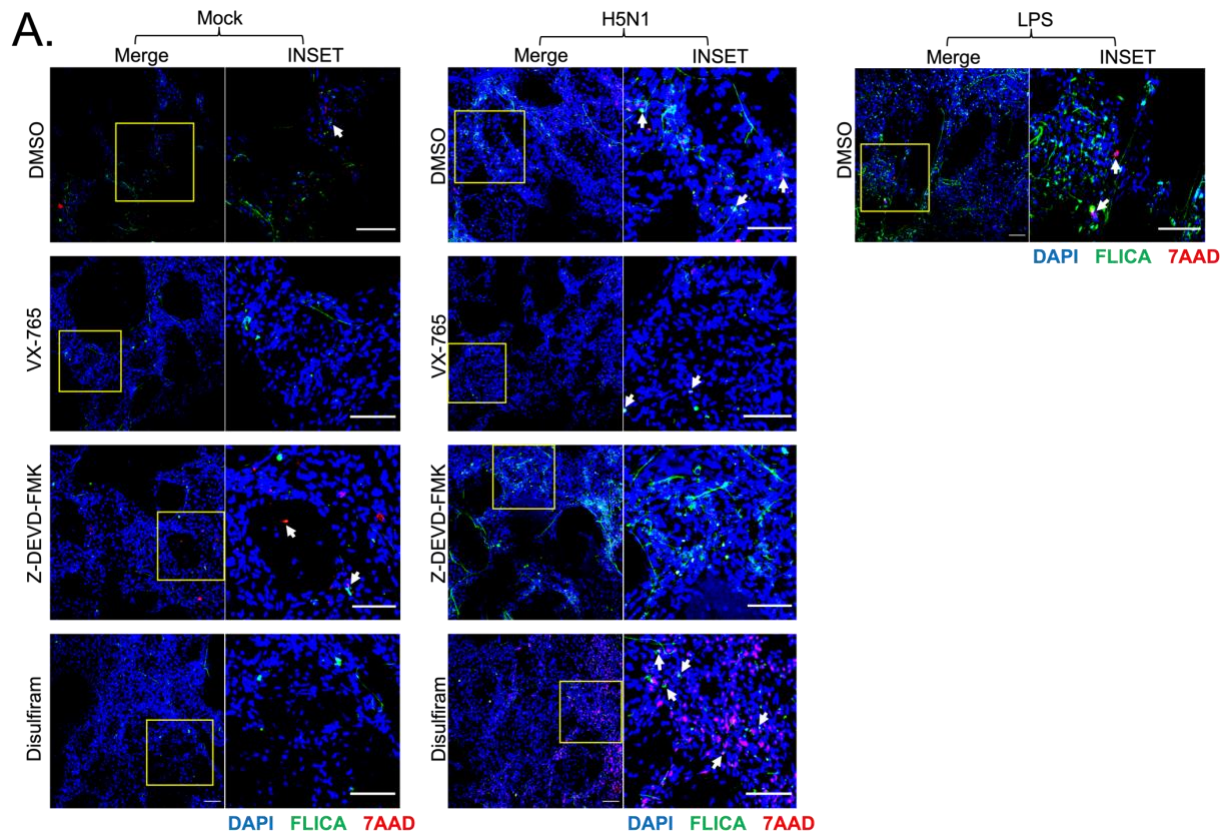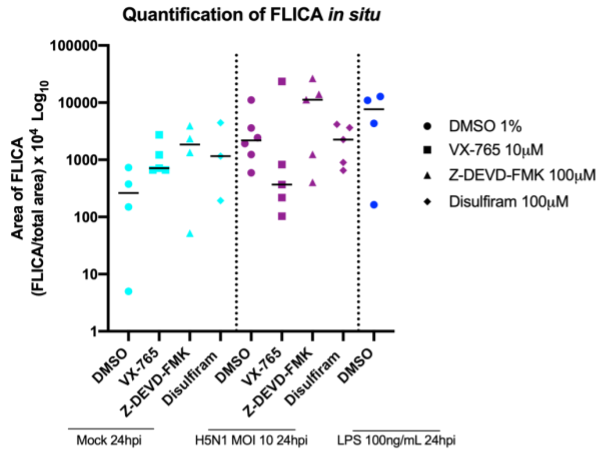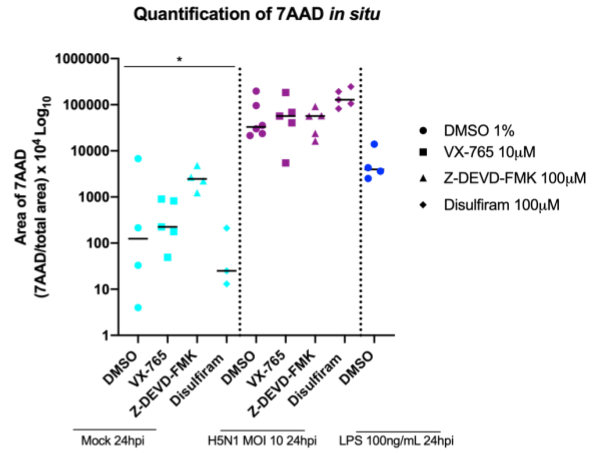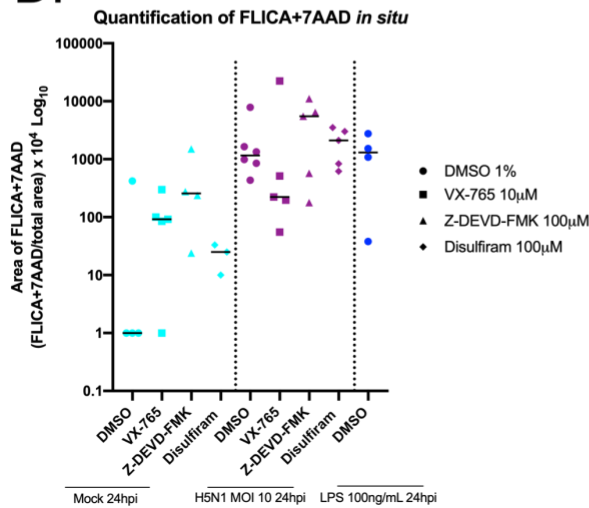
Figure 14: Cell Death in H5N1 Infected Porcine Lung

(A) Porcine lung PCLS stained with antibodies to 7AAD (red) and FLICA (green). DAPI was used to identify nuclei in cells. Scale bar is 100μm. Arrowheads point to representative co-localization. (B) Quantification of cell marker for FLICA within PCLS. (C) Quantification of cell marker for 7-AAD within PCLS. (D) Quantification of colocalization of cell markers for FLICA and 7-AAD within PCLS. Horizontal lines on graphs represent medians and results were statistically analyzed through Kruskal-Wallis tests followed by Dunn's multiple comparisons. *$p<0.05$. Conditions: H5N1 MOI 10, LPS 100ng/mL. Treatments: DMSO 1%, VX-765 10μM, Z-DEVD-FMK 100μM, disulfiram 100μM. Each dot is an individual image and this figure represents one donor.

5.3.2 Cell Death is Observed in Human PCLS and Reversed by Caspase Inhibitors

In human lung, there was a great deal of difficulty in staining with FLICA due to the stain nonspecifically binding to what was determined most likely to be elastin in the lung, so cell death is determined primarily solely through 7-AAD staining. Staining with other antibodies after staining with 7-AAD and subsequent paraformaldehyde fixing also interfered with the final staining panel, and it was difficult to observe co-localization of 7-AAD with other markers such as Influenza A NP (data not shown, determined through preliminary testing).

In human lung AGIE005, the LPS treated PCLSs showed the most dramatic change in cell death, with widespread 7-AAD in vehicle control treated DMSO and a significant decrease after treatment with VX-765 within the LPS treated group (Figure 15). In H5N1 treated PCLSs, there was a slight decrease in 7-AAD after treatment with caspase-1 inhibitor VX-765 but not as dramatic as the decrease seen after treatment with caspase-3 inhibitor Z-DEVD-FMK (Figure 15). This lung donor was the earliest lung with presentable data for 7-AAD, and the results provided warrant further investigation to determine if the same changes in cell death were observed after treatments in other lung donors.

A.
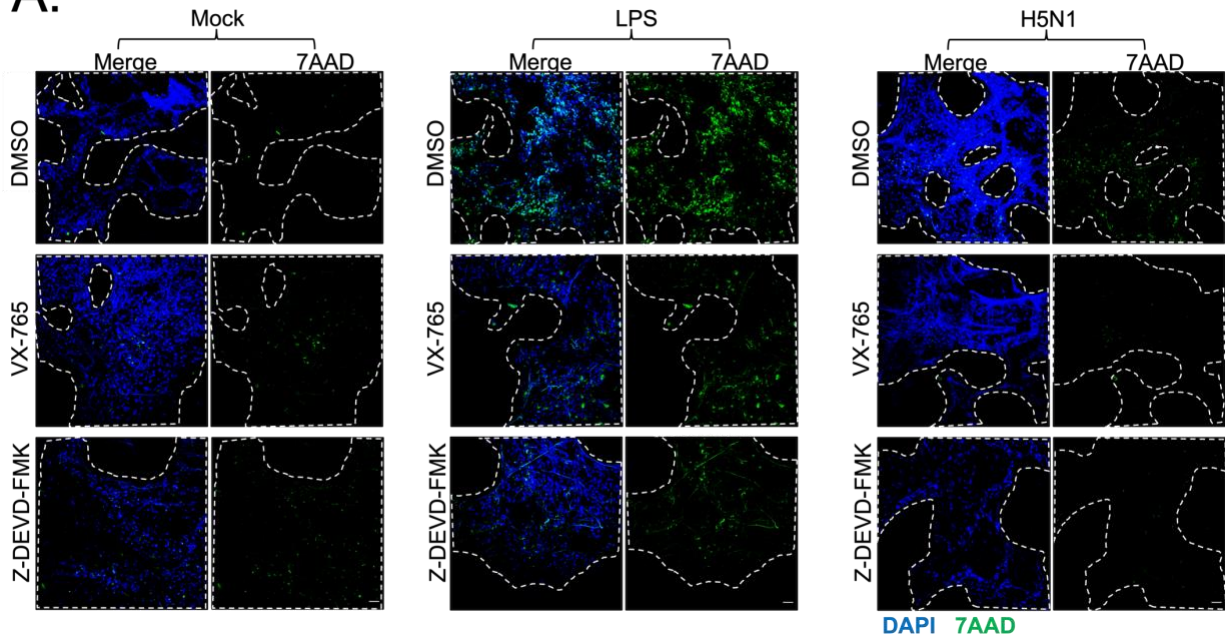
B.

Figure 15: Cell Death from H5N1 in AGIE005 Human Lung

(A) Human lung AGIE005 PCLS stained with antibodies to 7-AAD (green). DAPI was used to identify nuclei in cells. Scale bar is 100μm. Dotted lines mark areas of tissue. (B) Quantification of cell marker for 7-AAD within PCLS. Horizontal lines on graphs represent medians and results were statistically analyzed through Kruskal-Wallis tests followed by Dunn's multiple comparisons. $*p<0.05$, $**p<0.01$. Conditions: H5N1 MOI 10, LPS 100ng/mL. Treatments: DMSO 1%, VX-765 10μM, Z-DEVD-FMK 100μM. Each dot is an individual image and this figure represents one donor.

In human lung AHCG011 (the most recently procured lung), the concentration of disulfiram was changed from 100μM to 5μM to eliminate potential toxicity from the drug itself and to better reflect what I have seen in literature concerning the suggested concentration to use (125).

I used multiphoton imaging to generate Z-stacks of PCLS to obtain more representative images of thicker tissue. In these images was widespread 7-AAD throughout all conditions except those treated with disulfiram (Figure 16). The presence of 7-AAD that appears to be in a higher quantity after treatment with Z-DEVD-FMK than the DMSO vehicle control (Figure 16) indicates that this concentration may possibly be too high and in future studies this will need to be adjusted to make sure no cell toxicity is happening directly from the drug treatment.

Due to time constraints, only one image per condition was able to be taken for the multiphoton imaging (Figure 16), so the same PCLSs were imaged on a confocal microscope (Figure 17), taking 5 images per condition to be able to quantify the experiment. In this experiment, there was a visible drop in 7-AAD after VX-765 and after treatment with disulfiram (Figure 17A). Even though all results were nonsignificant, there is a slight drop in 7-AAD after treatment with VX-765 and disulfiram (Figure 17B).
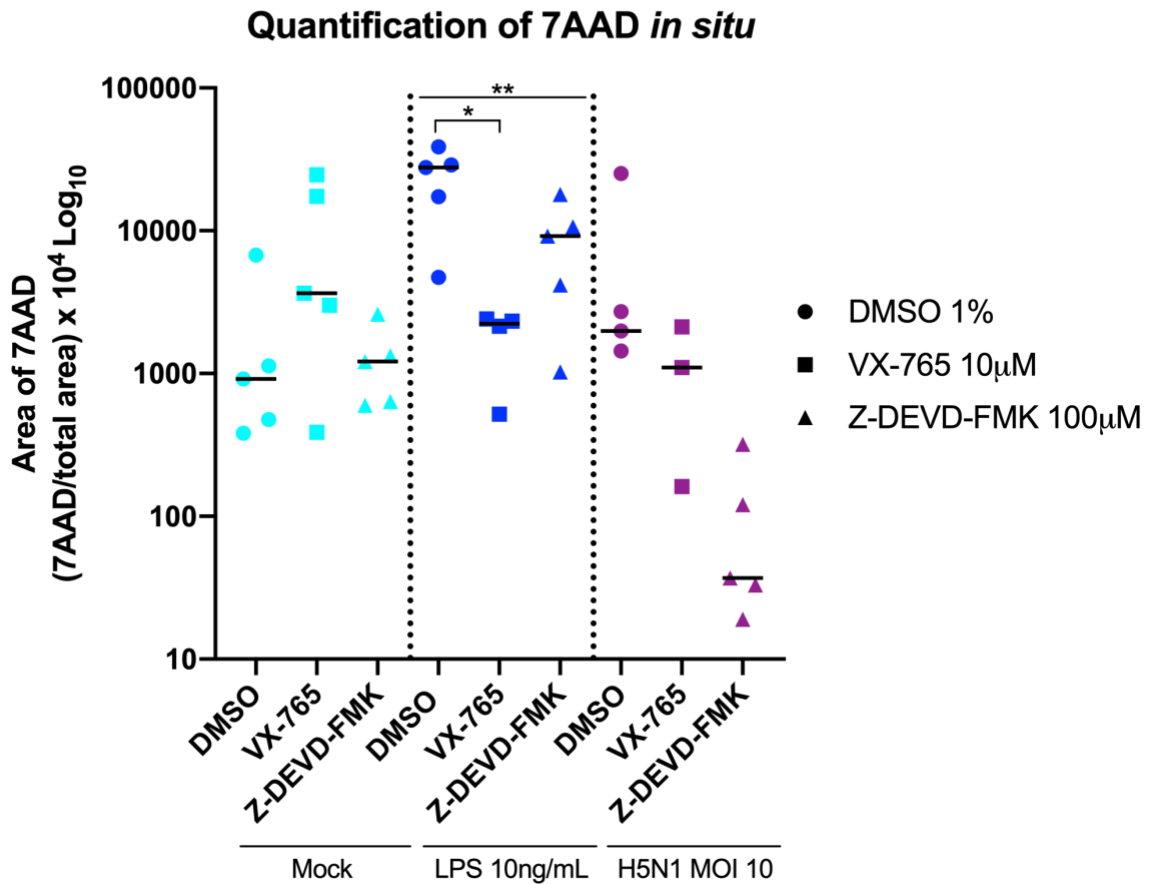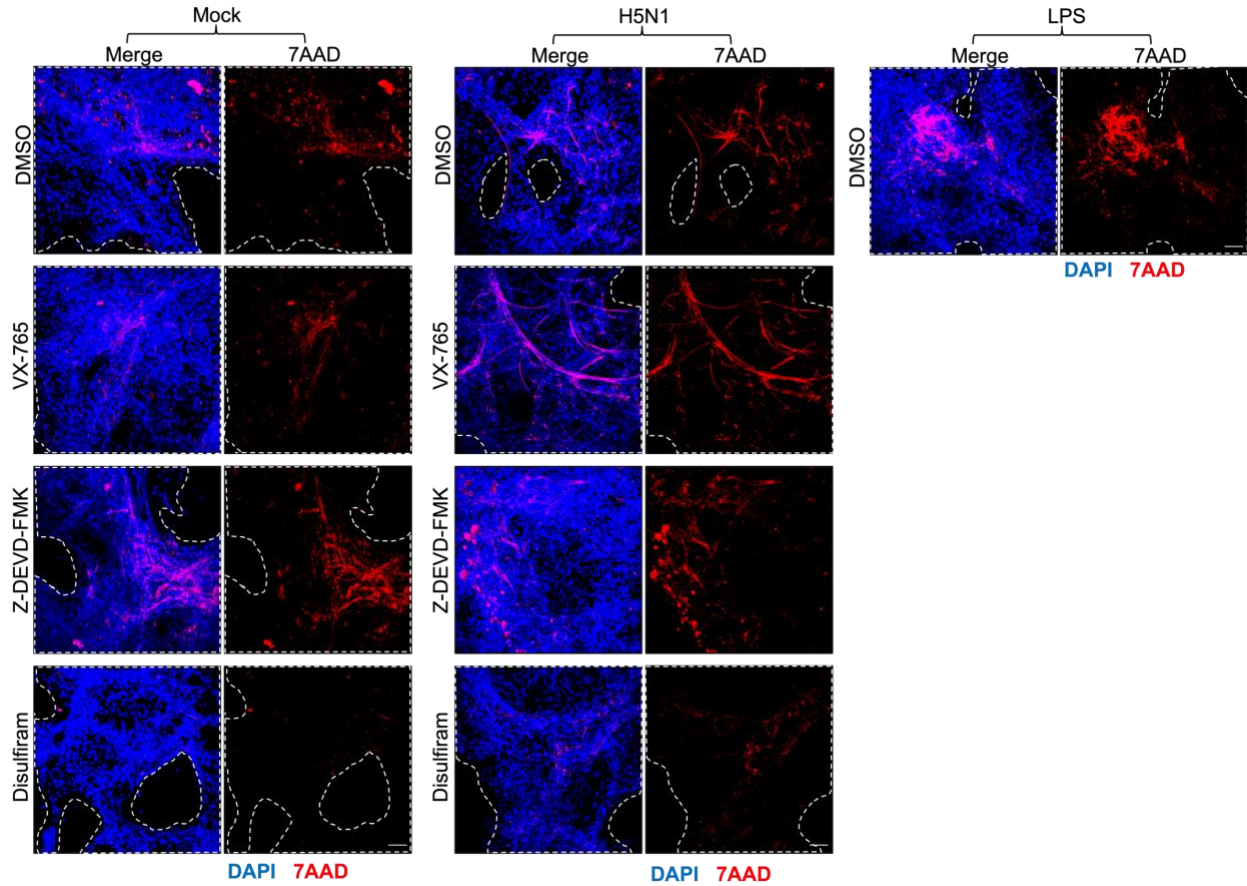
Figure 16: Cell Death from H5N1 in AHCG011 Human Lung

Human lung AHCG011 PCLS stained with antibodies to 7AAD (red). DAPI was used to identify nuclei in cells. Scale bar is 100μm. Images are Z-stack projections taken on an Olympus Mumultiphoton microscope encompassing 23 images with each image representing a 2 micron thick section. Dotted lines mark areas of tissue. Conditions: H5N1 MOI 10, LPS 100ng/mL. Treatments: DMSO 1%, VX-765 10μM, Z-DEVD-FMK 100μM, disulfiram 100μM.
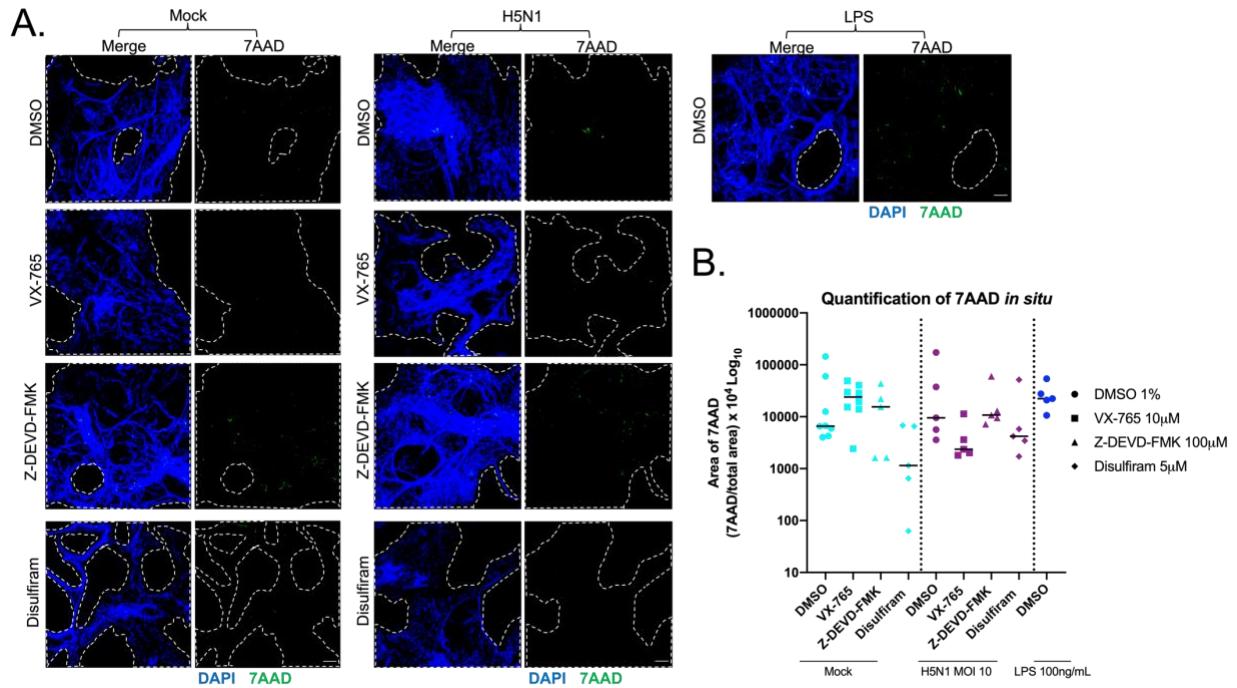
Figure 17: Cell Death from H5N1 in AHCG011 Human Lung

(A) Human lung AHCG011 PCLS stained with antibodies to 7AAD (green). DAPI was used to identify nuclei in cells. Scale bar is 100μm. Dotted lines mark areas of tissue. (B) Quantification of cell marker for 7-AAD within PCLS. Horizontal lines on graphs represent medians and results were statistically analyzed through Kruskal-Wallis tests followed by Dunn's multiple comparisons. All results were nonsignificant. Conditions: H5N1 MOI 10, LPS 100ng/mL. Treatments: DMSO 1%, VX-765 10μM, Z-DEVD-FMK 100μM, disulfiram 5μM. Each dot is an individual image and this figure represents one donor.

Overall, caspase-1 inhibitor VX-765 at 10μM and GSDMD-inhibitor disulfiram at 5μM are the most effective in reducing cell death, indicating that a pyroptotic pathway may be involved in HPAI H5N1 pathogenesis, as we have seen in transcriptomics in our previous study. The use of 7-AAD with these results also indicates that pyroptosis may be happening since 7-AAD labels cells with a compromised membrane, which is more consistent with an inflammatory method of cell death rather than apoptosis where the cell membrane can remain intact.

5.3.3 Downstream IL-1β is Reduced After Treatment with Caspase and Gasdermin-D Inhibitors

With evidence with 7-AAD showing effectiveness of caspase and GSDMD inhibitors, further investigation was needed to assess downstream cytokines and other members of the pyroptotic pathway. IL-1β ELISAs were completed on supernatants from 400-micron thick PCLS that were used in IHC, along with supernatants from 900-micron thick PCLS that were used for downstream Western blotting analysis. All supernatants were treated with non-denaturing lysis buffer to inactivate them so that the assay could be performed in BSL2 conditions; independent testing found no impact of non-denaturing lysis buffer on the quality of the ELISA (data not shown). From the most recent human lung, AHCG011, IL-1β increased after infection with H5N1 but was brought down after treatment with caspase-1/4 inhibitor VX-765, caspase-3 inhibitor Z-DEVD-FMK, and GSDMD inhibitor disulfiram, but the most dramatic change was after treatment with VX-765 and disulfiram (Figure 18). In 400-micron slices, the most significant results arose after 48 hours of infection, which did not change much from 24 hours besides Z-DEVD-FMK becoming slightly less effective (Figure 18B). In 900-micron PCLS, H5N1 infection still induces IL-1β production that can be almost completely reversed after treatments with VX-765 and disulfiram (Figure 19A), but this effect of VX-765 was only seen at 24 hours and was passed in effectiveness by Z-DEVD-FMK, but the effectiveness of disulfiram remained the same (Figure 19B).
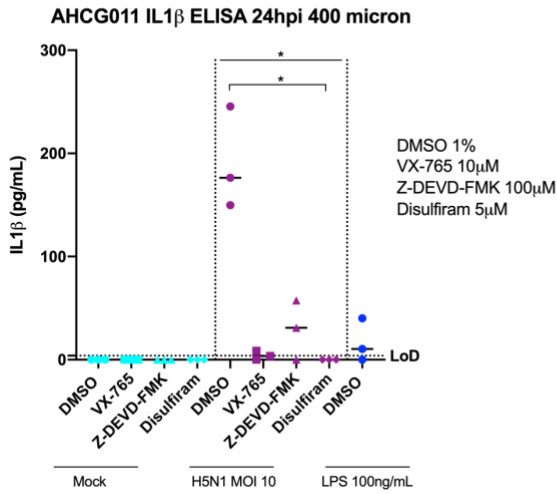
Figure 18: IL-1β ELISA from Human Lung AHCG011 400-Micron Slices

Supernatant from human lung AHAU189 400-micron PCLS was inactivated with NDLB and subjected to an ELISA for IL-1β at (A) 24hpi and (B) 48hpi. (B) IL-1β is most dramatically reduced after treatment with VX-765 and disulfiram after 48 hours. Horizontal lines on graphs represent medians and results were statistically analyzed through Kruskal-Wallis tests followed by Dunn's multiple comparisons. *$p<0.05$, ***$p<0.001$. Each dot is an individual image and this figure represents one donor.
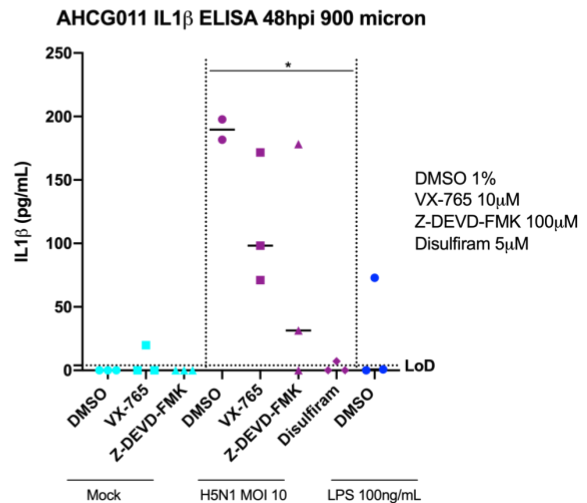
Figure 19: IL-1β ELISA from Human Lung AHCG011 900-Micron Slices

Supernatant from human lung AHAU189 900-micron PCLS was inactivated with NDLB and subjected to an ELISA for IL-1β at (A) 24hpi and (B) 48hpi. Horizontal lines on graphs represent medians and results were statistically

analyzed through Kruskal-Wallis tests followed by Dunn's multiple comparisons. *p<0.05. Each dot is an individual image and this figure represents one donor.

5.3.4 ASC and IL-1β are Reduced After Treatment with Caspase and Gasdermin-D

  Inhibitors in Lung Tissue

  In addition to observing IL-1β in ELISAs, I wanted to see if the same drug effects were present in the tissue through IHC. In figure 20, markers to the ASC inflammasome complex and the cytokine IL-1β were observed in human PCLS. In this lung, AHAU189, disulfiram was used at a concentration of 100μM. ASC was higher in LPS and H5N1 conditions in comparison with mock, although IL-1β through IHC remained fairly consistent among all conditions (Figure 20). In tissue, disulfiram 100μM also reduced levels of ASC and IL-1β (Figure 20). In the IL-1β ELISA results for the same donor as the tissue stained for IL-1β, AHAU189, VX-765 10μM dramatically reduced IL-1β levels, further confirming the important role in caspase-1/4 in the pathogenesis of H5N1 (Figure 21).

A.

B. Quantification of ASC *in situ*

C. Quantification of IL1β *in situ*

D. Quantification of ASC+IL1β *in situ*
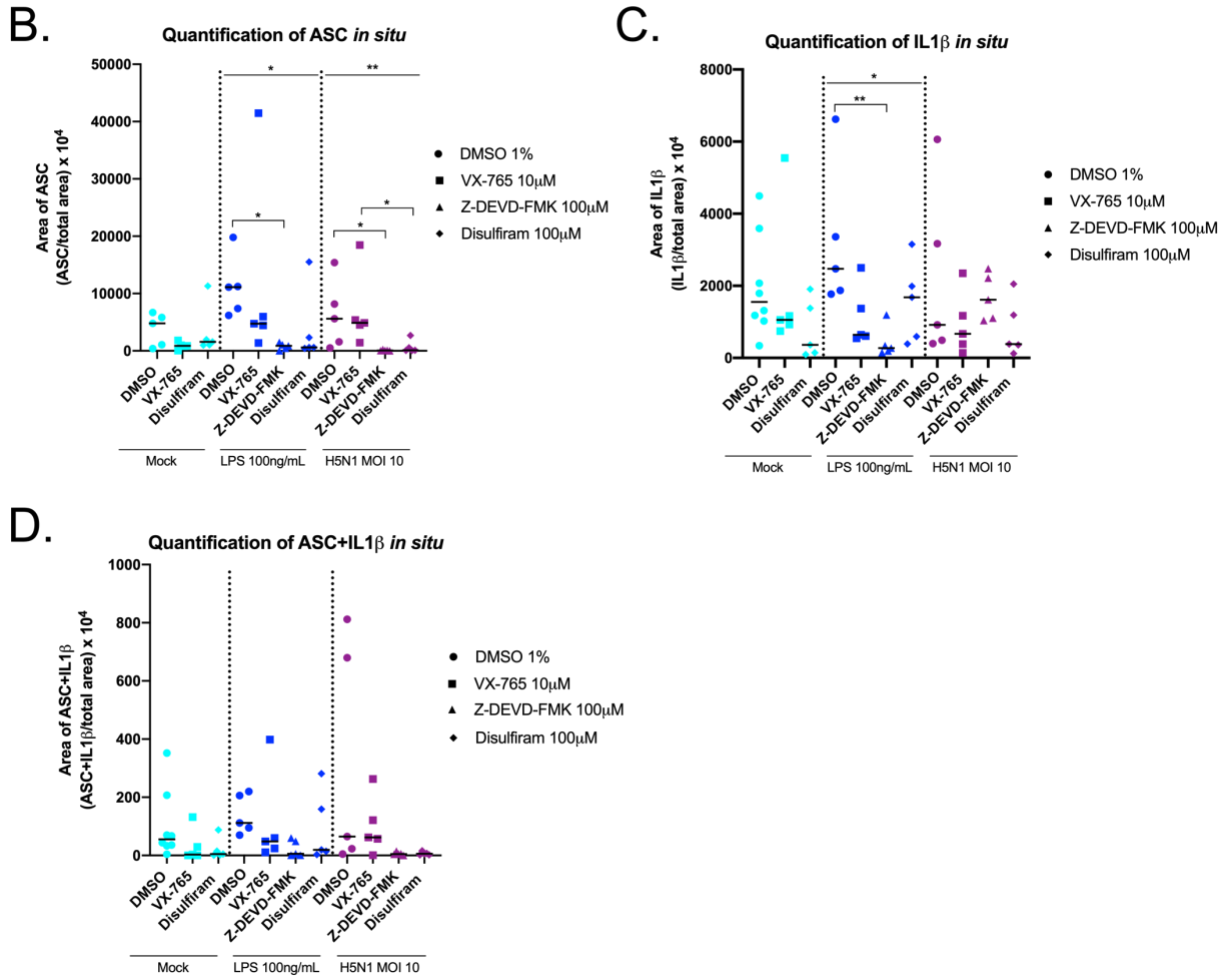
Figure 20: Markers of Pyroptotic Pathway in Human Lung AHAU189

(A) Human lung AHAU189 PCLS stained with antibodies to ASC (red) and IL-1β (green). DAPI was used to identify nuclei in cells. Scale bar is 100μm. Arrowheads highlight representative co-localization. (B) Quantification of cell marker for ASC within PCLS. (C) Quantification of cell marker for IL-1β. (D) Quantification of colocalization of ASC and IL-1β. Horizontal lines on graphs represent medians and results were statistically analyzed through Kruskal-Wallis tests followed by Dunn's multiple comparisons. *$p<0.05$, **$p<0.01$. Conditions: H5N1 MOI 10, LPS 100ng/mL. Treatments: DMSO 1%, VX-765 10μM, Z-DEVD-FMK 100μM, disulfiram 100μM. Each dot is an individual image and this figure represents one donor.

AHAU189 IL1β ELISA 24hpi 400 micron

DMSO 1%
VX-765 10μM
Z-DEVD-FMK 100μM
Disulfiram 100μM

Mock   LPS 100ng/mL   H5N1 MOI 10
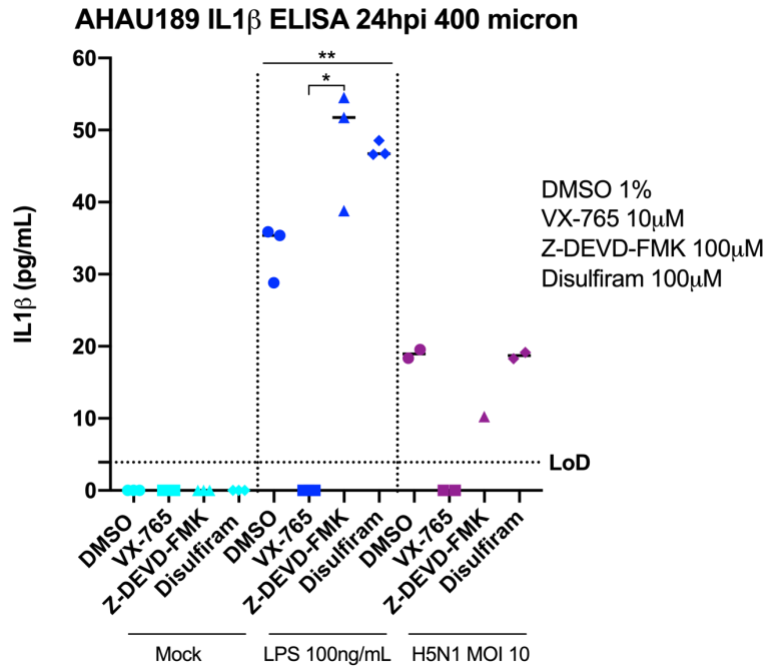
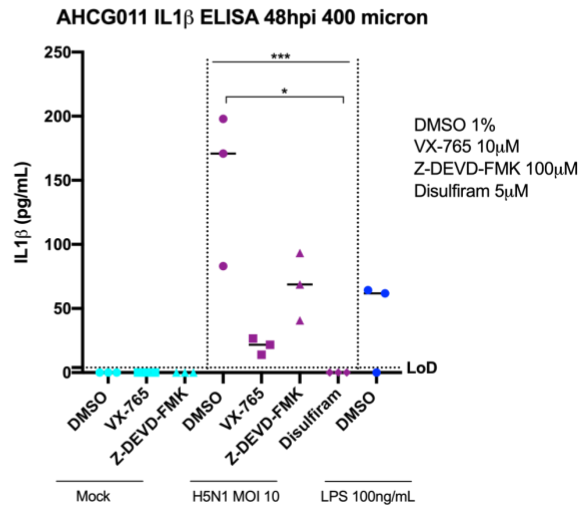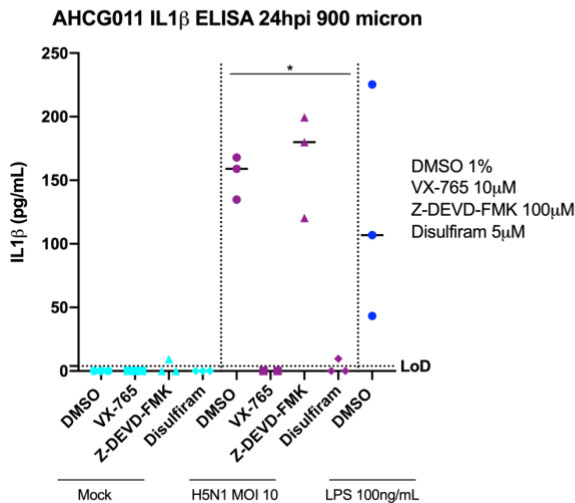**Figure 21: IL-1β ELISA from Human Lung AHAU189**

Supernatant from human lung AHAU189 400-micron PCLS was inactivated with NDLB and subjected to an ELISA for IL-1β. Horizontal lines on graphs represent medians and results were statistically analyzed through Kruskal-Wallis tests followed by Dunn's multiple comparisons. *$p<0.05$, **$p<0.01$. Each dot is an individual image and this figure represents one donor.
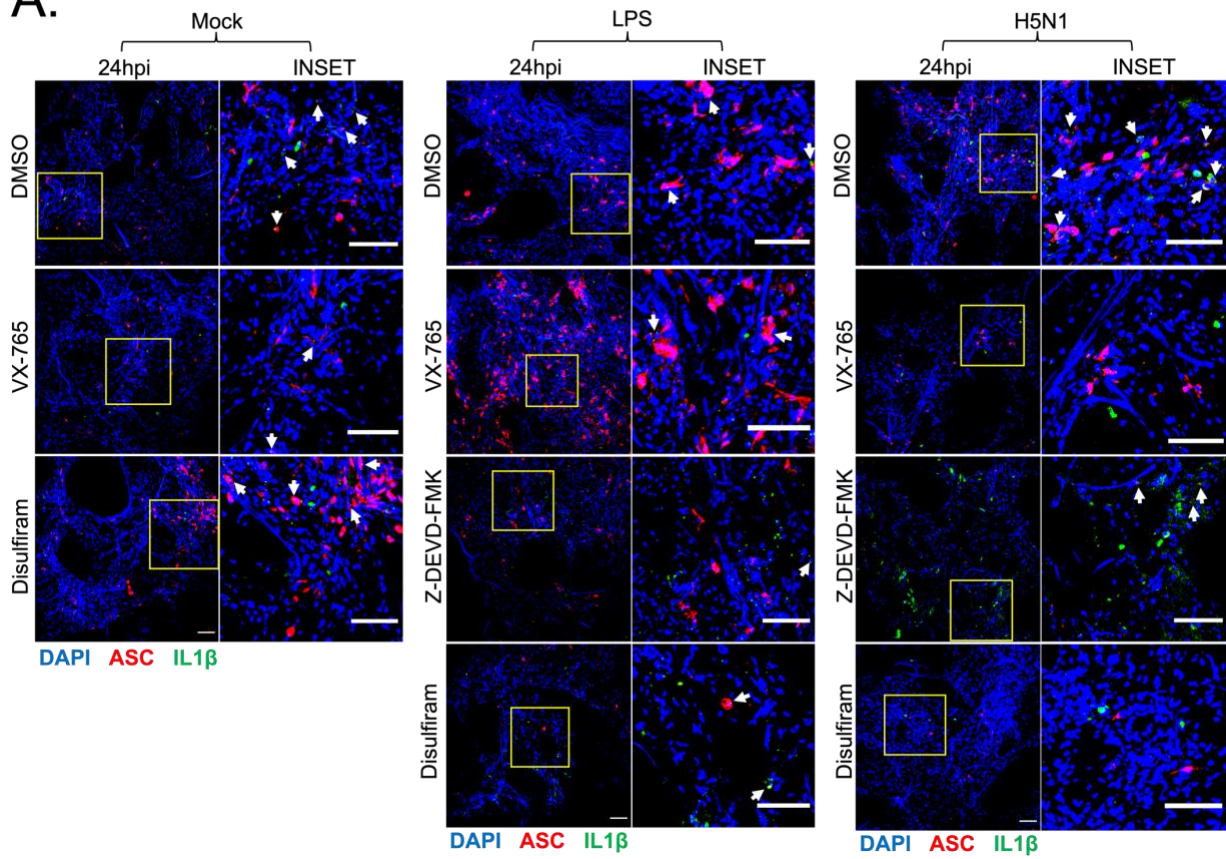
5.3.5 Interferon Response in Macaque Lungs

Macaques from our previous study demonstrated ARDS upon a high dose of aerosolized H5N1 of 6.72 log$_{10}$ PFU as seen by impressive inflammation through PET-CT scans, and an increase in IFNα, IL-6, TNF-α (43). From this same study, transcriptomics revealed higher expression of ISG in H5N1-infected macaques in comparison to naïve animals (Corry et al. manuscript in preparation). In lung samples from this study, I show an increase in IFNα in H5N1 infected tissue from a day 4 necropsy which matches what I have seen in this previous study, but also a visible increase in antiviral protein MxA/Mx1 (Figure 22) in the same tissue. These results suggest that upon H5N1 infection, the innate immune system goes through a type I interferon

64

response, corroborating what we have seen in our previous study and in a PCLS model of H5N1 infection (43, 131, 133, 134).
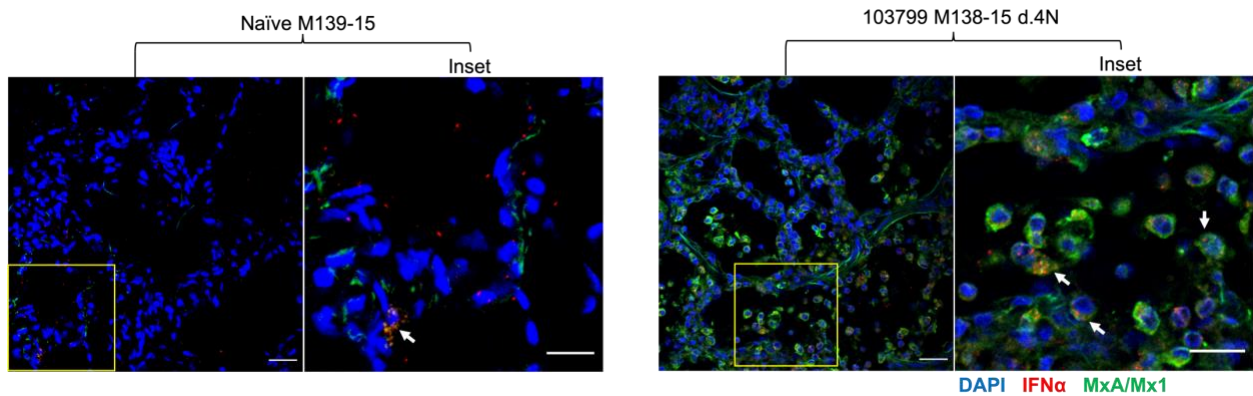
Figure 22: Interferon-Related Markers in Macaque Lungs

Immunofluorescence staining of lung sections from naive and infected macaque lungs stained with antibodies to IFNα (red) and MxA/Mx1 (green). Arrowheads point to representative co-localization. Scale bar is 100μm.

5.3.6 IFNα and MxA/Mx1 Reduction After Treatment with Inhibitors

In order to see if human PCLSs are susceptible to a type I IFN response similar to what was seen in monkey lungs, lung slices were stained with antibodies to IFNα and MxA/Mx1 and observed via IHC. The LPS inflammasome control condition was relatively comparable to mock conditions (Figure 23). LPS can induce type I IFN responses, although the lack of induction could be due to a different inflammasome activation other than TLR4 (135, 136). IFNα and MxA/Mx1 were reduced with all caspase and GSDMD inhibitors, although most dramatically with disulfiram (Figure 23), providing further evidence for a pyroptotic involvement in H5N1 pathogenesis.

A.

Mock — 24hpi | INSET
H5N1 — 24hpi | INSET
LPS — 24hpi | INSET

DMSO
VX-765
Z-DEVD-FMK
Disulfiram

DAPI IFNα MxA/Mx1

DAPI IFNα MxA/Mx1
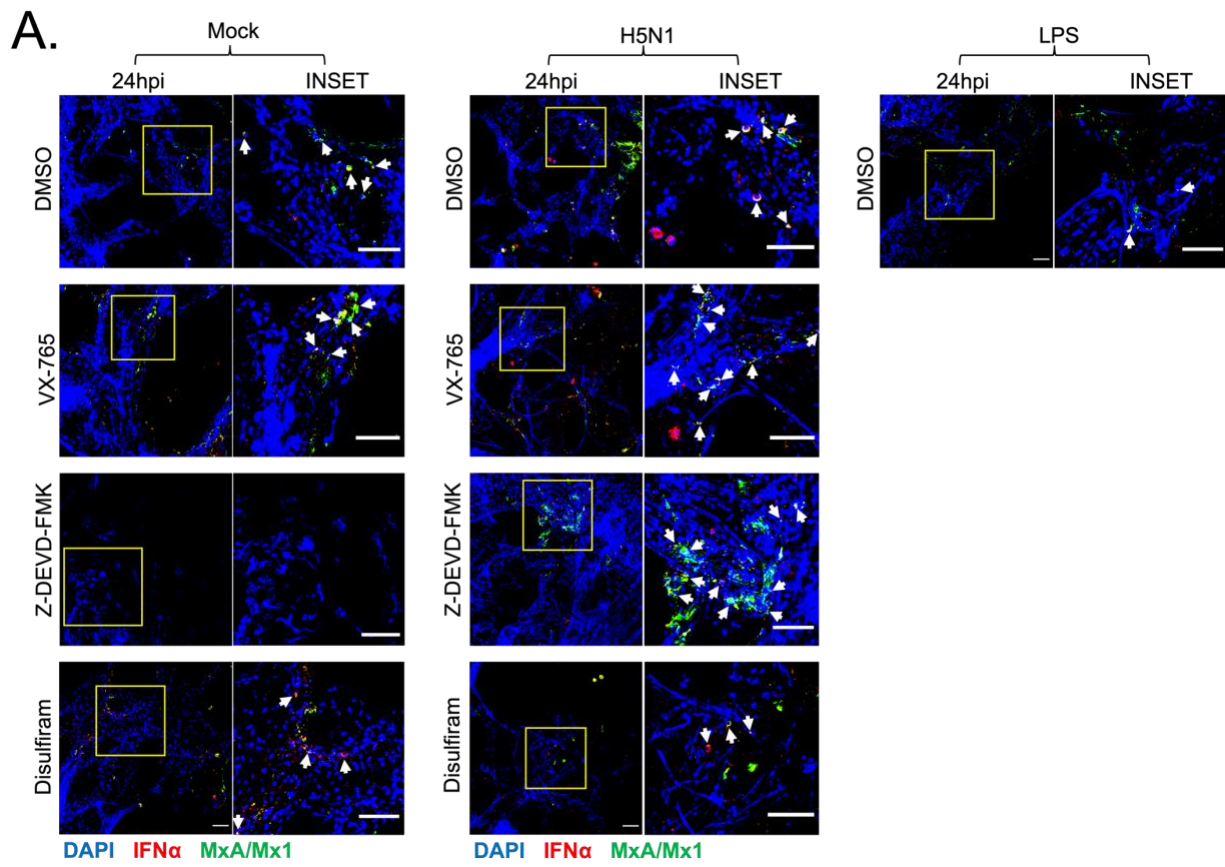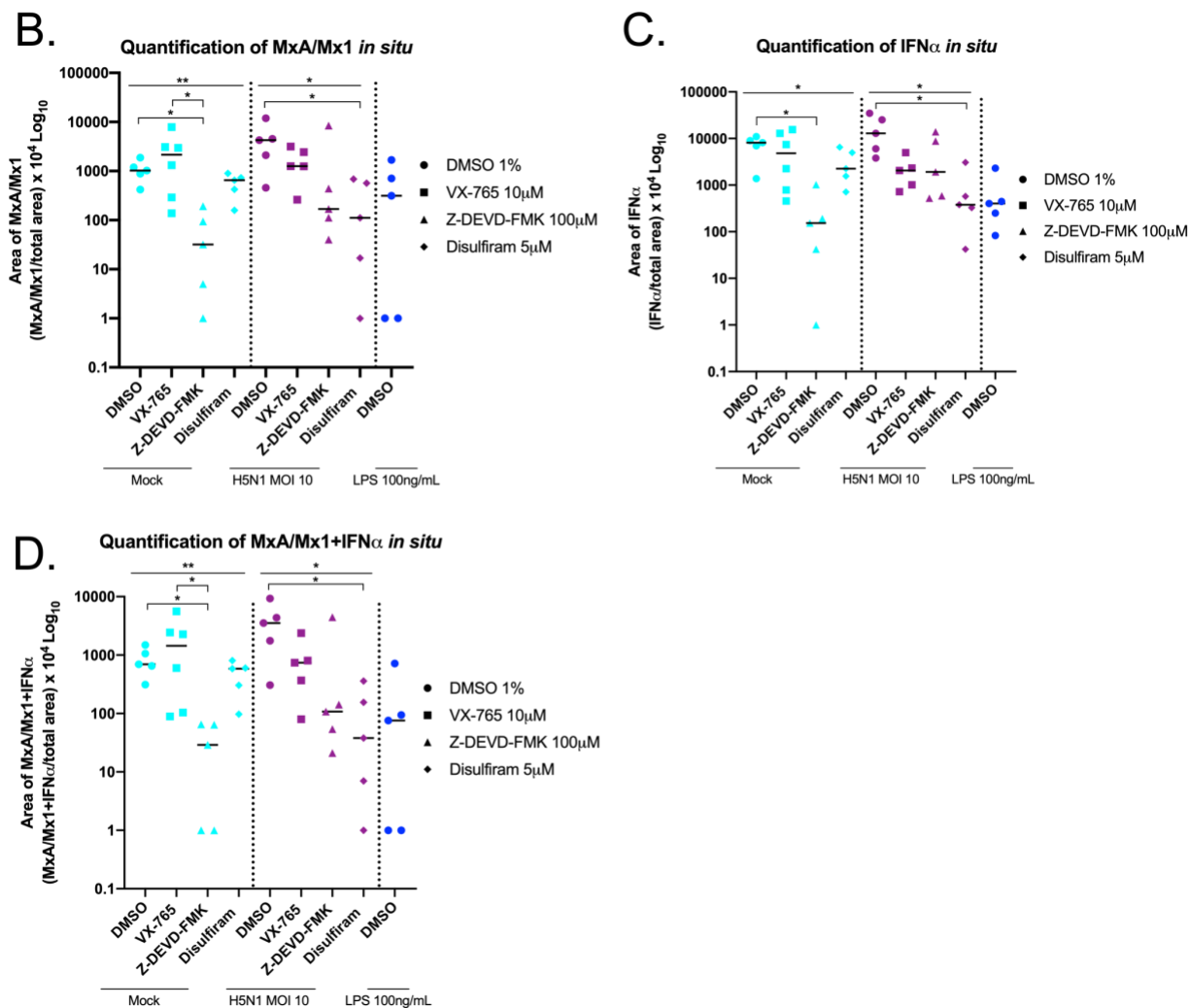
Figure 23: Markers of Interferon Stimulation in Human Lung AHCG011

(A) Human lung AHCG011 PCLS stained with antibodies to IFN-α (red) and MxA/Mx1 (green). DAPI was used to identify nuclei in cells. Scale bar is 100μm. Arrowheads highlight representative co-localization. (B) Quantification of cell marker for MxA/Mx1 within PCLS. (C) Quantification of cell marker for IFNα. (D) Quantification of colocalization of MxA/Mx1 and IFNα. Horizontal lines on graphs represent medians and results were statistically analyzed through Kruskal-Wallis tests followed by Dunn's multiple comparisons. *$p<0.05$, **$p<0.01$. Conditions: H5N1 MOI 10, LPS 100ng/mL. Treatments: DMSO 1%, VX-765 10μM, Z-DEVD-FMK 100μM, disulfiram 5μM. Each dot is an individual image and this figure represents one donor.

Finally, other quantitative methods of measuring cell death were explored. An LDH assay was tested to try and measure pyroptosis as LDH is released once the cell membrane loses integrity. In figure 24, LDH is increased after treatment with LPS and H5N1 in human lung AHAU189 and was reduced after treatment with caspase 1/4 inhibitor VX-765 across all exposure conditions. This

67

provides yet another piece of evidence that would suggest that pyroptosis plays a part in HPAI H5N1 pathogenesis.
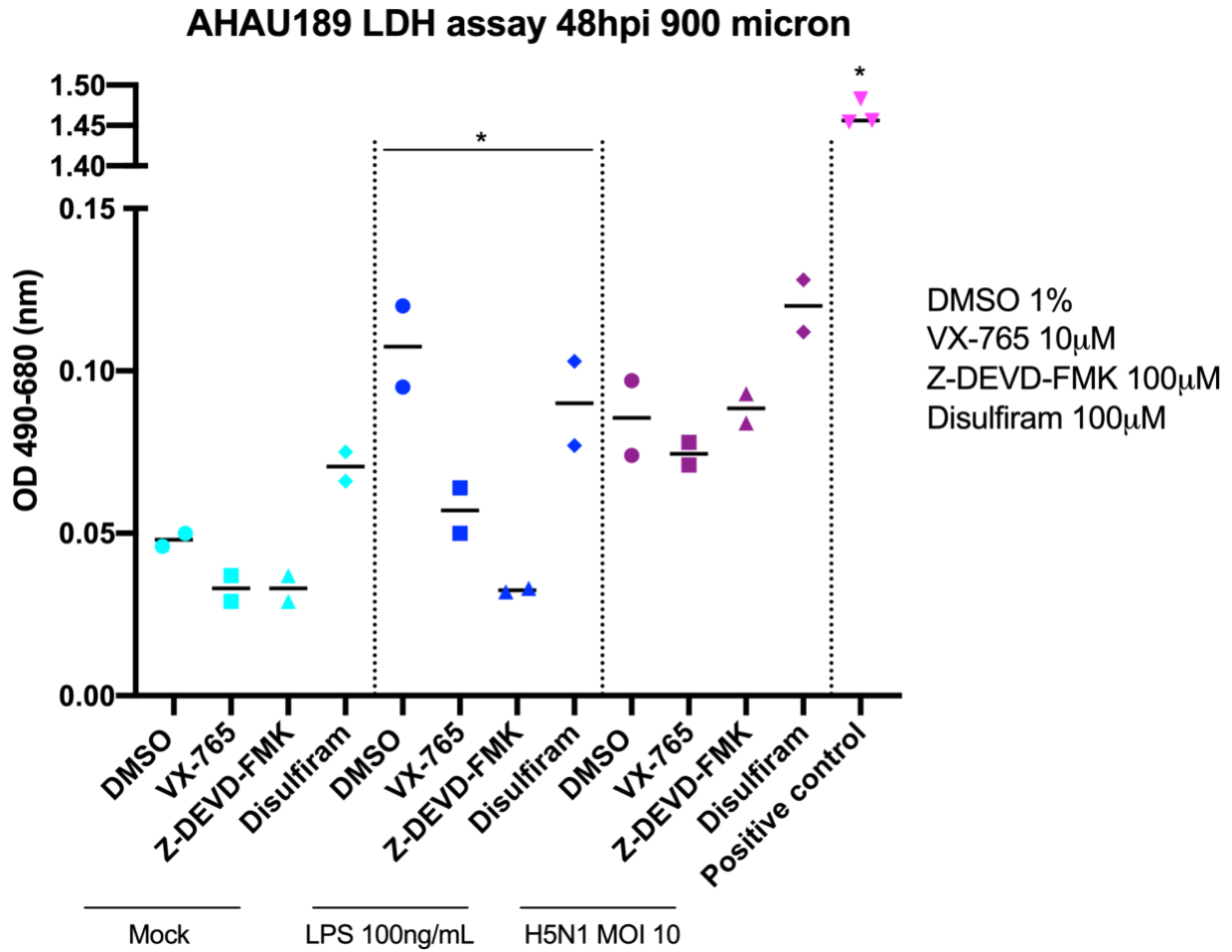
Figure 24: LDH Assay of Human Lung AHAU189

Supernatants from 900-micron human lung AHAU189 PCLS were collected and subjected to a LDH assay. Horizontal lines on graphs represent medians and results were statistically analyzed through Kruskal-Wallis tests followed by Dunn's multiple comparisons. *$p<0.05$. Each dot is an individual image and this figure represents one donor.

5.3.7 Aim 3 Conclusions

In conclusion, aim 3 successfully provides early evidence that pyroptosis plays a role in H5N1 pathogenesis, as we have seen in a macaque model via transcriptional analysis. This aim used a multitude of methods that examine different parts of the pyroptotic pathway, from beginning

(ASC), to the executioners of the pathway (caspase-1 and GSDMD) and ending with secreted cytokines and enzymes such as IL-1β and LDH.

5.4 Final Conclusions

In this study, I have accomplished the task of developing a PCLS model of H5N1 infection in both human and porcine lungs and have utilized this model to observe replicating virus and its subsequent cellular targets, AMs and AECs (Figures 5-13). Cell death data in porcine lung showed treatment with VX-765 10μM yielded the most dramatic decrease in FLICA labeled despite 7-AAD labeled cells remaining relatively the same (Figure 14). Also, in the human PCLS model I have investigated the possible cell death pathway that plays a role in the cytokine dysregulation that we have seen in our macaque model (43) and through transcriptomic analysis (Corry et al. manuscript in preparation), by employing ELISAs and IHC to observe multiple players of the pathway and response to infection: IL-1β, ASC, caspase-1, MxA/Mx1, IFNα, FLICA, and 7-AAD. I found that VX-765 10μM widely decreases IL-1β in supernatant (Figures 18, 19, 21), reduced levels of LDH in supernatant (Figure 24), and decreased levels of 7-AAD (Figures 15, 16, 17). While limited in data, experiments with human lung AHCG011 using a non-toxic concentration of disulfiram at 5μM showed exciting results, decreasing 7-AAD levels (Figures 16 and 17), and lowering the amount of secreted IL-1β to below the limit of detection of the ELISA in 400-micron PCLS and slightly higher but still dramatic reductions in 900-micron PCLS (Figures 18 and 19). In addition to 7-AAD and IL-1β reductions, disulfiram at 5μM significantly decreased both

MxA/Mx1 and IFNα in H5N1 infected conditions in comparison to the DMSO 1% vehicle control (Figure 23).

In our previous study, we showed a massive mobilization of cytokines (especially IFNα) (Figure 22) in response to infection, and recruitment of neutrophils and destruction of alveolar macrophages (43), it is encouraging to see a similar IFNα response in our PCLS model (Figure 23), giving validation that out PCLS model in at least some aspects can be substituted for animals models for early experiments as predecessors to determining what would be most important to study in an animal model, since many experiments in NHP models do not the capacity to test multiple factors at once due to cost, housing requirements, and difficulty of working with animals in a higher biosafety level. A graphical summary of this conclusion is shown in figure 25.
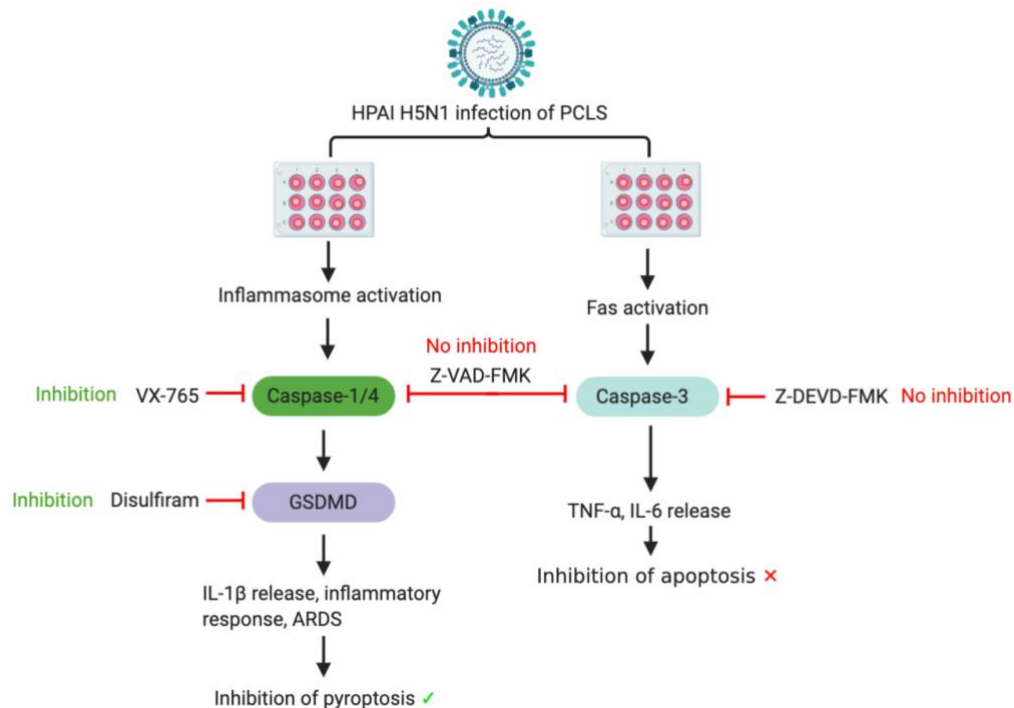
Figure 25: Graphical Summary of Study Findings

Through successful inhibition of pyroptotic pathway members, pyroptotosis can be linked to HPAI H5N1 pathogenesis in PCLS.

6.0 Discussion

6.1 HPAI H5N1 Infection in PCLS

Infection of both porcine and human PCLS was successful, yielding productive replication in both conditions (Figures 9 and 11) as seen via plaque assays. In IHC, drug treatment with VX-765 $10\mu M$ yielded higher levels of influenza A NP (Figures 10 and 12), although replicating virus remained equal among drug treatments at respective timepoints (24, 48, and 72hpi), implicating that they have no real effect on viral replication. In literature, AECs were shown to be targets of HPAI H5N1 infection, especially type I pneumocytes, which is comparable to what I have seen in the human PCLS model (132). However, in multiphoton imaging of human lung AHAU189, filamentous staining of AEC that seemed to be non-specific showed up throughout the tissue. As suggested by colleagues, filamentous staining of AEC within the tissue and not near the alveolar space may be nonspecific staining of elastin of collagen in the lung (Figure 12A). Further experimentation using specific stains would be needed to conclude this. AMs were reduced after HPAI H5N1 infection, suggesting that HPAI H5N1 may also be replicating in these cell types and/or targeting these cells to undergo cell death (Figure 13). As mentioned before, influenza A NP was not consistent between both porcine lungs (Figures 10 and 13) despite keeping infection and processing protocols consistent. This may be due to the general health of the porcine lung, perhaps a porcine lung that was less hemorrhaged would be more susceptible to infection.

6.2 HPAI H5N1 and Pyroptosis

Upon infection with influenza, the virulence factor PB1-F2 has been shown to activate the NLRP3 inflammasome and induce IL-1β production, indicating that NLRP3 plays an important role in the progression of disease (137). ASC knockout, caspase-1 knockout, and NLRP3 knockout mice reveal a lessened disease status, characterized by lower levels of IL-1β, ASC, and caspase-1, further supporting the involvement of the pyroptotic cell death response in another HPAI virus, H7N9, and H5N1 infection (56, 130, 138). These results corroborate what was seen in this study, since targeting caspase-1 and GSDMD resulted in a drop of IL-1β and therefore a reduction in pyroptosis. In IHC, levels of IL-1β were relatively low in tissue but very high in supernatant for human lung AHAU189 (Figures 20 and 21). This may be because at timepoints where lung slices were fixed in PFA (24, 48, or 72 hpi depending on the experiment), IL-1β had already been secreted into the media, which would explain these differences. In human lung AHCG011, IL-1β levels were significantly reduced after treatment with disulfiram at 5 μM at both 24 and 48 hpi in both 400 and 900-micron PCLS (Figures 18 and 19). Furthermore, differences in IL-1β levels became highly significant among all treatments due to an increase in IL-1β after 48 hpi in comparison to 24hpi in 400-micron slices in response to increase in cytokine levels in both VX-765 10μM and Z-DEVD-FMK 100μM conditions.

In macaque lung tissue observed through IHC, transcriptomics (Corry *et al.* manuscript in preparation), and in PCLS from human lung AHCG011, ISG-associated members IFN-α and MxA/Mx1 were found to be increased after HPAI H5N1 infection (Figures 22 and 23). All caspase and GSDMD inhibitors decreased IFN-α and MxA/Mx, with disulfiram at 5μM providing a significant decrease of both cell markers (Figure 23). This corroborates evidence that suggests that

72

a type I ISG response triggers a pyroptotic response and an apoptotic response in response to influenza infection (56, 139), and more specifically a pyroptotic response that we have seen in our studies (43) (Corry *et al.* manuscript in preparation).

Finally, 7-AAD serves as a simple and easy to use marker of cell death that stains cells that possess permeabilized membranes. Cell death remained relatively even across all drug treatments in porcine lung, although I believe this is due to the hemorrhaged nature and general diminished health of the porcine lungs upon arrival and throughout processing (Figure 14). FLICA stain was successful in porcine lungs, so this marker of active caspase-1 shows me that VX-765 10μM decreases the amount of active caspase-1 in tissue (Figure 14). Other experiments with healthy human lungs, while lacking in FLICA due to issues with nonspecific staining, provide valuable data on 7-AAD reduction upon both VX-765 10μM and disulfiram 5μM treatment in human lungs AHCG011 and AGIE005 (Figures 15, 16, 17). Only in one human lung, AGIE005, showed a decrease in 7-AAD in response to Z-DEVD-FMK 100μM treatment (Figure 15). The main difference between this human lung and the others is that this donor had Lupus, so perhaps cell death from this, which usually follows a caspase-3 dependent pathway (140), precedes cell death from H5N1 and is preferentially reduced from Z-DEVD-FMK 100μM treatment.

Overall, my data in addition to our lab's data shows pyroptosis plays at least some role in H5N1 pathogenesis (Figure 25).

6.3 Pyroptosis and Neutrophils

There have been studies recently that link GSDMD activation in neutrophils and the generation of neutrophil extracellular traps (NETs) (141, 142). Specifically, GSDMD is cleaved

73

when NETs are formed and travels to the plasma membrane, implicating that through multiple stimuli GSDMD is essential in NETosis (141, 142). However caspase 1/4 inhibitor VX-765 did not impact NET formation (142). Multiple studies have shown that neutrophils play an important role in H5N1 pathogenesis, as IL-1β aids in recruitment, so pyroptosis may have additional stimuli and pathway connections that warrant further exploration (43, 56, 96, 138, 143-146). Additionally, neutrophils activate the NLRP3 inflammasome in AM's, and their presence in the lower respiratory tract are correlated with disease severity (143, 144, 146). With evidence in our study implicating that GSDMD plays an important role in H5N1 pathogenesis, it will be important in the future to investigate the role of NET formation and NETosis using the PCLS model of infection. However, since neutrophils are part of a recruitable immune response, they would need to be added to PCLS separately in order to assess their role in infection by artificially adding a recruitable immune response to this system.

6.4 Contributions to Field of Influenza Research

As mentioned previously, the pandemic potential of avian influenza viruses, particularly H5N1, make for a public health concern due to the high mortality rate and lack of a specific immune response in the general human population to H5 influenza subtypes. There are mitigation efforts in place, but these are more so to protect vulnerable poultry populations. Seasonal influenza vaccination is recommended to prevent H5N1 infection in case cross-protection (18), but a vaccine for H5N1 does not exist for use in humans, only in poultry. Research into a universal influenza vaccine targeting the stem of the HA protein is in process among many groups, including our own, but the process to develop, test, and approve a vaccine for use is long. Instead, broadly acting

targets of the innate immune system's overactive response would be useful for not only protection against HPAI H5N1 pathogenesis, but other HPAI avian influenza viruses, and highly pathogenic coronaviruses (MERS-CoV, SARS-CoV, SARS-CoV-2) that have also been associated with ARDS as a severe disease outcome (147-150).

By assessing the roles of caspase and GSDMD inhibitors in PCLS, preparation for potential new infections would allow for a broadly acting treatment that could prove effective for multiple pathogens, something a vaccine cannot do. Additionally, these inhibitors could potentially be combined in treatment strategies to account for immune evasion strategies presented by different pathogens.

6.5 Limitations

The major limitation in this study is the statistical analysis of the image quantification through IHC. Because of smaller sample sizes of images, it is difficult to determine if the tests run should be parametric or nonparametric, but could possibly be improved by the addition of more images, such as a sample size of at least 10. PCLS were mounted in ProLong Diamond (Thermo Fisher), improving the condition of the slides enough to revisit older experiments if necessary, since all slides were saved.

Another limitation was the lack of donors to run comparisons along them to observe possible individual related differences in H5N1 pathogenesis and cell death responses. Two porcine lungs, denoted for the months received: 8/19 and 11/19, represent the data presented in this study, and 4 human donors were used to generate data for this project: AGIE005, AGHH267 (was used to examine H1N1 infection but data was not shown), AHAU189, and AHCG011 (Table

1). Donors with matched treatments were statistically compared, but no significant results were found due to low sample sizes. This is due to the fact that the model was adjusted to become more streamlined as time went on, and now that I have identified conditions and treatments of interest, experiments could be reduced and kept the same for each lung in the future, allowing for a better power analysis. Finally, a limitation is the lack of a recruitable immune response in these PCLS, as mentioned before. This makes it a bit difficult to make sure every slice is comparable to each other, especially in different sections of the lung, raising the concern that some sections may be skewed in the cell populations that already reside in those lung slices.

7.0 Future Directions

With an established PCLS model in place, I would like to use this to further investigate the role of GSDMD inhibitor disulfiram against H5N1 infection, in anticipation of using this drug in our aerosolized H5N1 model in macaques to prevent pyroptosis and possibly NETosis. With this in mind the PCLS model will be used to evaluate other cell death pathways to match what we have seen in transcriptomic analysis. Additionally, neutrophils activate the NLRP3 inflammasome in alveolar macrophages by providing the second signal which leads to caspase-1 cleavage and IL-1β release, and the level of them in the lower respiratory tract are correlated with disease severity (143, 144, 146). With disulfiram showing effectiveness in reducing pyroptosis through cell death and IL-1β reduction throughout my results and downregulation of GSDMD in transcriptomics , we believe GSDMD plays an important role in pathogenesis and will be important in the future to investigate the role of NET formation and NETosis using the PCLS model of infection. However, since neutrophils are part of a recruitable immune response, they would need to be added to PCLS separately in order to assess their role in infection by artificially adding a recruitable immune response to this system.

Another GSDMD inhibitor, LDC7559, necrosulfonamide as a MLKL inhibitor (part of the necroptotic pathway) will be used, for example to further explore the cell death pathways, but in investigation into an animal model we will use an inhibitor of NETosis in combination with a GSDMD inhibitor to provide a two-punch approach to reducing lung injury. The opportunity to test the effectiveness of these inhibitors and tease out the pathogenesis mechanisms before moving to an animal model is an exciting opportunity to test many other forms of cell death and their associated inhibitors.

Additionally, this PCLS model may not be limited to just H5N1. Other respiratory pathogens such as other influenzas and coronaviruses could be adapted to a PCLS model as we have done with H5N1. The added benefit of already having this PCLS system working with BSL3 pathogens has allowed for us to begin considering how this system may fare with a relevant virus that is affecting our everyday lives: SARS-CoV-2. While most research is preliminary, there are some studies that indicate pyroptosis may be involved in pathogenesis through assumptions that is shares some of the same inflammatory responses as SARS-CoV with data to support that both coronaviruses secrete the same cytokines that have been implicated in H5N1 pathogenesis, such as IL-1β, MIP-1A, and TNF-α (113, 151). Future studies in both of these areas could pave the way to testing important therapeutics that could help curb future epidemics in the absence of a vaccine.

Bibliography

1.   Neumann G, Chen H, Gao GF, Shu Y, Kawaoka Y. 2010. H5N1 influenza viruses: outbreaks and biological properties. Cell Research 20:51-61.
2.   Peiris JSM, de Jong MD, Guan Y. 2007. Avian Influenza Virus (H5N1): a Threat to Human Health. Clinical Microbiology Reviews 20:243.
3.   Zhang H, Hale BG, Xu K, Sun B. 2013. Viral and host factors required for avian H5N1 influenza A virus replication in mammalian cells. Viruses 5:1431-1446.
4.   Bouvier NM, Palese P. 2008. The biology of influenza viruses. Vaccine 26 Suppl 4:D49-D53.
5.   Prevention CfDCa. 2017 2017. Avian Influenza Type A Viruses. https://www.cdc.gov/flu/avianflu/influenza-a-virus-subtypes.htm. Accessed
6.   Chan MC, Chan RW, Chan LL, Mok CK, Hui KP, Fong JH, Tao KP, Poon LL, Nicholls JM, Guan Y, Peiris JS. 2013. Tropism and innate host responses of a novel avian influenza A H7N9 virus: an analysis of ex-vivo and in-vitro cultures of the human respiratory tract. Lancet Respir Med 1:534-42.
7.   Wilks S, de Graaf M, Smith DJ, Burke DF. 2012. A review of influenza haemagglutinin receptor binding as it relates to pandemic properties. Vaccine 30:4369-4376.
8.   Shinya K, Ebina M, Yamada S, Ono M, Kasai N, Kawaoka Y. 2006. Influenza virus receptors in the human airway. Nature 440:435-436.
9.   van Riel D, Munster VJ, de Wit E, Rimmelzwaan GF, Fouchier RAM, Osterhaus ADME, Kuiken T. 2007. Human and avian influenza viruses target different cells in the lower respiratory tract of humans and other mammals. The American journal of pathology 171:1215-1223.
10.   Zeng H, Goldsmith CS, Maines TR, Belser JA, Gustin KM, Pekosz A, Zaki SR, Katz JM, Tumpey TM. 2013. Tropism and Infectivity of Influenza Virus, Including Highly Pathogenic Avian H5N1 Virus, in Ferret Tracheal Differentiated Primary Epithelial Cell Cultures. Journal of Virology 87:2597.
11.   Zhao H, Zhou J, Jiang S, Zheng B-J. 2013. Receptor binding and transmission studies of H5N1 influenza virus in mammals. Emerging microbes & infections 2:e85-e85.
12.   Belshe RB. 2005. The origins of pandemic influenza--lessons from the 1918 virus. N Engl J Med 353:2209-11.
13.   Kaye D, Pringle CR. 2005. Avian Influenza Viruses and their Implication for Human Health. Clinical Infectious Diseases 40:108-112.
14.   Meseko C, Globig A, Ijomanta J, Joannis T, Nwosuh C, Shamaki D, Harder T, Hoffman D, Pohlmann A, Beer M, Mettenleiter T, Starick E. 2018. Evidence of exposure of domestic pigs to Highly Pathogenic Avian Influenza H5N1 in Nigeria. Scientific Reports 8:5900.
15.   Poovorawan Y, Pyungporn S, Prachayangprecha S, Makkoch J. 2013. Global alert to avian influenza virus infection: from H5N1 to H7N9. Pathogens and global health 107:217-223.
16.   de Graaf M, Fouchier RAM. 2014. Role of receptor binding specificity in influenza A virus transmission and pathogenesis. The EMBO journal 33:823-841.
17.   Eisfeld AJ, Neumann G, Kawaoka Y. 2014. Influenza A virus isolation, culture and identification. Nature Protocols 9:2663.

18. Centers for Disease Control and Prevention. 11/8/2019 2019. Influenza (Flu). https://www.cdc.gov/flu/index.htm. Accessed 11/13.

19. Kalthoff D, Globig A, Beer M. 2010. (Highly pathogenic) avian influenza as a zoonotic agent. Vet Microbiol 140:237-45.

20. Organization WH. 2019. Cumulative number of confirmed human cases of avian influenza A(H5N1) reported to WHO. https://www.who.int/influenza/human_animal_interface/H5N1_cumulative_table_archives/en/. Accessed 11/25.

21. Petrova VN, Russell CA. 2017. The evolution of seasonal influenza viruses. Nature Reviews Microbiology 16:47.

22. Cattoli G, Milani A, Temperton N, Zecchin B, Buratin A, Molesti E, Aly MM, Arafa A, Capua I. 2011. Antigenic drift in H5N1 avian influenza virus in poultry is driven by mutations in major antigenic sites of the hemagglutinin molecule analogous to those for human influenza virus. Journal of virology 85:8718-8724.

23. Li FCK, Choi BCK, Sly T, Pak AWP. 2008. Finding the real case-fatality rate of H5N1 avian influenza. Journal of Epidemiology and Community Health 62:555.

24. Ma W, Kahn RE, Richt JA. 2008. The pig as a mixing vessel for influenza viruses: Human and veterinary implications. Journal of molecular and genetic medicine : an international journal of biomedical research 3:158-166.

25. Ahmed SSU, Ersbøll AK, Biswas PK, Christensen JP, Hannan ASMA, Toft N. 2012. Ecological determinants of highly pathogenic avian influenza (H5N1) outbreaks in Bangladesh. PloS one 7:e33938-e33938.

26. Lai S, Qin Y, Cowling BJ, Ren X, Wardrop NA, Gilbert M, Tsang TK, Wu P, Feng L, Jiang H, Peng Z, Zheng J, Liao Q, Li S, Horby PW, Farrar JJ, Gao GF, Tatem AJ, Yu H. 2016. Global epidemiology of avian influenza A H5N1 virus infection in humans, 1997-2015: a systematic review of individual case data. The Lancet Infectious diseases 16:e108-e118.

27. Jiang W, Liu S, Hou G, Li J, Zhuang Q, Wang S, Zhang P, Chen J. 2012. Chinese and global distribution of H9 subtype avian influenza viruses. PloS one 7:e52671-e52671.

28. Li Q, Zhou L, Zhou M, Chen Z, Li F, Wu H, Xiang N, Chen E, Tang F, Wang D, Meng L, Hong Z, Tu W, Cao Y, Li L, Ding F, Liu B, Wang M, Xie R, Gao R, Li X, Bai T, Zou S, He J, Hu J, Xu Y, Chai C, Wang S, Gao Y, Jin L, Zhang Y, Luo H, Yu H, He J, Li Q, Wang X, Gao L, Pang X, Liu G, Yan Y, Yuan H, Shu Y, Yang W, Wang Y, Wu F, Uyeki TM, Feng Z. 2013. Epidemiology of Human Infections with Avian Influenza A(H7N9) Virus in China. New England Journal of Medicine 370:520-532.

29. Yu D, Xiang G, Zhu W, Lei X, Li B, Meng Y, Yang L, Jiao H, Li X, Huang W, Wei H, Zhang Y, Hai Y, Zhang H, Yue H, Zou S, Zhao X, Li C, Ao D, Zhang Y, Tan M, Liu J, Zhang X, Gao GF, Meng L, Wang D. 2019. The re-emergence of highly pathogenic avian influenza H7N9 viruses in humans in mainland China, 2019. Euro surveillance : bulletin Europeen sur les maladies transmissibles = European communicable disease bulletin 24:1900273.

30. Gambotto A, Barratt-Boyes SM, de Jong MD, Neumann G, Kawaoka Y. 2008. Human infection with highly pathogenic H5N1 influenza virus. Lancet 371:1464-75.

31. Uyeki TM. 2009. Human Infection with Highly Pathogenic Avian Influenza A (H5N1) Virus: Review of Clinical Issues. Clinical Infectious Diseases 49:279-290.

32. To KKW, Ng KHL, Que T-L, Chan JMC, Tsang K-Y, Tsang AKL, Chen H, Yuen K-Y. 2012. Avian influenza A H5N1 virus: a continuous threat to humans. Emerging Microbes & Infections 1:1-12.

33. Lipatov AS, Kwon YK, Sarmento LV, Lager KM, Spackman E, Suarez DL, Swayne DE. 2008. Domestic Pigs Have Low Susceptibility to H5N1 Highly Pathogenic Avian Influenza Viruses. PLOS Pathogens 4:e1000102.

34. Nidom CA, Takano R, Yamada S, Sakai-Tagawa Y, Daulay S, Aswadi D, Suzuki T, Suzuki Y, Shinya K, Iwatsuki-Horimoto K, Muramoto Y, Kawaoka Y. 2010. Influenza A (H5N1) viruses from pigs, Indonesia. Emerging infectious diseases 16:1515-1523.

35. Capua I, Cattoli G. 2013. Prevention and control of highly pathogenic avian influenza with particular reference to H5N1. Virus Res 178:114-20.

36. Reece PA. 2010. Treatment options for H5N1: lessons learned from the H1N1 pandemic. Postgrad Med 122:134-41.

37. Couch RB, Davis BR. 2010. Has Oseltamivir been shown to be Effective for Treatment of H5N1 Influenza? The Journal of Infectious Diseases 202:1149-1151.

38. Tomar J, Biel C, de Haan CAM, Rottier PJM, Petrovsky N, Frijlink HW, Huckriede A, Hinrichs WLJ, Peeters B. 2018. Passive inhalation of dry powder influenza vaccine formulations completely protects chickens against H5N1 lethal viral challenge. Eur J Pharm Biopharm 133:85-95.

39. Li C, Bu Z, Chen H. 2014. Avian influenza vaccines against H5N1 'bird flu'. Trends Biotechnol 32:147-56.

40. Yassine HM, Boyington JC, McTamney PM, Wei CJ, Kanekiyo M, Kong WP, Gallagher JR, Wang L, Zhang Y, Joyce MG, Lingwood D, Moin SM, Andersen H, Okuno Y, Rao SS, Harris AK, Kwong PD, Mascola JR, Nabel GJ, Graham BS. 2015. Hemagglutinin-stem nanoparticles generate heterosubtypic influenza protection. Nat Med 21:1065-70.

41. Sautto GA, Kirchenbaum GA, Ross TM. 2018. Towards a universal influenza vaccine: different approaches for one goal. Virol J 15:17.

42. Eisenstein M. 2019. Towards a universal flu vaccine. Nature 573:S50-s52.

43. Wonderlich ER, Swan ZD, Bissel SJ, Hartman AL, Carney JP, O'Malley KJ, Obadan AO, Santos J, Walker R, Sturgeon TJ, Frye LJ, Jr., Maiello P, Scanga CA, Bowling JD, Bouwer AL, Duangkhae PA, Wiley CA, Flynn JL, Wang J, Cole KS, Perez DR, Reed DS, Barratt-Boyes SM. 2017. Widespread Virus Replication in Alveoli Drives Acute Respiratory Distress Syndrome in Aerosolized H5N1 Influenza Infection of Macaques. Journal of immunology (Baltimore, Md : 1950) 198:1616-1626.

44. Soloff AC, Bissel SJ, Junecko BF, Giles BM, Reinhart TA, Ross TM, Barratt-Boyes SM. 2014. Massive Mobilization of Dendritic Cells During Influenza A Virus Subtype H5N1 Infection of Nonhuman Primates. The Journal of Infectious Diseases 209:2012-2016.

45. Short KR, Kroeze E, Fouchier RAM, Kuiken T. 2014. Pathogenesis of influenza-induced acute respiratory distress syndrome. Lancet Infect Dis 14:57-69.

46. Peiris JSM, Cheung CY, Leung CYH, Nicholls JM. 2009. Innate immune responses to influenza A H5N1: friend or foe? Trends in immunology 30:574-584.

47. Peiris JS, Hui KP, Yen HL. 2010. Host response to influenza virus: protection versus immunopathology. Curr Opin Immunol 22:475-81.

48. Ichinohe T, Pang IK, Iwasaki A. 2010. Influenza virus activates inflammasomes via its intracellular M2 ion channel. Nat Immunol 11:404-10.

49.   Huo C, Xiao K, Zhang S, Tang Y, Wang M, Qi P, Xiao J, Tian H, Hu Y. 2018. H5N1 Influenza a Virus Replicates Productively in Pancreatic Cells and Induces Apoptosis and Pro-Inflammatory Cytokine Response. Frontiers in Cellular and Infection Microbiology 8.

50.   Hui KPY, Lee SMY, Cheung C-y, Mao H, Lai AKW, Chan RWY, Chan MCW, Tu W, Guan Y, Lau Y-L, Peiris JSM. 2011. H5N1 Influenza Virus–Induced Mediators Upregulate RIG-I in Uninfected Cells by Paracrine Effects Contributing to Amplified Cytokine Cascades. The Journal of Infectious Diseases 204:1866-1878.

51.   Herold S, Becker C, Ridge KM, Budinger GRS. 2015. Influenza virus-induced lung injury: pathogenesis and implications for treatment. European Respiratory Journal 45:1463.

52.   de Jong MD, Simmons CP, Thanh TT, Hien VM, Smith GJ, Chau TN, Hoang DM, Chau NV, Khanh TH, Dong VC, Qui PT, Cam BV, Ha do Q, Guan Y, Peiris JS, Chinh NT, Hien TT, Farrar J. 2006. Fatal outcome of human influenza A (H5N1) is associated with high viral load and hypercytokinemia. Nat Med 12:1203-7.

53.   Chan RWY, Leung CYH, Nicholls JM, Peiris JSM, Chan MCW. 2012. Proinflammatory Cytokine Response and Viral Replication in Mouse Bone Marrow Derived Macrophages Infected with Influenza H1N1 and H5N1 Viruses. PLOS ONE 7:e51057.

54.   Baskin CR, Bielefeldt-Ohmann H, Tumpey TM, Sabourin PJ, Long JP, Garcia-Sastre A, Tolnay AE, Albrecht R, Pyles JA, Olson PH, Aicher LD, Rosenzweig ER, Murali-Krishna K, Clark EA, Kotur MS, Fornek JL, Proll S, Palermo RE, Sabourin CL, Katze MG. 2009. Early and sustained innate immune response defines pathology and death in nonhuman primates infected by highly pathogenic influenza virus. Proc Natl Acad Sci U S A 106:3455-60.

55.   Menachery VD, Eisfeld AJ, Schäfer A, Josset L, Sims AC, Proll S, Fan S, Li C, Neumann G, Tilton SC, Chang J, Gralinski LE, Long C, Green R, Williams CM, Weiss J, Matzke MM, Webb-Robertson B-J, Schepmoes AA, Shukla AK, Metz TO, Smith RD, Waters KM, Katze MG, Kawaoka Y, Baric RS. 2014. Pathogenic influenza viruses and coronaviruses utilize similar and contrasting approaches to control interferon-stimulated gene responses. mBio 5:e01174.

56.   Lee S, Hirohama M, Noguchi M, Nagata K, Kawaguchi A. 2018. Influenza A Virus Infection Triggers Pyroptosis and Apoptosis of Respiratory Epithelial Cells through the Type I Interferon Signaling Pathway in a Mutually Exclusive Manner. Journal of Virology 92:e00396-18.

57.   Kobasa D, Jones SM, Shinya K, Kash JC, Copps J, Ebihara H, Hatta Y, Kim JH, Halfmann P, Hatta M, Feldmann F, Alimonti JB, Fernando L, Li Y, Katze MG, Feldmann H, Kawaoka Y. 2007. Aberrant innate immune response in lethal infection of macaques with the 1918 influenza virus. Nature 445:319-23.

58.   Muramoto Y, Shoemaker JE, Le MQ, Itoh Y, Tamura D, Sakai-Tagawa Y, Imai H, Uraki R, Takano R, Kawakami E, Ito M, Okamoto K, Ishigaki H, Mimuro H, Sasakawa C, Matsuoka Y, Noda T, Fukuyama S, Ogasawara K, Kitano H, Kawaoka Y. 2014. Disease severity is associated with differential gene expression at the early and late phases of infection in nonhuman primates infected with different H5N1 highly pathogenic avian influenza viruses. J Virol 88:8981-97.

59.   Guillot L, Nathan N, Tabary O, Thouvenin G, Le Rouzic P, Corvol H, Amselem S, Clement A. 2013. Alveolar epithelial cells: master regulators of lung homeostasis. Int J Biochem Cell Biol 45:2568-73.

60. Cline TD, Beck D, Bianchini E. 2017. Influenza virus replication in macrophages: balancing protection and pathogenesis. The Journal of general virology 98:2401-2412.

61. Takano R, Nidom CA, Kiso M, Muramoto Y, Yamada S, Shinya K, Sakai-Tagawa Y, Kawaoka Y. 2009. A comparison of the pathogenicity of avian and swine H5N1 influenza viruses in Indonesia. Archives of virology 154:677-681.

62. Kim HM, Lee YW, Lee KJ, Kim HS, Cho SW, van Rooijen N, Guan Y, Seo SH. 2008. Alveolar macrophages are indispensable for controlling influenza viruses in lungs of pigs. J Virol 82:4265-74.

63. Heidemann S, Nair A, Bulut Y, Sapru A. 2017. Pathophysiology and Management of Acute Respiratory Distress Syndrome in Children. Pediatric Clinics of North America 64:1017-1037.

64. Barnard DL. 2009. Animal models for the study of influenza pathogenesis and therapy. Antiviral research 82:A110-A122.

65. Belser JA, Katz JM, Tumpey TM. 2011. The ferret as a model organism to study influenza A virus infection. Disease Models &amp; Mechanisms 4:575.

66. Fujiyuki T, Yoneda M, Yasui F, Kuraishi T, Hattori S, Kwon H-j, Munekata K, Kiso Y, Kida H, Kohara M, Kai C. 2013. Experimental Infection of Macaques with a Wild Water Bird-Derived Highly Pathogenic Avian Influenza Virus (H5N1). PLOS ONE 8:e83551.

67. Lipatov AS, Kwon YK, Pantin-Jackwood MJ, Swayne DE. 2009. Pathogenesis of H5N1 Influenza Virus Infections in Mice and Ferret Models Differs According to Respiratory Tract or Digestive System Exposure. The Journal of Infectious Diseases 199:717-725.

68. Lu X, Tumpey TM, Morken T, Zaki SR, Cox NJ, Katz JM. 1999. A Mouse Model for the Evaluation of Pathogenesis and Immunity to Influenza A (H5N1) Viruses Isolated from Humans. Journal of Virology 73:5903.

69. Rimmelzwaan GF, Kuiken T, van Amerongen G, Bestebroer TM, Fouchier RAM, Osterhaus ADME. 2001. Pathogenesis of Influenza A (H5N1) Virus Infection in a Primate Model. Journal of Virology 75:6687.

70. Watanabe T, Iwatsuki-Horimoto K, Kiso M, Nakajima N, Takahashi K, Jose da Silva Lopes T, Ito M, Fukuyama S, Hasegawa H, Kawaoka Y. 2018. Experimental infection of Cynomolgus Macaques with highly pathogenic H5N1 influenza virus through the aerosol route. Scientific Reports 8:4801.

71. Zitzow LA, Rowe T, Morken T, Shieh WJ, Zaki S, Katz JM. 2002. Pathogenesis of avian influenza A (H5N1) viruses in ferrets. J Virol 76:4420-9.

72. Ilyushina NA, Khalenkov AM, Seiler JP, Forrest HL, Bovin NV, Marjuki H, Barman S, Webster RG, Webby RJ. 2010. Adaptation of Pandemic H1N1 Influenza Viruses in Mice. Journal of Virology 84:8607.

73. Zimmermann KC, Green DR. 2001. How cells die: Apoptosis pathways. Journal of Allergy and Clinical Immunology 108:S99-S103.

74. Green DR. 1998. Apoptotic Pathways: The Roads to Ruin. Cell 94:695-698.

75. Geske FJ, Gerschenson LE. 2001. The biology of apoptosis. Human Pathology 32:1029-1038.

76. Elmore S. 2007. Apoptosis: a review of programmed cell death. Toxicol Pathol 35:495-516.

77. Bohm I, Schild H. 2003. Apoptosis: the complex scenario for a silent cell death. Mol Imaging Biol 5:2-14.

78. Loreto C, La Rocca G, Anzalone R, Caltabiano R, Vespasiani G, Castorina S, Ralph DJ, Cellek S, Musumeci G, Giunta S, Djinovic R, Basic D, Sansalone S. 2014. The Role of Intrinsic Pathway in Apoptosis Activation and Progression in Peyronie's Disease. BioMed Research International 2014:616149.

79. Yuen KM, Chan RW, Mok CK, Wong AC, Kang SS, Nicholls JM, Chan MC. 2011. Differential onset of apoptosis in avian influenza H5N1 and seasonal H1N1 virus infected human bronchial and alveolar epithelial cells: an in vitro and ex vivo study. Influenza Other Respir Viruses 5:437-438.

80. Uiprasertkul M, Kitphati R, Puthavathana P, Kraivong R, Kongchanagul A, Ungchusak K, Angkasekwinai S, Srisook K, Vanprapar N, Auewarakul P. 2007. Apoptosis and Pathogenesis of Avian Influenza A (H5N1) Virus in Humans. Emerging infectious diseases 13:708-12.

81. Ueda M, Daidoji T, Du A, Yang C-S, Ibrahim MS, Ikuta K, Nakaya T. 2010. Highly pathogenic H5N1 avian influenza virus induces extracellular Ca2+ influx, leading to apoptosis in avian cells. Journal of virology 84:3068-3078.

82. Mao H, Liu Y, Sia SF, Peiris JSM, Lau YL, Tu W. 2017. Avian influenza virus directly infects human natural killer cells and inhibits cell activity. Virol Sin 32:122-129.

83. Daidoji T, Koma T, Du A, Yang C-S, Ueda M, Ikuta K, Nakaya T. 2008. H5N1 avian influenza virus induces apoptotic cell death in mammalian airway epithelial cells. Journal of virology 82:11294-11307.

84. Bian Q, Lu J, Zhang L, Chi Y, Li Y, Guo H. 2017. Highly pathogenic avian influenza A virus H5N1 non-structural protein 1 is associated with apoptotic activation of the intrinsic mitochondrial pathway. Experimental and therapeutic medicine 14:4041-4046.

85. Hui KPY, Li HS, Cheung MC, Chan RWY, Yuen KM, Mok CKP, Nicholls JM, Peiris JSM, Chan MCW. 2016. Highly pathogenic avian influenza H5N1 virus delays apoptotic responses via activation of STAT3. Scientific Reports 6:28593.

86. Chang P, Kuchipudi SV, Mellits KH, Sebastian S, James J, Liu J, Shelton H, Chang K-C. 2015. Early apoptosis of porcine alveolar macrophages limits avian influenza virus replication and pro-inflammatory dysregulation. Scientific Reports 5:17999.

87. Tsuchiya K. 2020. Inflammasome-associated cell death: Pyroptosis, apoptosis, and physiological implications. Microbiol Immunol 64:252-269.

88. Place DE, Kanneganti T-D. 2019. On the Road to Discovering the Elusive Executioner of Pyroptosis. The Journal of Immunology 202:1911.

89. Man SM, Karki R, Kanneganti T-D. 2017. Molecular mechanisms and functions of pyroptosis, inflammatory caspases and inflammasomes in infectious diseases. Immunological reviews 277:61-75.

90. Kuriakose T, Kanneganti TD. 2019. Pyroptosis in Antiviral Immunity. Curr Top Microbiol Immunol doi:10.1007/82_2019_189.

91. Frank D, Vince JE. 2019. Pyroptosis versus necroptosis: similarities, differences, and crosstalk. Cell Death & Differentiation 26:99-114.

92. Fink SL, Cookson BT. 2005. Apoptosis, Pyroptosis, and Necrosis: Mechanistic Description of Dead and Dying Eukaryotic Cells. Infection and Immunity 73:1907.

93. de Vasconcelos NM, Lamkanfi M. 2019. Recent Insights on Inflammasomes, Gasdermin Pores, and Pyroptosis. Cold Spring Harb Perspect Biol doi:10.1101/cshperspect.a036392.

94. Bergsbaken T, Fink SL, Cookson BT. 2009. Pyroptosis: host cell death and inflammation. Nature reviews Microbiology 7:99-109.

95.   Wang Y-Y, Liu X-L, Zhao R. 2019. Induction of Pyroptosis and Its Implications in Cancer Management. Frontiers in Oncology 9.

96.   Ichinohe T, Lee HK, Ogura Y, Flavell R, Iwasaki A. 2009. Inflammasome recognition of influenza virus is essential for adaptive immune responses. Journal of Experimental Medicine 206:79-87.

97.   Ong JD, Mansell A, Tate MD. 2017. Hero turned villain: NLRP3 inflammasome-induced inflammation during influenza A virus infection. J Leukoc Biol 101:863-874.

98.   Cilloniz C, Shinya K, Peng X, Korth MJ, Proll SC, Aicher LD, Carter VS, Chang JH, Kobasa D, Feldmann F, Strong JE, Feldmann H, Kawaoka Y, Katze MG. 2009. Lethal influenza virus infection in macaques is associated with early dysregulation of inflammatory related genes. PLoS Pathog 5:e1000604.

99.   Banerjee SK, Huckuntod SD, Mills SD, Kurten RC, Pechous RD. 2019. Modeling Pneumonic Plague in Human Precision-Cut Lung Slices Highlights a Role for the Plasminogen Activator Protease in Facilitating Type 3 Secretion. Infection and Immunity 87:e00175-19.

100.   Liu G, Betts C, Cunoosamy DM, Åberg PM, Hornberg JJ, Sivars KB, Cohen TS. 2019. Use of precision cut lung slices as a translational model for the study of lung biology. Respiratory Research 20:162.

101.   Meng F, Punyadarsaniya D, Uhlenbruck S, Hennig-Pauka I, Schwegmann-Wessels C, Ren X, Dürrwald R, Herrler G. 2013. Replication characteristics of swine influenza viruses in precision-cut lung slices reflect the virulence properties of the viruses. Veterinary Research 44:110.

102.   Niehof M, Hildebrandt T, Danov O, Arndt K, Koschmann J, Dahlmann F, Hansen T, Sewald K. 2017. RNA isolation from precision-cut lung slices (PCLS) from different species. BMC Res Notes 10:121.

103.   Rosales Gerpe MC, van Vloten JP, Santry LA, de Jong J, Mould RC, Pelin A, Bell JC, Bridle BW, Wootton SK. 2018. Use of Precision-Cut Lung Slices as an Ex Vivo Tool for Evaluating Viruses and Viral Vectors for Gene and Oncolytic Therapy. Molecular therapy Methods & clinical development 10:245-256.

104.   Temann A, Golovina T, Neuhaus V, Thompson C, Chichester JA, Braun A, Yusibov V. 2017. Evaluation of inflammatory and immune responses in long-term cultured human precision-cut lung slices. Human vaccines & immunotherapeutics 13:351-358.

105.   Bryson KJ, Garrido D, Esposito M, McLachlan G, Digard P, Schouler C, Guabiraba R, Trapp S, Vervelde L. 2020. Precision cut lung slices: a novel versatile tool to examine host–pathogen interaction in the chicken lung. Veterinary Research 51:2.

106.   Brann KR, Fullerton MS, Onyilagha FI, Prince AA, Kurten RC, Rom JS, Blevins JS, Smeltzer MS, Voth DE. 2019. Infection of Primary Human Alveolar Macrophages Alters Staphylococcus aureus Toxin Production and Activity. Infection and Immunity 87:e00167-19.

107.   Delgado-Ortega M, Melo S, Punyadarsaniya D, Rame C, Olivier M, Soubieux D, Marc D, Simon G, Herrler G, Berri M, Dupont J, Meurens F. 2014. Innate immune response to a H3N2 subtype swine influenza virus in newborn porcine trachea cells, alveolar macrophages, and precision-cut lung slices. Vet Res 45:42.

108. Graham JG, Winchell CG, Kurten RC, Voth DE. 2016. Development of an Ex Vivo Tissue Platform To Study the Human Lung Response to Coxiella burnetii. Infection and immunity 84:1438-1445.
109. Sellwood C, Asgari-Jirhandeh N, Salimee S. 2007. Bird flu: if or when? Planning for the next pandemic. Postgraduate medical journal 83:445-450.
110. Taubenberger JK, Morens DM. 2009. Pandemic influenza--including a risk assessment of H5N1. Revue scientifique et technique (International Office of Epizootics) 28:187-202.
111. Herfst S, Schrauwen EJA, Linster M, Chutinimitkul S, de Wit E, Munster VJ, Sorrell EM, Bestebroer TM, Burke DF, Smith DJ, Rimmelzwaan GF, Osterhaus ADME, Fouchier RAM. 2012. Airborne Transmission of Influenza A/H5N1 Virus Between Ferrets. Science 336:1534.
112. Imai M, Watanabe T, Hatta M, Das SC, Ozawa M, Shinya K, Zhong G, Hanson A, Katsura H, Watanabe S, Li C, Kawakami E, Yamada S, Kiso M, Suzuki Y, Maher EA, Neumann G, Kawaoka Y. 2012. Experimental adaptation of an influenza H5 HA confers respiratory droplet transmission to a reassortant H5 HA/H1N1 virus in ferrets. Nature 486:420-428.
113. Fu Y, Cheng Y, Wu Y. 2020. Understanding SARS-CoV-2-Mediated Inflammatory Responses: From Mechanisms to Potential Therapeutic Tools. Virologica Sinica doi:10.1007/s12250-020-00207-4.
114. Yang Y, Peng F, Wang R, Guan K, Jiang T, Xu G, Sun J, Chang C. 2020. The deadly coronaviruses: The 2003 SARS pandemic and the 2020 novel coronavirus epidemic in China. Journal of autoimmunity 109:102434-102434.
115. Rosales Gerpe MC, van Vloten JP, Santry LA, de Jong J, Mould RC, Pelin A, Bell JC, Bridle BW, Wootton SK. 2018. Use of Precision-Cut Lung Slices as an Ex Vivo Tool for Evaluating Viruses and Viral Vectors for Gene and Oncolytic Therapy. Mol Ther Methods Clin Dev 10:245-256.
116. Ghonime MG, Shamaa OR, Das S, Eldomany RA, Fernandes-Alnemri T, Alnemri ES, Gavrilin MA, Wewers MD. 2014. Inflammasome priming by lipopolysaccharide is dependent upon ERK signaling and proteasome function. J Immunol 192:3881-8.
117. Yang Y, Wang H, Kouadir M, Song H, Shi F. 2019. Recent advances in the mechanisms of NLRP3 inflammasome activation and its inhibitors. Cell Death & Disease 10:128.
118. Deng H, Maitra U, Morris M, Li L. 2013. Molecular mechanism responsible for the priming of macrophage activation. The Journal of biological chemistry 288:3897-3906.
119. Meng F, Lowell CA. 1997. Lipopolysaccharide (LPS)-induced macrophage activation and signal transduction in the absence of Src-family kinases Hck, Fgr, and Lyn. The Journal of experimental medicine 185:1661-1670.
120. Moscovis S, Hall S, Burns C, Scott R, Blackwell C. 2014. Development of an experimental model for assessing the effects of cigarette smoke and virus infections on inflammatory responses to bacterial antigens. Innate Immun 20:647-58.
121. Liu W, Chen Y, Meng J, Wu M, Bi F, Chang C, Li H, Zhang L. 2018. Ablation of caspase-1 protects against TBI-induced pyroptosis in vitro and in vivo. Journal of neuroinflammation 15:48-48.
122. Doitsh G, Galloway NL, Geng X, Yang Z, Monroe KM, Zepeda O, Hunt PW, Hatano H, Sowinski S, Munoz-Arias I, Greene WC. 2014. Cell death by pyroptosis drives CD4 T-cell depletion in HIV-1 infection. Nature 505:509-14.
123. Wang W, Li G, De W, Luo Z, Pan P, Tian M, Wang Y, Xiao F, Li A, Wu K, Liu X, Rao L, Liu F, Liu Y, Wu J. 2018. Zika virus infection induces host inflammatory responses by

facilitating NLRP3 inflammasome assembly and interleukin-1β secretion. Nature Communications 9:106.

124. Zahid A, Li B, Kombe AJK, Jin T, Tao J. 2019. Pharmacological Inhibitors of the NLRP3 Inflammasome. Frontiers in Immunology 10.

125. Hu JJ, Liu X, Zhao J, Xia S, Ruan J, Luo X, Kim J, Lieberman J, Wu H. 2018. Identification of pyroptosis inhibitors that target a reactive cysteine in gasdermin D. bioRxiv doi:10.1101/365908:365908.

126. Wurzer WJ, Planz O, Ehrhardt C, Giner M, Silberzahn T, Pleschka S, Ludwig S. 2003. Caspase 3 activation is essential for efficient influenza virus propagation. The EMBO journal 22:2717-2728.

127. Lee ACY, Zhang AJX, Chu H, Li C, Zhu H, Mak WWN, Chen Y, Kok K-H, To KKW, Yuen K-Y. 2019. H7N9 influenza A virus activation of necroptosis in human monocytes links innate and adaptive immune responses. Cell Death & Disease 10:442.

128. Daidoji T, Koma T, Du A, Yang C-S, Ueda M, Ikuta K, Nakaya T. 2008. H5N1 Avian Influenza Virus Induces Apoptotic Cell Death in Mammalian Airway Epithelial Cells. Journal of Virology 82:11294.

129. Manzoor R, Sakoda Y, Nomura N, Tsuda Y, Ozaki H, Okamatsu M, Kida H. 2009. PB2 Protein of a Highly Pathogenic Avian Influenza Virus Strain A/chicken/Yamaguchi/7/2004 (H5N1) Determines Its Replication Potential in Pigs. Journal of Virology 83:1572.

130. Huang CH, Chen CJ, Yen CT, Yu CP, Huang PN, Kuo RL, Lin SJ, Chang CK, Shih SR. 2013. Caspase-1 deficient mice are more susceptible to influenza A virus infection with PA variation. J Infect Dis 208:1898-905.

131. Westenius V, Mäkelä SM, Julkunen I, Österlund P. 2018. Highly Pathogenic H5N1 Influenza A Virus Spreads Efficiently in Human Primary Monocyte-Derived Macrophages and Dendritic Cells. Frontiers in immunology 9:1664-1664.

132. Weinheimer VK, Becher A, Tönnies M, Holland G, Knepper J, Bauer TT, Schneider P, Neudecker J, Rückert JC, Szymanski K, Temmesfeld-Wollbrueck B, Gruber AD, Bannert N, Suttorp N, Hippenstiel S, Wolff T, Hocke AC. 2012. Influenza A Viruses Target Type II Pneumocytes in the Human Lung. The Journal of Infectious Diseases 206:1685-1694.

133. Fujikura D, Miyazaki T. 2018. Programmed Cell Death in the Pathogenesis of Influenza. International journal of molecular sciences 19:2065.

134. Schmolke M, Viemann D, Roth J, Ludwig S. 2009. Essential Impact of NF-κB Signaling on the H5N1 Influenza A Virus-Induced Transcriptome. The Journal of Immunology 183:5180.

135. Karimi Y, Poznanski SM, Vahedi F, Chen B, Chew MV, Lee AJ, Ashkar AA. 2017. Type I interferon signalling is not required for the induction of endotoxin tolerance. Cytokine 95:7-11.

136. Vadiveloo PK, Vairo G, Hertzog P, Kola I, Hamilton JA. 2000. Role Of Type I Interferons During Macrophage Activation By Lipopolysaccharide. Cytokine 12:1639-1646.

137. Tate MD, Ong JDH, Dowling JK, McAuley JL, Robertson AB, Latz E, Drummond GR, Cooper MA, Hertzog PJ, Mansell A. 2016. Reassessing the role of the NLRP3 inflammasome during pathogenic influenza A virus infection via temporal inhibition. Scientific Reports 6:27912.

138. Ren R, Wu S, Cai J, Yang Y, Ren X, Feng Y, Chen L, Qin B, Xu C, Yang H, Song Z, Tian D, Hu Y, Zhou X, Meng G. 2017. The H7N9 influenza A virus infection results in lethal

inflammation in the mammalian host via the NLRP3-caspase-1 inflammasome. Scientific reports 7:7625-7625.

139. Malireddi RKS, Kanneganti T-D. 2013. Role of type I interferons in inflammasome activation, cell death, and disease during microbial infection. Frontiers in Cellular and Infection Microbiology 3.

140. Mistry P, Kaplan MJ. 2017. Cell death in the pathogenesis of systemic lupus erythematosus and lupus nephritis. Clinical immunology (Orlando, Fla) 185:59-73.

141. Chen KW, Monteleone M, Boucher D, Sollberger G, Ramnath D, Condon ND, von Pein JB, Broz P, Sweet MJ, Schroder K. 2018. Noncanonical inflammasome signaling elicits gasdermin D–dependent neutrophil extracellular traps. Science Immunology 3:eaar6676.

142. Sollberger G, Choidas A, Burn GL, Habenberger P, Di Lucrezia R, Kordes S, Menninger S, Eickhoff J, Nussbaumer P, Klebl B, Kruger R, Herzig A, Zychlinsky A. 2018. Gasdermin D plays a vital role in the generation of neutrophil extracellular traps. Sci Immunol 3.

143. Camp JV, Jonsson CB. 2017. A Role for Neutrophils in Viral Respiratory Disease. Frontiers in Immunology 8.

144. Peiró T, Patel DF, Akthar S, Gregory LG, Pyle CJ, Harker JA, Birrell MA, Lloyd CM, Snelgrove RJ. 2018. Neutrophils drive alveolar macrophage IL-1β release during respiratory viral infection. Thorax 73:546.

145. Zhao Y, Lu M, Lau LT, Lu J, Gao Z, Liu J, Hoi Yu AC, Cao Q, Ye J, McNutt MA, Gu J. 2008. Neutrophils May Be a Vehicle for Viral Replication and Dissemination in Human H5N1 Avian Influenza. Clinical Infectious Diseases 47:1575-1578.

146. Zhu L, Liu L, Zhang Y, Pu L, Liu J, Li X, Chen Z, Hao Y, Wang B, Han J, Li G, Liang S, Xiong H, Zheng H, Li A, Xu J, Zeng H. 2018. High Level of Neutrophil Extracellular Traps Correlates With Poor Prognosis of Severe Influenza A Infection. The Journal of Infectious Diseases 217:428-437.

147. Anonymous. 2013. Middle East Respiratory Syndrome (MERS) - An update. International journal of health sciences 7:V-VI.

148. Baas T, Taubenberger JK, Chong PY, Chui P, Katze MG. 2006. SARS-CoV virus-host interactions and comparative etiologies of acute respiratory distress syndrome as determined by transcriptional and cytokine profiling of formalin-fixed paraffin-embedded tissues. J Interferon Cytokine Res 26:309-17.

149. Li H, Weng H, Lan C, Zhang H, Wang X, Pan J, Chen L, Huang J. 2018. Comparison of patients with avian influenza A (H7N9) and influenza A (H1N1) complicated by acute respiratory distress syndrome. Medicine 97:e0194-e0194.

150. Singhal T. 2020. A Review of Coronavirus Disease-2019 (COVID-19). Indian journal of pediatrics 87:281-286.

151. Yang Y, Peng F, Wang R, Guan K, Jiang T, Xu G, Sun J, Chang C. 2020. The deadly coronaviruses: The 2003 SARS pandemic and the 2020 novel coronavirus epidemic in China. Journal of Autoimmunity 109:102434.